BOTSWANA INTERNATIONAL UNIVERSITY
OF SCIENCE & TECHNOLOGY

Faculty of Engineering

Department of Mechanical, Energy and Industrial
Engineering

# MODELING, SIMULATION, AND ENERGY MANAGEMENT OF SOLAR PV-BASED MICROGRIDS USING REAL-TIME RESIDENTIAL DATA

By

TUMELO BOITSHOKO SEANE

Student ID number: 13000423

BEng Energy Engineering (BIUST)

A Dissertation/thesis Submitted to the Faculty of Engineering and
Technology in Fulfilment of the Requirements for the Award of the
Degree of Master of Engineering in Mechanical and Energy in
BIUST

**Supervisor: Professor Ravi Samikannu**

Department of Electrical, Telecommunications and Computer Engineering

Faculty of Engineering, BIUST

Ravis@biust.ac.bw

August 2022

## DECLARATION REGARDING THE WORK AND COPYRIGHT

**Candidate**: _TUMELO BOITSHOKO SEANE_____

**Student ID:** _____13000423_____

Thesis Titled: MODELING, SIMULATION, AND ENERGY MANAGEMENT OF SOLAR PV-BASED MICROGRIDS USING REAL-TIME RESIDENTIAL DATA_____

I, the **Candidate**, certify that the Thesis is all my own original work and that I have not obtained a degree in this University or elsewhere on the basis of any of this work.

Signed: _____Date: _____18/08/2022_____

**Primary Supervisor**: __PROFESSOR RAVI SAMIKANNU___

I, the Candidate's **Primary Supervisor**, hereby confirm that I have inspected the above titled thesis and, to the best of my knowledge, it is based on the original work of the candidate.

Signed:_____Date: _____18.08.2021_____

i

## CERTIFICATION

The undersigned certifies that they have read and hereby recommend for acceptance by the Faculty of Engineering a thesis titled: ***Modeling, Simulation, and Energy Management of Solar PV-Based Microgrids using Real-Time Residential Data,*** in fulfilment of the requirements for the degree of Master of Engineering in (*Electrical and Electronics*) of the BIUST.

**Prof. Ravi Samikannu**

Date: 18.08.2022

## ACKNOWLEDGMENTS

**ABSTRACT**

The research aims at defining and analyzing an energy solution that incorporates renewable energy, thereby giving rise to improving energy security and providing grid stability for the grid networks located in urban residential areas. The urbanization growth in Botswana coincides with the increase in electricity consumption. The electricity load demand in the country outlasts the local supply and thereby the need for importing electricity from the Southern Africa Power Pool (SAPP). To address grid stability and reliable power supply issues, the research aims to design a microgrid system for an urban settlement by matching the electric load demand with solar photovoltaic (PV) generation in a residential district. The initial stages of the research include measuring electrical loads in a single household for a certain period. The energy data collected from residential homes were subjected to a smart metering examination. The analysis revealed high variability in the daily energy usage of the household. The dataset was tabulated through the two seasons experienced in Botswana, summer, and winter. Following a study using clustering techniques, three clusters with outliers' data identified the optimum monthly energy use with the lowest Mean Squared Error (MSE) after ten iterations. The peak hourly profiles from the metered residential household were used to represent a cumulative 250-kW planned power solar PV microgrid system. The design and simulation were conducted on the simulation environment MATLAB/Simulink with real-time daily irradiation and temperature profiles from the metered household location.

Proportional Integral Derivative (PID) controllers could achieve a desired DC microgrid voltage throughout the day. The boost converter through a signal from the Maximal Power Point Tracking (MPPT) could achieve the maximum voltage of the solar PV module. For energy management optimization, Fuzzy Logic Control (FLC) was incorporated for the grid-connected microgrid with battery support. The FLC simulation analysis demonstrated that the battery offered energy stability inside the microgrid system during the shift from island mode to a grid-connected mode of operation. The economic study was conducted in HOMERPro, and it revealed the levelized cost of electricity at USD 10.90/ kWh. The nature of the solar PV microgrid design revealed the system's lifetime cost savings worth USD 99,248.6. A microgrid system is a subpart of a smart grid; thus,

the proposed system aids in achieving the quick restoration of electricity when a power outage occurs while also enhancing local energy resiliency.

# TABLE OF CONTENTS

# LIST OF FIGURES

# LIST OF TABLES

**NOMENCLATURE**

**Notation**

| | |
|---|---|
| Ah | Ampere hour |
| I | Current |
| $I_D$ | Diode current |
| $I_L$ | Light generated current |
| $I_{mpp}$ | Current at maximum power point |
| $I_{sc}$ | Short circuit current |
| $I_{sh}$ | Shunt leakage current |
| KToe | Kilotonnes per oil equivalent |
| kW | Kilowatt |
| $kW/m^2$ | Kilowatt per square meter |
| kWh | Kilowatt hour |
| $L_{DP}$ | Frequency-dependent active coefficients |
| $L_{DQ}$ | Frequency-dependent reactive coefficients |
| MW | Megawatt |
| $MW_p$ | Megawatt peak |
| $^o$C | Degree Celsius |
| P | Active power |
| $P_{in}$ | Input power |
| $P_o$ | Nominal power |
| Q | Reactive power |
| $R^2$ | Coefficient of determination |
| $R_s$ | Series resistance |
| $R_{sh}$ | Shunt resistance |
| TWh | Terawatt hours |
| V | Voltage |
| $v_c$ | Carrier wave voltage |
| $V_{dc}$ | Volts of direct current |
| $V_{in}$ | Input voltage |

| $V_{mpp}$ | Voltage at maximum point |
|---|---|
| $V_o$ | Nominal voltage |
| $V_{oc}$ | Open circuit voltage |
| $v_{ref}$ | Reference voltage |
| $W/m^2$ | Watts per square meter |
| $W_p$ | Watt peak |

## Abbreviations

| AC | Alternating current |
|---|---|
| ANN | Artificial neural networks |
| ARIMA | Autoregressive integrated moving average |
| BESS | Battery energy storage system |
| DC | Direct current |
| DG | Distributed generation |
| ESS | Energy storage system |
| FLC | Fuzzy logic control |
| IoT | Internet of Things |
| LCL | Inductor-current-inductor |
| LCOE | Levelized cost of electricity |
| MAPE | Mean absolute percentage error |
| MOSFET | Metal Oxide Silicon Field Effect Transistors |
| MPPT | Maximum power point tracking |
| NPC | Net present cost |
| PEM | Proton-exchange membrane |
| PID | Proportional integral derivative |
| PVSyst | Photovoltaic (PV) System (SYST) |
| PWM | Pulse width modulation |
| RES | Renewable energy source |
| RET | Renewable energy technologies |
| RSME | Root mean square error |

| | |
|---|---|
| SARIMA | Seasonal autoregressive integrated moving average |
| SMPWM | Sinusoidal pulse width modulation |
| SOC | State of charge |
| SPSS | Statistical Package for Social Sciences |
| SSA | Sub-Sahara Africa |
| SVM | Support vector machine |
| THD | Total harmonic distortion |
| USD | United states dollar |
| VSI | Voltage source inverter |
| ZI | Hybrid constant impedance current model |
| ZIP | Zero-inflated Poisson |
| HOMER | Hybrid Optimization Model for Electric Renewables |
| PV | Photovoltaic |
| MATLAB | Matrix laboratory |
| MSE | Mean square error |

# 1    CHAPTER 1: INTRODUCTION

## 1.1    Overview

The following chapter defines the research goal, objectives, scope and provides an overview of the entire thesis structure. The thesis style described at the end of the chapter allows for reflection on material as a whole covered by the author.

## 1.2    Introduction

Rapid urbanization severely limits cities' environments and architecture, particularly in developing countries (Donahue 2019). Countries' energy security is enhanced by the resilience and effectiveness of local energy-generating structures and distribution systems. Botswana's urbanization is accelerating, and the increased electricity demands that come with it put a strain on the country's fragile electricity grid. Implementing an energy solution for urban dwellers would alleviate the energy supply issues that would arise due to increasing urbanization in a growing city like Gaborone. 'Mini-grids and microgrids are prospective renewable energy solutions capable of providing the most inexpensive production cost for three-quarters of all the connections necessary in Sub-Sahara Africa,' according to the (IEA 2014). The solutions serve as a foundation for integrating Renewable Energy Technologies (RETs) that promote local energy generation from low-carbon sources. The utilization of renewables, particularly solar energy, to meet local electrical load demands in cities via microgrids offers hope for the divisive issue of central transmission distribution (Halu et al. 2016). Botswana enjoys a high sun intensity throughout the year, making solar photovoltaics a viable energy source. An energy analysis of residential building usage provides the sizing and design information necessary for constructing solar PV-based microgrid systems.

1.3    Background to the problem

Botswana's existing power grid is incapable of providing the country's electricity load requirement. To meet the country's electrical consumption, the government must purchase electricity from the Southern Africa Power Pool (SAPP) (Botswana Power Corporation (BPC) 2019). Botswana is classified as an upper-middle-income country, but it has several obstacles, including a lack of infrastructure and poor production and skills (Essah and Ofetotse 2014). Electricity consumption has been steadily increasing in the past two decades, as indicated in Figure 1.1.
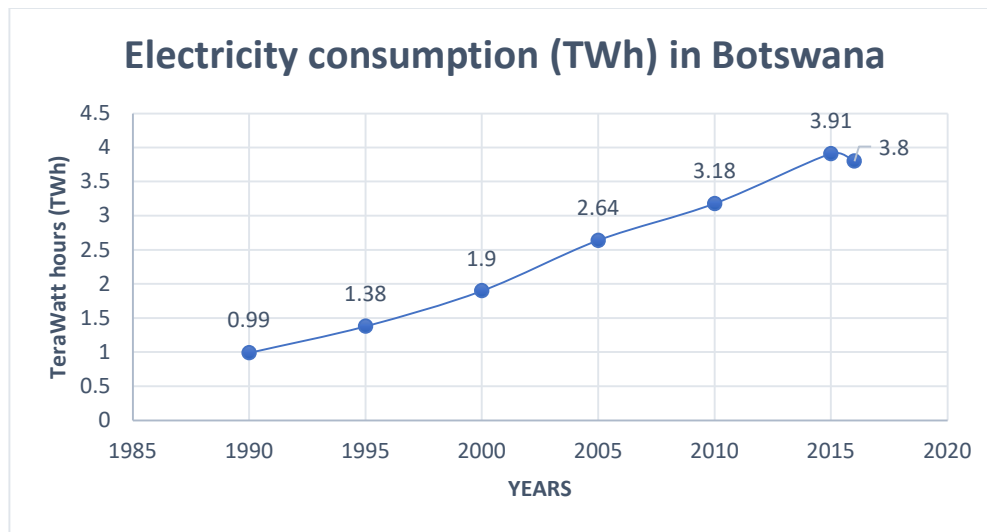


Figure 1.1: The electricity consumption in Botswana between the years 1990 and 2016. SOURCE: (IEA 2019)

The capital city's rapid urbanization necessitates an increase in electrical supplies. The country has been subjected to load shedding systems since 2013. The load-shedding schemes are a result of the continued rise in energy usage in domestic areas. Statistics reveal that from the overall energy consumption in Botswana, domestic energy usage accounts for slightly above one-third (Ofetotse, E., Essah, E. and Yao 2015).

### 1.4    Problem statement

The reliability of energy delivery to consumers is affected by the stability of the utility system. Electricity supply unreliability will primarily affect residential consumers in urban areas. Due to many electrical appliances and structures in use every day of the year, metropolitan areas have high electricity consumption. According to the World Energy Balances 2019, residential power usage climbed from 42 kilotonnes of oil equivalent (KToe) in 2004 to 88 KToe in 2017 (IEA 2019). Energy provision from solar photovoltaics presents an innovative method to alleviate the electricity need mainly among people living in residential areas. The cost-effectiveness of a microgrid, which incorporates solar photovoltaics primarily for residential spaces, appears to be profitable and valuable to consumers.

### 1.5    Research Aim

The aim of the research is stated as follows:

➢ The sizing and design of a community solar PV microgrid system through analysis of residential energy usage

### 1.6    Research Scope

An assessment on the rooftop solar PV system (microgrid) design for an urban settlement will be conducted whereby people will be sharing electrical loads through the system. The system to be designed will be connected to the grid. The research begins with the measurement of the electricity load in an exemplary building over a period. Afterward, a solar PV system will be designed and simulated for a single household. After that, a solar PV microgrid system will be modeled and simulated for the urban residential quarter (25 residential houses with similar load profiles). The control and energy management approach used will assure optimal energy generation by the solar PV system, resulting in

lower monthly electricity expenditures. An overview will be undertaken to emphasize the need for microgrid systems through a brief economic assessment.

### 1.7    Research Objectives

The research objectives of the project are articulated as follows:

- To measure the annual electricity usage in a residential household in Botswana.
- To execute smart meter data analytics for the identification of energy usage behavior characteristics.
- To design a grid-connected rooftop solar PV system for the house in experimentation.
- To model and simulate a solar PV microgrid system in both stand-alone and grid-connected mode.
- To carry out optimization analysis and evaluate the solar PV microgrid system's economic viability.

### 1.8    Research Questions

Several questions were prepared to kick-start the idea generation, planning, and execution. The research questions present an overview or guide to the utilization of distributed energy generation resources such as solar in microgrids for urban areas:

⇒ How are electrical loads characterized for large area settlements such as urban areas?

⇒ What are the technological trends of controller capabilities in microgrids?

⇒ How can solar PV generation be integrated within a microgrid?

⇒ Which type of inverter control is best suited for urban solar PV microgrids?

⇒ Are energy storage systems necessary for the optimum operation of solar PV microgrids?

⇒ How is the load-based solar PV system for a typical residential household in Botswana designed and dimensioned?

⇒ What control schemes are necessary for the management of power flow within a microgrid system?

⇒ What are the optimization techniques to improve the performance of microgrids?

⇒ What are the economic ramifications for a design of a solar PV microgrid in communities in Botswana?

1.9    Research work plan
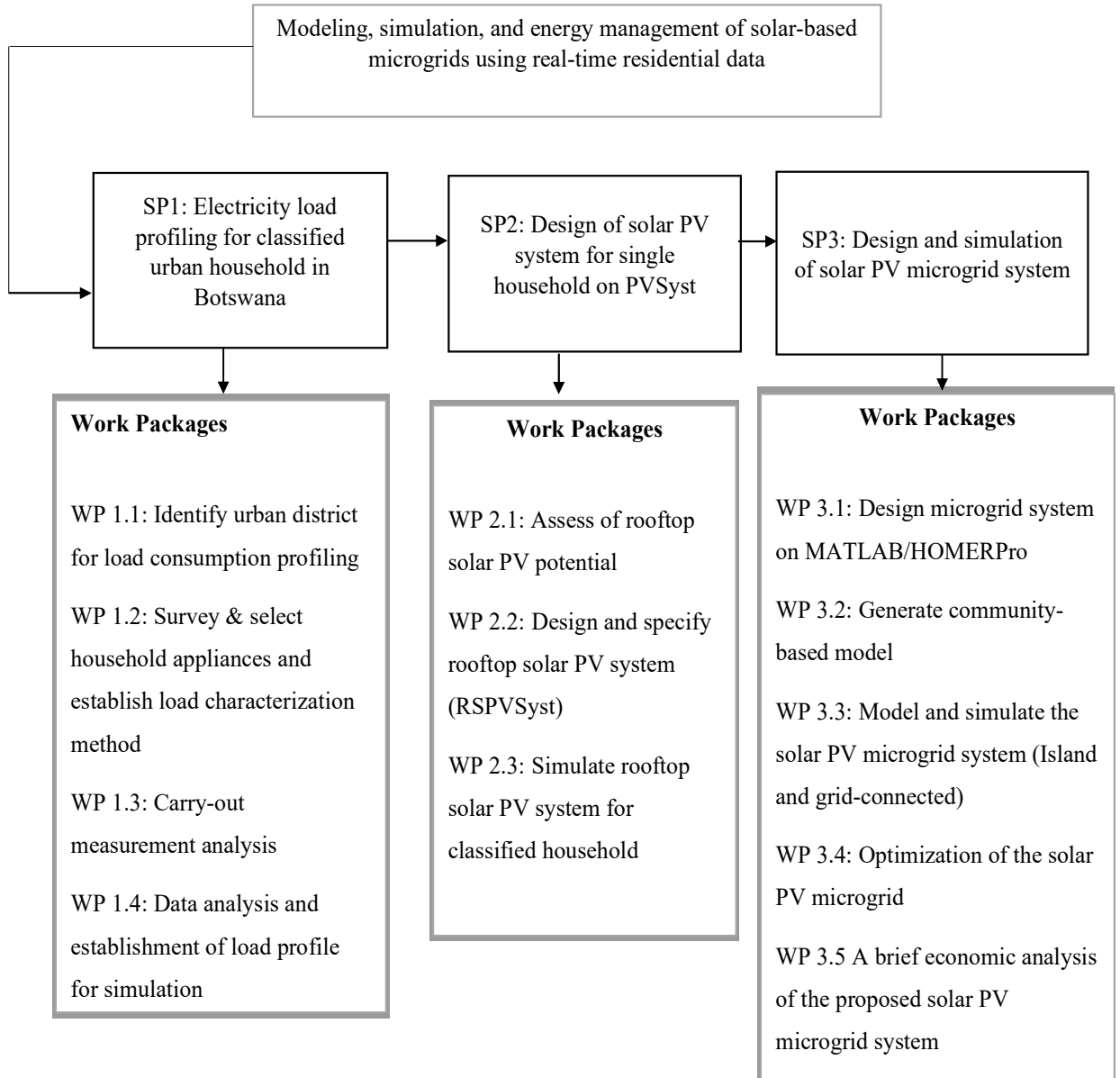


Figure 1.2: Research work plan

The research work plan in Figure 1.2 was divided into three sub-projects and their respective work packages.

    I.     Sub-project 1: Electricity load profiling for classified urban household in Botswana

This part of the research includes activities related to smart meters and the analysis of energy consumption data in a residential household. Smart meters were installed in a residential household for a period of 12 months to record energy consumption. Data analysis techniques were then used to the data collected by smart meters.

    II.    Sub-project 2: Design of solar PV system for single household on PVSyst

Subproject 2 involves using smart meter data analytics to design and size a residential solar PV system. The design and simulation of the solar PV system was performed in the PVSyst simulation environment.

    III.    Sub-project 3: Design and simulation of the solar PV microgrid system

This component of the research involved modeling and simulating the solar PV microgrid using MATLAB and HOMERPro software environments. The MATLAB environment was used for most of the design modeling of the microgrid and its components. Activities such as microgrid design and simulation in both island and grid-connected modes of operation were completed. Simulation in HOMERPro provided the economic analysis of the microgrid system.

### 1.10  Research design and methodology

The author provides an overview of the project's research strategy, technique, methodology, data gathering methods, research process, and restrictions.

### 1.10.1 Research method - Quantitative

A quantitative study will be conducted through energy usage analysis to meet the research objectives. The energy analysis will also be utilized to size a community solar PV microgrid system.

### 1.10.2 Data gathering

The investigation begins with the collection of data from a single residential household. The following methodologies and research procedures will be used to obtain primary data.

i. Observation and questionnaire: gather electrical loads data from house owners in the identified good household in the urban settlement.

ii. Experimentation /Monitoring: the measurement of electrical loads in households and the creation of a load profile.

iii. Interviews through various communication media as well as personal contact.

### 1.10.3 Research Process

Below is a workflow schematic linking the research methods by the sub-projects detailed in the Research work plan. Figure 1.3 provides a schematic description of the research workflow.

Electric Load Profiling
- Questionnaire
- Experimentation (energy load analysis)
- Developing energy load profile

Developing load model for an urban household
- Load modelling using clustering technique
- Modelling load profile for district size

Microgrid modelling and simulation
- Simulate a solar PV system for singular household
- Modelling of a solar driven microgrid system for district

Figure 1.3: Workflow schematic of the research design

The workflow schematic depicted in Figure 1.3 represents the sequential flow of work activities done towards the success of the research. The activities in the load profiling section describe work duties such as questionnaires, smart meter experimentation, and developing daily energy load profiles. The next section of the workflow flowchart involves the development of load models through the analysis of smart metering data. Data analytics techniques include clustering, time series and regression. The smart meter analysis data provides information on the design and size of the community solar photovoltaic microgrid system. Following that, modeling, and simulation analyses of the microgrid system were carried out in a simulation environment.

### 1.11  Project management

### 1.1 Overview

The chapter comprises the authors' planning and works via a timeline to achieve the research objectives.

1.2 Project milestones

Below are the critical project milestones of the research in order of execution:

I.      Research proposal (May 2019 – July 2019)

II.      Literature review (August 2019 – April 2020)

III.      Research methodology design (May 2020 – July 2020)

IV.      Electricity load profiling in a residential household in Botswana (August 2020 – August 2021)

V.      Simulation of solar PV system for a single home in PVSyst (September 2020)

VI.      Smart meter data analytics (August 2021 – September 2021)

VII.      Design and simulation of solar PV microgrid system on MATLAB (May 2021 – September 2021)

VIII.      Simulation of a microgrid on HOMER (September 2021)

IX.      Economic analysis of the microgrid system (September 2021)

## 1.3 Gantt chart

| Project lead: **Tumelo Seane** | | Supervisor: **Professor Ravi Samikannu** Co-supervisor: **Dr Tobias Bader** | |
|---|---|---|---|

| Modeling, simulation, and energy management of solar-based microgrids using real-time residential data | Due Date | Lead | Year 1 (2019) / Year 2 (2020) / Year 3 (2021) |
|---|---|---|---|
| **Sub-Project 1: Electricity load profiling for classified urban household in Botswana** | | | |
| **WP1.1: Identify urban district for load consumption profiling** | | | |
| **Activity 1.1.1:** Determine geographical location of | Aug-19 | Tumelo | |
| **Activity 1.1.2:** Classify urban households according to energy demand, determined installed capacity, occupancy, building type | Sep-19 | Tumelo | |
| **Activity 1.1.3:** Acquire permission for analyses purposes | Nov-19 | Tumelo | |
| **Activity 1.1.4:** Define residential district parameters | Nov-19 | Tumelo | |
| **WP1.2: Survey & selection of household appliances and establishment of load characterization method** | | | |
| **Activity 1.2.1:** Review appliances and electric capacity for smart metering concept for urban household | Sep-19 | Tumelo | |
| **Activity 1.2.2:** Define appliance for example household to be investigated and determine installed capacity | Oct-19 | Tumelo | |
| **Activity 1.2.3:** Review methods of characterizing electricity load profiles | Oct-19 | Tumelo | |
| **Activity 1.2.4:** Evaluate and select aloud characterization method based on the residential arrangement/household classification | Oct-19 | Tumelo | |
| **WP1.3: Carry-out load measurement analysis** | | | |
| **Activity 1.3.1:** Install smart meters in a household | Aug-20 | Tumelo | |
| **Activity 1.3.2:** Record electricity usage and relevant data | Jun-21 | Tumelo | |
| **Activity 1.3.3:** Monitor/Estimate building occupancy | Jun-21 | Tumelo | |
| **Activity 1.3.4:** Continuous analysis of measurement data | Jun-21 | Tumelo | |
| **WP1.4: Data analysis and establishment of load profile for simulation** | | | |
| **Activity 1.4.1:** Interpret analyzed data and correlation | Jul-21 | Tumelo | |
| **Activity 1.4.2:** Deduce load model for classified single | May-21 | Tumelo | |
| **Activity 1.4.3:** Scale load model on the main grid for entire district based on single household model | Mar-20 | Tumelo | |
| **Sub-Project 2: Design of solar PV system for single household on PVSyst** | | | |
| **WP2.1: Assessment of rooftop solar PV potential** | | | |
| **Activity 2.1.1:** Review solar PV potential of urban districts | Feb-20 | Tumelo | |
| **Activity 2.1.2:** Discuss solar PV-system potential based on | Sep-20 | Tumelo | |
| **WP2.2: Simulation of rooftop solar PV system for classified household** | | | |
| **Activity 2.2.1:** Identify solar PV planning method and | Aug-19 | Tumelo | |
| **Activity 2.2.2:** Define system requirements and functionality | Mar-20 | Tumelo | |
| **Activity 2.2.3:** Dimension rooftop PV solar system | May-20 | Tumelo | |
| **Activity 2.2.4:** Dimension system for high efficient appliance portfolio and compare | May-20 | Tumelo | |
| **Activity 2.2.5:** Select system components determine component capacities | May-20 | Tumelo | |
| **WP2.3: Establish electricity load profile for simulation** | | | |
| **Activity 2.3.1:** Prepare simulation environment | Mar-20 | Tumelo | |
| **Activity 2.3.2:** Model rooftop solar PV system in simulation environment | Apr-20 | Tumelo | |
| **Activity 2.3.3:** Define system parameters and profiles | May-20 | Tumelo | |
| **Activity 2.3.4:** Carry-out simulation calculations for the | May-20 | Tumelo | |
| **Activity 2.3.5:** Sensitivity Analysis with parameter variation | Jun-20 | Tumelo | |
| **Activity 2.3.6:** Analyze, interpret and document simulation | Jul-20 | Tumelo | |
| **Sub-Project 3: Design and simulation of solar PV microgrid system** | | | |
| **WP3.1: Define RSPVSyst on District System Level** | | | |
| **Activity 3.1.1:** Design and define system functionality | Feb-20 | Tumelo | |
| **Activity 3.1.2:** Define system objectives | Mar-20 | Tumelo | |
| **Activity 3.1.3:** Carry-out system sizing based on simulation load profiles of selected households | May-20 | Tumelo | |
| **WP3.2: Generate community-based model** | | | |
| **Activity 3.2.1:** Generate occupant behavior model based clustering method | Mar-21 | Tumelo | |
| **Activity 3.2.2:** Generate building energy demand model | Feb-21 | Tumelo | |
| **Activity 3.2.3:** Summarize the district energy flow | Apr-21 | Tumelo | |
| **WP3.3: Model and simulate the solar PV microgrid system (Island and grid-connected) Level** | | | |
| **Activity 3.3.1:** Prepare simulation environment | Aug-21 | Tumelo | |
| **Activity 3.3.2:** Model district load in simulation | Oct-21 | Tumelo | |
| **Activity 3.3.3:** Model rooftop solar PV system in simulation environment | Sep-21 | Tumelo | |
| **Activity 3.3.4:** Define system parameters and profiles | Aug-21 | Tumelo | |
| **Activity 3.3.5:** Carry-out simulation calculations for the RSPVSyst | Aug-21 | Tumelo | |
| **Activity 3.3.6:** Sensitivity Analysis with parameter variation | Jul-21 | Tumelo | |
| **Activity 3.3.7:** Analyze, interpret and document simulation results for RSPVSyst | Aug-21 | Tumelo | |
| **Activity 3.3.8:** Determine RSPVSyst size of system on District System Level | Aug-21 | Tumelo | |
| **WP3.4: Optimization of the solar PV microgrid** | | | |
| **Activity 3.4.1:** Establishment of fuzzy logic control inputs | Sep-21 | Tumelo | |
| **Activity 3.4.2:** Establish the set of rules for the FLC | Sep-21 | Tumelo | |
| **Activity 3.4.3:** Analysis of the FLC optimization results | Sep-21 | Tumelo | |
| **Activity 3.4.3:** Summary of the integration of the FLC optimization | Sep-21 | Tumelo | |
| **WP3.5: A brief economic analysis of the proposed solar PV microgrid system** | | | |
| **Activity 3.4.1:** Input the proposed microgrid design into HOMERPro | Octoer 20 | Tumelo | |
| **Activity 3.4.2:** Sensitive analysis simulation of the proposed microgrid | Oct-21 | Tumelo | |
| **Activity 3.4.3:** Analysis of the HOMERPro economic overview | Oct-21 | Tumelo | |
| **Activity 3.4.3:** Recommend further research, discuss challenges and limitations of the model | Oct-21 | Tumelo | |

Figure 1.4: Gantt chart for the research

1.4  Budget

Table 1.1: Proposed budget for the research project

| Item | Estimated Cost |
|---|---|
| 6.1 Labor related Costs *(specify)* | P 0 |
| 6.2 Consumables (General Expenses) *(specify)*<br>- Trip 1: Refreshments and water during a visit to BHC Gaborone<br>- Trip 2: Refreshments and water during a visit to the Ministry of Lands & Housing | P 200<br><br>P 200 |
| 6.3 Travel (Internal & External) (*specify, if applicable*)<br>- Day Trip 1: Botswana Housing Corporation (BHC) Gaborone<br>- Day Trip 2: Ministry of Land & Housing, Gaborone<br>- Flight expenses to Dubai, United Arab Emirates (Round trip)<br>- Accommodation expenses in Dubai ( P 700/night) – 2 nights | P 250<br>P 250<br>P 7 000<br>P 1 400 |
| 6.4 Workshops & Conference Expenses *(not more than 15% of total cost)*<br>- ICMRES 2021: 15. International Conference on Microgrids and Renewable Energy Systems. January 28-29, 2021<br>Dubai, United Arab Emirates | Registration<br><br>(P 3 400) |
| 6.5 Equipment/Asset Expenditure *(specify)*<br><br>- iCarbon Energy Management package x2: To be used for energy analysis in residential home | P 17 200 |
| **TOTAL** | P 29 900 |

### 1.5  Communication

- o  Meetings with supervisor and co-supervisor once a week
- o  Email
- o  Instant Messaging

### 1.6 Support staff

The primary work of the research will be undertaken by the author specifically with the assistance of Supervisor Professor Ravi Samikannu and previous supervisor Dr. Tobias Bader.  The Faculty of Engineering and Technology will assist with software tools and packages. The services provided by the library, such as e-learning the school offers, also have played an instrumental role in the research. In addition, the internet through search engines such as Google Scholar and SciVal assisted in the study.

### 1.7 Conclusion

This chapter details all the activities planned for the success of the research project. It details the objectives and scope of the research project.

## 2    CHAPTER 2: LITERATURE REVIEW

### 2.1    Overview

A literature assessment of the structure and functioning of solar PV microgrids is presented in this chapter. It contains an overview of the individual components and the control strategies utilized for power management flow within the microgrid system. It concludes with the challenges and future work on solar PV-based microgrid systems.

### 2.2    Introduction

Microgrids are characterized as small to medium-scale solutions that include Distributed Generation (DG), electrical loads, control, and energy management components (Ustun, Ozansoy, and Zayegh 2011). Renewable and nonrenewable energy resources are used in DG units. Integrating Renewable Energy Resources (RES), such as solar energy, in microgrids promotes environmental sustainability by producing minimal carbon emissions (Basak et al. 2012; F. Wang, Zhu, and Yan 2018). Community solar microgrids are described as ten or more residential households alongside the local businesses to attain the microgrid system's affordability and resilience traits (Qazi 2017). Community microgrids in cities have been reported in the literature to make electricity more affordable to individual customers through the shared usage of RES (Palaniappan et al. 2017). The affordability of solar PV systems has made renewable energy resources more appealing to integration in microgrid systems. The decrease in solar PV module costs is based on technological improvement, and authors' (Mayer et al. 2015) forecast that PV module costs will fall from USD 0.61 per Wp to USD 0.16 per Wp between 2015 and 2050. Solar energy is an intermittent energy source, and thereby remote microgrid systems are equipped with Energy Storage Systems (ESS), which keeps the flow of electricity to power consumers uninterrupted. A control and energy management strategy accomplishes the communication between the components of a microgrid system. Some of the control schemes for microgrid systems include hierarchical and droop control (Meng et al. 2016; Planas et al. 2013; Tayab et al. 2017).

### 2.3    Microgrid architecture

A microgrid is defined as an electrically bounded section of the transmission distribution network that brings together local distributed generation sources, energy storage devices, and regulated electrical loads to produce a self-sufficient energy system (Cagnano, Tuglie, and Mancarella 2020). A microgrid system comprises three major sections; generation, loads, and controls, and these three operate inside a specialized regulated structure in conjunction with the utility grid (Donahue 2019). The Point of Common Coupling (PCC) is a transformer feature that connects the microgrid to the primary grid.

### 2.3.1    Microgrid topology

Three types of microgrid topologies may be identified based on the operating frequency of power generation (Hossain et al. 2019).

#### 2.3.1.1   DC Microgrid System

DC microgrids are characterized by low to medium-voltage DC distribution networks. A DC transmission bus line connects DG units with DC power output to the other components of the microgrid (Fusheng, Ruisheng, and Fengquan 2016). The inception of low voltage DC microgrids is increasingly more common when the bulk of the load demand is from receptive electronic devices (Salomonsson, Söder, and Sannino 2009). Microgrid systems with medium voltage direct current (MVDC) are frequently used for heavy industrial loads that support offshore oil and gas drilling (Kounev et al. 2014; Reed et al. 2012). A DC-DC converter is utilized to regulate the DC voltage output of a solar PV system. Because some electrical appliances are powered by an AC power supply, a DC/AC converter is necessary for the system depicted in Figure 2.1 (Justo et al. 2013). The ESS will store any excess power in the DC bus line. Figure 2.1 shows a typical microgrid system structure.
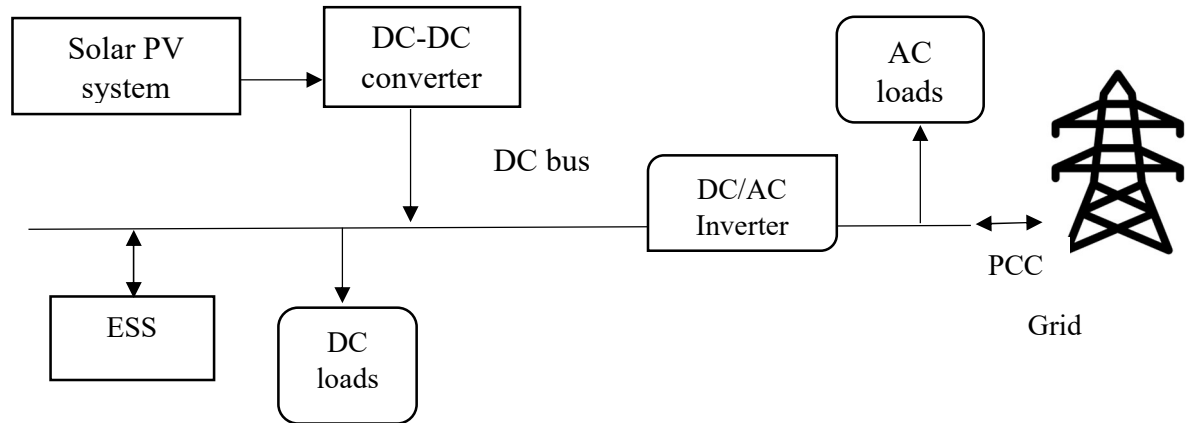
Figure 2.1: A microgrid system with both DC and AC loads. (Justo et al. 2013)

Because of the absence of converter requirements, DC microgrid systems are preferable over AC microgrid systems. Because energy losses occur at each conversion phase, the AC microgrid system has more energy losses than the DC microgrid system (Hossain et al. 2019; Shuai et al. 2018).

### 2.3.1.2   AC Microgrid System

A Low to Medium Voltage AC transmission network is part of an AC Microgrid system (LVAC). DG units that produce AC power link directly to the transmission line, whereas DG units with DC power are connected to the transmission line through a DC/AC converter(Hossain et al. 2019; Justo et al. 2013). DG units for the AC microgrid system include wave turbines, hydropower, and wind energy conversion system (WECS) (Baran and Mahajan 2003). AC/DC inverters convert AC power to a DC source to power DC and ESS loads. The use of an AC/DC inverter presents several issues, including infringement protection, communication, and microgrid operation (Phurailatpam, Rajpurohit, and Pindoriya 2011).

### 2.3.1.3   Hybrid AC/DC microgrid systems

Various AC and DC energy sources and multiple loads are connected to the corresponding AC and DC networks in a hybrid AC/DC microgrid system setup (Liu, Wang, and Loh 2011). The bidirectional inverter serves the role of facilitating the power supply between both buses as per the energy requirements of the microgrid system (Jain and Raju 2013). System components such as the ESS and DC loads communicate over the system's DC bus to facilitate power delivery. The hybrid system can achieve low conversion losses because the microgrid's separate components are individually linked to their power sources. (Hasan and Arif 2018). Figure 2.2 depicts the configuration of a hybrid AC/DC microgrid system.
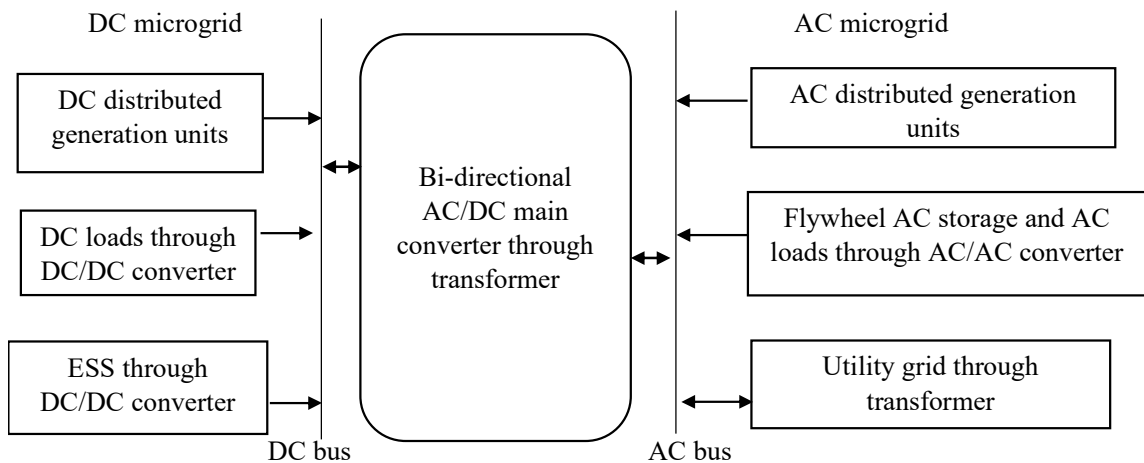
Figure 2.2: Structure of a hybrid AC/DC microgrid system (Jain and Raju 2013)

### 2.3.2 Community solar microgrids

Community solar microgrids can be found in either urban or remote settings. The creation of community solar microgrids in urban regions has more significant advantages than in remote areas due to the numerous benefits derived from energy exchanges with the utility grid (Faure et al. 2017). Benefits of grid-connected microgrids include improved power quality and reduced transmission power losses, thereby improving system finances (Da Marcello et al. 2017). In addition, urban microgrid systems serve as a foundation for smart grid technologies such as monitoring and control, essential for improving the electrical power grid's reliability (Howell et al. 2017). According to a 2017 survey conducted by the Italian Agency for New Technologies, Energy, and Sustainable Economic Development (ENEA), over 70 operational microgrid systems are established in urban areas worldwide (Faure et al. 2017). Load management is crucial in prioritizing load power-sharing between critical and low-priority loads. Power-sharing and self-sufficiency are two notable characteristics of community solar microgrids in urban areas.

### 2.3.2.1 Power-sharing

Power-sharing in a microgrid system allows individual customers in a community solar microgrid to utilize power from the solar PV system, thus saving money from their monthly electricity bill purchases (Palaniappan et al. 2017). Customers in a community solar microgrid may include local businesses, schools, hospitals, and residential households. For example, in Boston, Massachusetts (USA), several solar community microgrids are divided by district zones in the city. The community solar microgrids have been set up in locations with critical loads found in hospitals, emergency housing, and supermarkets, improving the utility grid network. The community solar microgrid establishment resulted in cost savings between $692 and $180,000 annually for the customers in Boston (Morgan et al. 2016). A campus community solar microgrid study by (Gašparović et al. 2016) investigated two microgrid community cases at the University of Split (Croatia) to identify optimum scenarios for the economic share of electrical loads in the settlement. The results from the study revealed that electricity purchases from the

national electricity grid were offset by 17% through the campus microgrid system. Another example of power-sharing among residential households in an urban microgrid system is reported in a DC community solar microgrid in the city of Wisconsin, Milwaukee. The DC community microgrid is made up of nine homes that are linked by a 380 Vdc transmission line. A solar PV system as the main DG unit, a Home Energy Management System (HEMS), and a Microgrid Energy Management System make up the microgrid system. Customers in the community solar microgrid take advantage of the HEMS and MEMS service platforms that are linked to the internet cloud to maximize cost reductions in their households (Palaniappan et al. 2017). Smart peak shaving in an urban community network through Demand Side Management (DSM) enables customers to make significant cost savings in their annual electricity purchases from the electric utility grid (Faure et al. 2017).

### 2.3.2.2   Self-sufficiency

The ability to detach from the utility grid and function in an island mode is another feature of urban microgrids. The microgrid system can operate in the island mode, such as a power outage or when the DG unit can provide exclusively continuous power to the electrical loads without support from the utility grid. According to (Wanitschke, Pieniak, and Schaller 2017), "Time-based autarky is defined as the degree of self-sufficiency of the microgrid as assessed by the total duration during which no power is taken or fed into the overlying energy grid-level." A key aspect of self-sufficiency in a microgrid system is the availability of an ESS. Examples of urban microgrid systems reported in the literature are listed in Table 2.1.

Table 2.1: Examples of urban microgrid systems

| Components | DG units' capacity | Performance |
|---|---|---|
| Hybrid microgrid for residential application (Bifaretti et al. 2017) | Solar PV: 3 $kW_p$, PEM fuel cell: 1.2 kW Battery capacity:8 kWh Maximum electronic load: 5 kW | The fuel cell, with grid assistance, was able to meet load surges in the early morning and late afternoon. The simulations show a maximum solar PV output of 1.5 kW between 11 a.m. and 2 p.m., with extra electricity sent into the grid. |
| Grid-connected microgrid system (Da Marcello et al. 2017) | Solar PV: 11.76 kW  Fuel cell: 10 kW,  Battery: 500Ah | During island mode, the battery meets the energy demands of the load from the grid. Once the grid is restored, the battery is charged within 4 seconds. |
| Campus University microgrid system (Borer 2013) | Gas turbine generator: 15 MW Solar PV: 4.5 $MW_p$ | The maximum gas-turbine power and solar PV generation recorded every day were 16 MW and 4 MW, respectively. |
| Grid-connected residential solar PV with battery backup. (Saxena et al. 2017) | Planned solar PV power: 5 kW | Simulation results reveal a 3 kW peak power at 700 $W/m^2$ and 4.4 kW peak power at 1000 $W/m^2$. |

2.4    Solar PV microgrids modeling and simulation

This chapter goes through the components used to simulate solar PV microgrids in both grid-connected and island modes of operation. DC/DC converter, inverter, solar PV modules, ESS, and electrical loads are all components of solar PV microgrids. The review encapsulates the developed solar PV modules and their performance under various software environments. The DC/DC converter performs the function of converting the DC voltage source to another DC voltage source of a different magnitude. The DC/AC inverter converts a DC voltage source to an AC voltage source and synchronizes the AC output to the utility grid (Yang et al. 2019). The usage of an inverter in a microgrid system results in drawbacks such as harmonics and voltage imbalances, to mention a few. The inverters are equipped with Pulse Width Modulation (PWM) to maintain stability in the output waveforms. An ESS is required to ensure the efficient operation of a solar PV microgrid by reducing the intermittent and variable solar PV production (D. W. Gao 2015a). There are two types of ESS designs for community solar microgrids: aggregate and distribution.  The use of a Battery Energy Storage System (BESS), a kind of ESS, in community solar microgrid systems has been widely described in the literature. Of the various BESS models, the lithium-ion battery models have displayed a higher efficiency than lead-acid and nickel-cadmium battery models (Breeze 2018; Kularatna 2015; Vetter and Rohr 2014).

2.4.1    Modeling of solar PV modules

A solar PV module is made up of several PV cells that are joined together. A solar PV array comprises modules connected in series or parallel (Villalva, Gazoli, and Filho 2009). A typical solar cell model is illustrated in Figure 2.3 as a single diode model that represents an ideal PV cell's equivalent circuit (Adhikari and Li 2014). The concept of a practical single solar cell is shown in Figure 2.3.
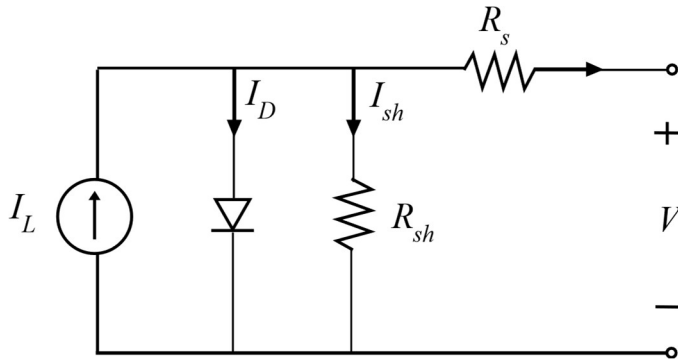
Figure 2.3: Design of a solar cell using an equivalent circuit (Adhikari and Li 2014)

$R_s$ represents the series resistance in the circuit diagram above, whereas $R_{sh}$ represents the shunt resistance, which has an inverse relationship with the leakage current. The diode current and shunt leakage current, respectively, are represented by $I_D$ and $I_{sh}$ (Prakash and Singh 2016). MATLAB/Simulink, Personal Simulation Program with Integrated Circuit Emphasis (PSpice), and PSCAD, to name a few, have all been used to create and integrate various solar PV modules (Ahlawat, Gupta, and Gupta 2017; Nguyen and Nguyen 2015). The Simscape toolbox in the MATLAB/Simulink environment provides a constructed solar PV module designed according to Equation 3.16. The model's principal characteristic is that it is easy to use and utilizes simulations to determine the PV module's radiation and temperature (Khalil and Ateea 2015). The PSpice software environment now contains PV modules created using a single PV cell and allows for PV module analysis by running simulations under various partially shadowed circumstances (PSC). The PSpice environment enables performance study for a PV module under PSC by adjusting the current source (Jiang et al. 2011). Table 2.2 summarizes the PV array modules produced in various software environments. It captures the performance of several PV module kinds and designs at different temperatures and irradiation levels. Table 2.2 represents various PV array model designs in different software environments.

Table 2.2: Solar PV array models performance

| Solar PV module type | Capacity | Performance |
|---|---|---|
| **Single diode model (SDM) in MATLAB/Simulink** (Dey et al. 2016) | 50 Wp solar module performance under various irradiance and temperature values | The simulation shows that the solar PV module generated a 46 W peak at 15º C. Still, it developed a peak of 46 W at 35º C, thereby revealing that the PV module performance does not positively correlate with temperature. |
| **Hybrid model on MATLAB/ PSpice environment** (Jiang et al. 2011) | The solar cell at irradiance values (0.4 $kW/m^2$ – 1.0 $kW/m^2$) in increments of 0.2 $kW/m^2$ | The solar PV module hybrid model produced 70 Wp under uniform shaded conditions (USC) and 76 Wp under partially shaded conditions (PSC). |
| **Multi-dimension diode PV module on the MATLAB/Simulink environment** (Soon and Low 2015) | Solar PV module under STC | When compared to the SDM, utilizing the double-diode model (DDM) enhances modeling accuracy. The proposed model simulation findings allow for the addition of diodes in series without impacting PV peak generation. |
| **Comparison of DDM (Model 1), iterative Newton-Raphson model (model 2), and proposed model (model 3) on MATLAB** (Bhuvaneswari and Annamalai 2011) | Solar PV module with capacity 50 Wp under STC | The PV curves of the three models under real-world testing settings (500 kW/m2) delivered model 1 and model with the highest peak power of 25 Wp, while model 2 produced 23 Wp. |

### 2.4.2   Battery Energy Storage System (BESS) modeling

The BESS is responsible for reducing power supply variability between electrical loads and generation units (Abdi, Mohammadi-ivatloo, and Javadi 2017; Alzahrani et al. 2017; D. W. Gao 2015a). A BESS is vital for urban microgrid systems to provide power to loads during the island mode. A BESS is required for urban microgrid systems to provide electricity to loads during the island mode. The BESS communicates with the DC/DC converter, DC/AC inverter, DC link capacitor, and the community solar PV microgrid system (Farrokhabadi et al. 2018). The buck-boost converter is a DC/DC converter topology utilized for urban microgrids to enable the charge and discharge of the BESS (Farrokhabadi et al. 2018; D. W. Gao 2015b; Nisha Kondrath 2018). The ESS can operate as the electrical load or generator through charging and discharging. ESS configurations exist in two states, namely distributed and aggregated ESS. When compared to distributed ESS, aggregated ESS is better suitable for microgrids because it efficiently suppresses power fluctuation in the microgrid system (D. W. Gao 2015a; Kook et al. 2006; Li and Joós 2007). The BESS manages energy in the microgrid system by performing load leveling and peak load shifting (Xia et al. 2015). Local voltage support, grid contingency assistance, and load shifting are ancillary services that the ESS provides to the microgrid system. (Farrokhabadi et al. 2018). The BESS models utilize the commonly established electrochemical batteries or regulated voltage sources (Tremblay, Dessaint, and Dekkiche 2007). BESS models can respond to the control system instructions and activate the reserve in approximately 20 milliseconds (Adrees, Andami, and Milanovic 2016). BESS capacity and lifetime are affected by variables such as depth of discharge (DOD), rate of discharge, and temperature. Equation 2.1 illustrates the capacity of a battery expression (Alzahrani et al. 2017):

$$B_{capacity} = \frac{E_{load} \, * \, D_{off}}{DOD_{max} \, * \, n_{temp}} \qquad\qquad 2.1$$

$E_{load}$ is the load supplied to the microgrid system during periods of low electrical power supply by the DG unit in ampere-hours, $D_{off}$ is the number of days the microgrid is

operating in island mode, $DOD_{max}$ is the depth of discharge at maximum level and $n_{temp}$ represents the temperature correction factor. Lithium-ion batteries are the most commonly used battery type for community solar PV microgrids because of their unique characteristics, including high energy density, low weight, and long life duration (Breeze 2018; Kularatna 2015). Table 2.3 presents an overview of the battery types and applications reported in the literature.

Table 2.3: Overview of BESS models

| Applications | Battery types | Overview |
|---|---|---|
| **Grid-connected solar PV system with battery support for residential usage in Dymola software environment** (Vetter and Rohr 2014) | Performance comparison of lead-acid battery with a lithium-ion battery <br><br> Battery capacity: 6.3 kWh | According to the simulation results, replacing a lead-acid battery with a lithium-ion battery improves functional capacity by up to 90%. |
| **Residential battery storage connected to the grid** (Bila, Opathella, and Venkatesh 2016) | Lithium-ion battery (3.88 kWh) <br><br> 75 Ah | The battery's cycle efficiency for charging and discharging is 91 percent and 87.5 percent, respectively. |
| **Modeling design of off-grid microgrid system** (Moncecchi et al. 2018) | Comparison of lead-acid and lithium-ion battery (94.5 kWh and 49.1 kWh) | The simulation cost analysis of the two batteries showed that the lead-acid batteries were replaced three times throughout the study period. In contrast, the lithium-ion battery was replaced just once. |

Lithium-ion batteries are commonly used in solar community solar microgrids because they have an 80% Depth of Discharge (DoD) compared to lead-acid batteries' 50% DoD (Vetter and Rohr 2014).

### 2.4.3    Inverter modeling

Energy conversion is required for a microgrid system to allow power flow exchanges between individual components (Shintre and Mulla 2016). In terms of power supply, inverters are divided into current source inverters (CSI) and voltage source inverters (VSIs). A VSI and CSI circuits are classified based on their DC input type, either voltage source or current source(D. W. Gao 2015b; D. Z. Gao and Sun 2016). Three-phase VSI features three inverter legs and is typically used in medium to high power (>5 kW). (Kharjule 2015; Siwakoti, Forouzesh, and Pham 2018). The inverter is designed with three half-bridge inverters that are coupled in a parallel manner. The three inverters have a 120-degree phase difference, and their combination produces a three-phase voltage source (Manias 2017). The power transfers between microgrid systems and the utility grid via a bidirectional inverter/rectifier are dictated by the microgrid system's power requirements (Debela, Ensermu, and Bhattacharya 2017).  A solar PV-BES microgrid system can integrate a multifunctional VSI to regulate the waveforms of parameters such as voltage, harmonic content, and frequency (Narayanan, Seema, and Singh 2018). The current and voltage waveforms of harmonics are characterized by distortion and divergence from sinusoidal output waveforms (Gray and Morsi 2015). Control and modulation techniques are used to ensure proper inverter operation and to eliminate harmonics in the system.

Techniques like the PWM and stepped-wave inverter are used to control three-phase VSI. Because of its capacity to work at lower frequencies, PWM is the most widely used technique for suppressing harmonics in machines with a history of more than fifty years (Aguilera et al. 2018). The amplitude output voltage of the VSI can be controlled using PWM inverters. The inverter undergoes multiple switching at a steady DC input voltage, and the inverter obtains fewer harmonics (Kim 2017). Single PWM, Multiple PWM, and Sinusoidal Pulse Width Modulation (SPWM) are the three most prevalent control mechanisms for PWM inverters. Because of its apparent use in industrial applications, the SPWM is the most commonly utilized modulation (Kim 2017). Every half cycle, there is one pulse for single PWM control. By altering the width of the single pulse, the voltage generated can be changed (Aguilera et al. 2018; Kharjule 2015).

2.4.3.1   SPWM Inverter

The SPWM approach can modulate voltage for each cycle (Kim 2017). The technique generates many pulses for each half-cycle. The duration of each pulse varies as per the sine wave scale. The sinusoidal waveform is created by comparing two waveforms: a triangle wave (carrier wave) and a control wave (control wave) (sinusoidal). The high-frequency carrier signal ($v_c$) and the sinusoidal AC voltage reference signal ($v_{ref}$) pass via a comparison device. The intersection of the two movements indicates the inverter's switching states (D. Z. Gao and Sun 2016; Manias 2017). Figure 2.4  depicts the operation of the SPWM technique.
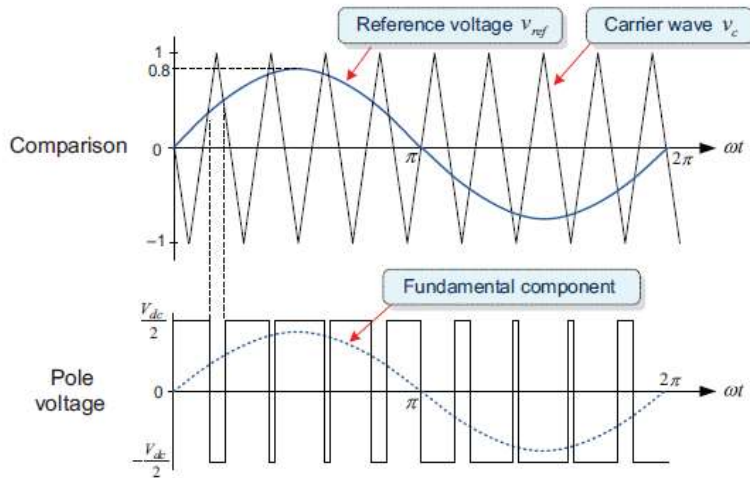


Figure 2.4: Operation of the SPWM technique  (Kim 2017)

It is visible that when $v_{ref} > v_c$, the pole voltage ($V_{dc}/2$) is at its maximum, and when $v_{ref} < v_c$, the pole voltage is at its minimum ($-V_{dc}/2$). Linear modulation can only be achieved when the amplitude of $v_{ref}$ remains below the peak of the $v_c$ i.e., $v_{ref} \leq V_{dc}/2$ (Aguilera et al. 2018). Changing the modulation waveform allows you to control the amplitude and frequency of the output. The modulation index MI denotes the relationship between the carrier and modulating waves (Equation 2.2).

$$MI = \frac{v_{ref}}{V_{dc}/2} \qquad\qquad 2.2$$

The linear modulation index range ($MI$) is between 0 and 1 when $v_{ref} \leq V_{dc}/2$ (Kim 2017). The inverter can generate an output voltage that is proportionate to the reference voltage (Kharjule 2015). Grid-forming and grid-following inverters are two types of inverters used in electricity systems. Grid-forming inverters can operate as voltage sources to lower output impedance in output voltage waveforms because of their design (Ashabani and Mohamed 2014). Grid-feeding/following inverters serve as current sources to control the output current waveforms' impedance (Unruh et al. 2020).

Table 2.4 presents the developed inverter models and their applications.

Table 2.4: Inverter models

| Inverter type | Usage | Overview |
|---|---|---|
| Grid forming converter (GFC) in an island AC microgrid system (E Silva, Luiz, and De Matos 2014) | Reduction of the energy generated in the microgrid system to safeguard the ESS | By switching the GFC frequency, the battery bank voltage was maintained at 280 V as the generation gradually decreased. |
| Bi-directional converters in a hybrid microgrid system (Debela, Ensermu, and Bhattacharya 2017) | Energy management in the microgrid system | The employment of the SPWM inverter resulted in a 300 V peak on the AC power supply, resulting in conversion efficiency of 95% in steady-state. |
| Parallel converters in an autonomous microgrid system (Vazquez et al. 2012) | Estimation of the correct number of inverters for improving power output. | The predicted three inverters could deliver 110V at a frequency of 60 Hz by balancing current and regulating the output voltage. |
| Hybrid current-controlled VSI and voltage-controlled VSI in an autonomous microgrid (Ashabani and Mohamed 2014). | Usage of controlled droop method to enable the smart power distribution in the microgrid. | (a) Grid-connected: Models A (current-dropping voltage-controlled VSI) and C (power-dropping voltage-controlled VSI) gave reaction times of 0.07 sec and 1.0 sec, respectively, indicating the system's capacity to monitor grid frequencies without Phase-Locked Loop (PLL) to synchronous machines. (b) Models A and C had a power-sharing and current-sharing inaccuracy of 0.5 percent and 1.0 percent, respectively, when connected to an island. |
| Multi-level inverter for solar PV-based grid-connected inverter (Sarwar and Asghar 2011). | Improvement of the wave shape and reduction of the total harmonic distortion (THD) in output voltage waveforms. | THD was reduced by changing the switching angles of the multi-winding transformer. The THD measured at $110^{\circ}$ was 22.9 percent, whereas the THD recorded at $125^{\circ}$ was roughly 32 percent. |
| Parallel-connected single-phase PV-based inverter (Kulkarni and Nehete 2014). | Comparison of the simulated and measured output voltage of the inverter with a 500 W resistive load. | The output voltage discrepancy between the simulated and measured values was about 6%, with the system's THD reported at 1.25 percent. |

### 2.4.4   Electrical load modeling

A load profile depicts energy use behavior in a residential household (Ihbal, Rajamani, and Jalboub 2011). The electrical loads of different residential families can be grouped to reflect a community's or district's profile. Due to many elements such as weather and dynamic human behaviors, creating load models is a massive undertaking. According to the authors, load models can be created by utilizing a constant electric impedance (Alzahrani et al. 2017). Load modeling aims to develop simple mathematical models that approximate load behavior (Arif et al. 2018). The objective of load modeling is to establish simple math modeling to approximate load conduct. Static and dynamic load models are the two types of load models. Due to the nature of modeling loads, the electrical loads in a residential house may be represented as static loads, as most of them do not exhibit highly non-linear behavior. A standard load modeling approach is measurement-based load modeling, which accumulates load data from data collection devices to generate load characteristics (Arif et al. 2018; M. Jin, Renmu, and Hill 2006). Component-based load modeling is another load modeling technique that derives energy information by evaluating the electrical load's composition (Ju et al. 2018). Residential electrical loads are aggregated using component-based load models. The household features in a residential household are inferred using energy usage data from smart meters (Fahim and Sillitti 2019). User behavior traits are represented by energy usage patterns (Collin et al. 2014; Mcloughlin, Duffy, and Conlon 2015). Authors (Labeeuw and Deconinck 2016) present a load model that generates load profiles using the clustering characterization technique. Clustering characterization is an independent technique for detecting various energy usage trends in large groups of residential users (L. Jin et al. 2017). Authors (Tang et al. 2019) present a data-driven online aggregated load modeling approach to mimic the load of aggregated users.

### 2.4.4.1   Static load models

Static load models depict active and reactive power in a microgrid system as a function of voltage and frequency fluctuations (Arif et al. 2018; EL-Shimy et al. 2018). The Zero-Inflated Poisson (ZIP), exponential, and frequency-dependent models are some of the static load models developed. Among the many literature studies for measuring the static characteristics of electrical loads, the ZIP model is the most extensively utilized (Arif et al. 2018; Gu, Ai, and Wu 2005). The ZIP load model for active and reactive power is mathematically represented by Equation 2.3 and Equation 2.4.

$$\frac{P}{P_o} = [P_1 (\frac{V}{V_0})^2 + P_2 \frac{V}{V_o} + Q_3 ] \, ( 1 + L_{DP} \, \Delta f) \qquad \qquad 2.3$$

$$\frac{Q}{Q_o} = [Q_1 (\frac{V}{V_o})^2 + Q_2 \frac{V}{V_o} + Q_3 ] \, ( 1 + L_{DQ} \, \Delta f ) \qquad \qquad 2.4$$

The active and reactive power absorbed by the static load is represented by $P$ and $Q$, respectively, $V$ is the terminal voltage of the electrical load, $P_1$ ,$P_2$, $P_3$ and $Q_1$, $Q_2$, $Q_3$ indicate the voltage-dependent active and reactive power coefficients, respectively. Where $L_{DP}$ stands for frequency-dependent active power coefficients, $L_{DQ}$ stands for frequency-dependent reactive power coefficients, $\Delta f$ stands for frequency variation, and subscript $o$ stands for standard value.

### 2.4.4.2   Dynamic models

The active and reactive powers in a microgrid system are represented as a function of voltage and time in dynamic load models (Arif et al. 2018). The exponential dynamic load model is a dynamic model for a residential dwelling (Yamashita et al. 2012). The induction motor (IM) model is distinguished by its time-based reaction to a voltage variation. The IM model is used for transient simulations due to the fast-changing nature

of dynamic loads (Abdelsalam et al. 2014; Yamashita et al. 2012). Table 2.5 shows a list of common electrical load components.

Table 2.5: Modeling of load components

| Electrical Load component | Model composition | Simulation results |
|---|---|---|
| (a) **Incandescent model** <br> (b) **Induction cooker model** (Zhao et al. 2010) | (a) Hybrid constant impedance and current model (ZI) and stable impedance model (Z) <br><br> (b) I model and ZI model | (a) The ZI model accurately reflected the measurement curve. However, the Z model did not. <br> (b) The I model could replicate the fluorescent active power's static properties. <br> (c) The I and Z models could represent the induction cooker's active and reactive power characteristics, respectively. |
| **A 22 kilovolts electrical substation** (Carneiro et al. 2017) | An exponential model and ZIP model | The simulation findings of the ZIP and exponential models were similar to the observed values of active power. However, the ZIP model did not appropriately represent values that were similar to the experimental reactive power. |
| **Modern household appliances test in a laboratory** (Bokhari et al. 2014) | Identification of ZIP load parameters through varying the voltage of the individual appliances | The experiment results show that current instruments are injected with a power correction factor, allowing the formulation of a precise ZIP load model compared to measured power levels. |

### 2.4.5    Challenges of solar community microgrids

The three modes of operation for community microgrids provide technological problems when integrating solar PV as DG units. The difficulties encountered by solar community microgrids in urban areas are particularly pronounced when operating during on-grid states (Hossain et al. 2019; Qazi 2017). Through islanding, a balance between the generation and load must be kept to avoid faults in distribution transmission lines, which can be harmful to the individual components in the microgrid system (Faure et al. 2017). The technical challenges of microgrids include control, protection, and re-synchronization, to mention a few.

### 2.4.5.1    Microgrid stability

Grid-connected microgrids are more prone to instability issues than island microgrids due to voltage and frequency synchronization with the primary utility grid. Conventional power stations in SSA are unidirectional, making them vulnerable to malfunctions resulting in power outages (Sampath, Prasad, and Samikannu 2018). As a result, improved control systems are necessary for the SSA area to ensure the integration of microgrids with utility grids. The link of the solar microgrids with the utility grid necessitates a control technique to avoid system voltage and frequency deviations from their setpoints (Kumar and Ravikumar 2016; Sivarasu, Chandira Sekaran, and Karthik 2015).

### 2.4.5.2    Protection

Analysis of the direction and amplitude of current flow in the system is complicated when micro-sources are integrated with a unidirectional power network. Because solar PV is a weather-dependent RET, it generates intermittent electricity throughout the day (Mariam, Basu, and Conlon 2016). Because the fault current path fluctuates depending on fault location, the unpredictability in current flow in the system causes protection devices in networks to malfunction (Hossain et al. 2019; Miveh et al. 2012). Authors (Salomonsson,

Söder, and Sannino 2009) propose a low-voltage DC microgrid safety system that combines fuses and circuit breakers to detach faults and minimize the impact of interruptions quickly. Control systems that can regulate and monitor energy flow while also protecting microgrid components are heavily reliant on the use of both grid-connected and island microgrids(Hasan and Arif 2018).

### 2.4.6   Future of solar community microgrids

The global expansion growth of solar microgrids has improved due to the inception of techniques and methods that alleviate the intermittency issue of solar as an energy source (Qazi 2017). Various solar microgrid systems utilize an additional DG unit or an ESS to maintain the power balance supply in the microgrid system. A rapidly rising technique used in the optimization of a microgrid is machine learning. Machine learning through linear programming, effective energy management within the microgrid is accomplished through the scheduled economic dispatch and unit commitments of the microgrid components (Shrivastwa et al. 2019). Optimization models such as DER-CAM have been utilized to encompass mixed-integer linear programming (MILP) for microgrids with various energy types. Authors (Mashayekh et al. 2017), through MILP, use multi-modeling nodes for optimal siting of electrical and heating/cooling networks. Through linear programming, the community's standard and forecast load profiles will aid in the microgrid system's adequate sizing and design techniques through control algorithms. Another machine learning technique for the optimization model of microgrid energy management is dynamic programming. Multi-parameter dynamic programming was utilized for optimization by addressing non-linear loads and power supply intermittency of DG units (X. Wang et al. 2020). Through technology advancement, projections indicate that by 2050, solar PV will be the cheapest source of power, with costs estimated at USD 0.014- 0.05/ kWh (IRENA 2019a). Therefore, solar microgrids are promising energy solution avenues for developing countries considering the high Global Horizontal Irradiation (GHI) values received in certain countries (Yekini et al. 2013).

2.5    Observations and gaps from the literature after critical review

Key observations and research gaps identified from the literature review include:

- The low-cost nature of solar PV system has made them attractive for integration in low to medium scale energy solutions such as microgrids systems.

- The microgrid system benefits consumers by reducing the costs of their monthly expenses through energy management systems (EMS).

- The intermittent nature of solar PV creates harmonics in the voltage output waveforms which are corrected by control and modulation techniques.

- Several studies have been conducted to evaluate the quality of energy in a microgrid based on the amount of total harmonic distortion (THD) in the supply voltage.

- Few studies have examined the comparative performance between PID controllers and fuzzy logic control by THD evaluation.

- Little work has been done on measurement-based load modeling of energy consumption for households in Botswana.

- Few studies have been conducted on the design simulation of solar PV microgrids in Botswana.

2.6    Conclusion

This chapter introduces a microgrid's general concept and working principles, especially solar PV community solar microgrids established in urban settlements. Solar PV microgrids in an urban settlement operate in two modes, namely grid-connected and island mode. Energy management in an urban microgrid settlement allows an individual customer to reap cost savings through the shared usage of RES integrated into their building. The droop control technique achieves effective management through voltage sag reduction that develops because of the intermittent nature of solar as a RES. The review then introspection on the historical modeling and simulation background of the individual components that make a microgrid system, especially solar-based. The performance assessment of the particular model components was reviewed under various software environments such as MATLAB/Simulink, PSCAD, and Pspice. For community solar microgrids, there are two forms of ESS configurations, namely aggregate and distribution. Battery Energy Storage System (BESS), a form of an ESS, has been widely reported in the literature for usage in community solar microgrid systems. Of the various BESS models, the lithium-ion battery models have displayed a higher efficiency than lead-acid and nickel-cadmium battery models. The integration of solar PV as a DG unit in community solar microgrids brings about technical challenges through the three modes of operation. The difficulties experienced by community solar microgrids in urban settlements are more prominent during the on-grid operation mode.

### 3 CHAPTER 3: RESEARCH DESIGN AND METHODOLOGY

### 3.1 Overview

The methodologies and strategies used to develop solar PV microgrids in urban environments are presented in this chapter. It comprises residential load metering in a Botswana setting, followed by the smart meter data analysis. After that, the single household Grid-connected solar PV system was designed in the simulation environment PVSyst. The solar PV system design in PVSyst then informs the creation of the solar PV community microgrid model in the software environment MATLAB/Simulink. The solar PV microgrid designs will be for the island and grid-connected mode for the settlement.

### 3.2 Introduction

The initial objectives of the research include the measurement of energy consumption in a typical urban household. Various techniques are utilized to identify residential load profile patterns through smart metering data. The measurement-based approach will be used for the load model design. The method retrieves load data from data acquisition equipment to deduce the electrical load characteristics in a residential home. A smart metering system will be utilized to extract the energy consumption information for the residential household in the experiment. A residential home grid-connected solar PV system will be sized and simulated as per the daily energy requirements of the family in experimentation in the software environment PVSyst. Descriptive and predictive analytics will be utilized to analyze the smart metering data through the programs Statistical Package for Social Sciences (SPSS) and the statistics toolbox in MATLAB. Techniques used to predict electricity usage include regression models, clustering techniques, Autoregressive Integrated Moving Average (ARIMA), and Support Vector Machines (SVM). The analytics are conducted to identify the best appropriate description of the load appliances in the residential household. The overview energy usage scenarios will aid the inception of demand-side management (DSM) schemes alongside implementing a solar PV microgrid system.

For this research, a grid-connected solar PV system will be designed for a single household with minimizing feed-in to the grid through PVSyst and MATLAB software environments. The smart metering data will then be utilized to forecast the demand for electrical appliances in the future. The medium-term (week to a year) forecasting will be applied through analytical programs such as SPSS and Microsoft excel. Forecasting offers a snapshot of future energy use in the home, which is critical information for designing the community solar PV microgrid system. The MATLAB/Simulink application will be used to develop the community solar PV microgrid system. The energy management plan for the community solar PV microgrid is based on the descriptive and predictive analysis results. Through energy management in the community microgrid system, the load profile from the residential households will match the rooftop solar PV microgrid system. The energy consumption data for a quarter of households in an urban community will be synthesized through a MATLAB program. The model design of the community solar PV microgrid system will be carried out in MATLAB/Simulink. Residential households play a crucial role in the forthcoming electricity systems as they emerge to become a substantial chunk of Africa's power generating power capacity. The design of a smart load management program is necessary for the effectiveness of a solar PV microgrid system in terms of energy production.

### 3.3    Residential load metering and design

Several methods and techniques characterize electrical energy usage in residential households (Issi and Kaplan 2018). The general techniques include the engineering method, statistical design, time-series, and clustering technique. The engineering method of characterization, also known as the bottom-up approach, is the most utilized to generate electricity consumption in a residential home. The system achieves electricity characterization in homes through function parameters such as occupancy and appliance ownership (Capasso et al. 1994). The statistical method accomplishes electricity characterization through figures and reports. Data estimations based on reports provide the time-use and quantity of energy usage in a residential home (Mcloughlin, Duffy, and Conlon 2015). The time-series method is often used for households' energy usage in

larger societies but is lesser in individual households (Mcloughlin, Duffy, and Conlon 2013). The final characterization method, namely the clustering technique, identifies similar electricity usage patterns in residential communities. The technology is new and unsupervised, yet it detects different sorts of energy consumption behavior in big groups of residential users (L. Jin et al. 2017). The bottom-up approach was utilized for this research, considering that it will be used for an individual household. The clustering technique will be used for the analysis of the energy consumption of the community households.

### 3.3.1    Proposed metering methodology

The measurement period will run for 6-12 months to have a yearly overview of appliance usage in a residential home. Electric characteristics such as voltage, current, and power factors for electrical appliances will be identified through data recording. The medium and long-term monitoring period is to have a seasonal overview of load consumption throughout the year.

#### 3.3.1.1    Study area

Botswana International University of Science & Technology (BIUST)

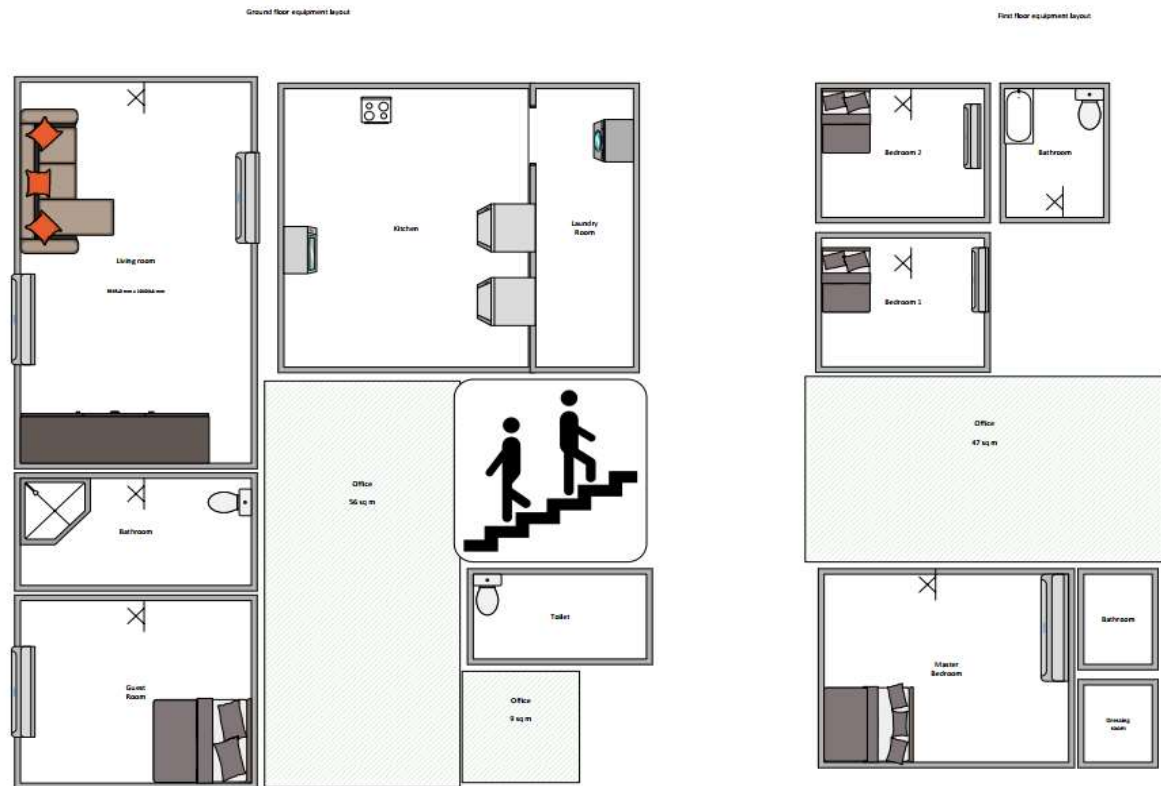BIUST Staff senior houses

Palapye, Botswana

Figure 3.1: The electrical appliances layout of the building in the experiment

Figure 3.1 represents the layout of the building. The residential building comprises one room downstairs, three rooms upstairs, a sitting room, a kitchen, three bathrooms, and toilets. There are multiple appliances in the building, but only the major appliances will be metered.

### 3.3.1.2  Initial survey and questionnaire

A preliminary study will be undertaken in the experimental household for a certain period to identify household occupancy patterns and appliance ownership. The study will include a survey and a questionnaire. A questionnaire sample to be administered to the people living in the household is listed in Table 3.1.

Table 3.1: Preliminary questionnaire to identify the energy consumption pattern in the household.

| Question # | Description |
|---|---|
| Q1 | How many inhabitants are in the household? |
| Q2 | What is the employment status of the inhabitants in the household? |
| Q3 | How many rooms are in the household? |
| Q4 | What is the quantity and types of electrical appliances per room in the household? |
| Q6 | What is the energy use behavior on a weekday and weekends? |
| | |

The questionnaire provides the occupancy scenarios and energy usage behaviors in the household.

### 3.3.1.3   Metering equipment

The metering equipment for the measurement period is the Smart Gateway (Energy Management & IoT Gateway). The system is an intelligent energy system capable of monitoring, controlling, and optimizing energy usage in the household via an app or online dashboard (CarbonTRACK 2019). Smart meters can detect electrical home appliances consumption, and dependent on the end-usage application, they can be utilized for various analysis methods and procedures under forecasts (Yildiz et al. 2017). The techniques used for load forecasting include regression analysis, exponential smoothing, and weighted iteration (Wen et al. 2018). A significant function of forecasting is to promote power generation planning for an electric power system.

The functional capabilities of the Smart Gateway include but are not limited to (CarbonTRACK 2019):

- Management of peak loads for an entire house
- Creation and management of digital essential loads panel
- Remote control and monitoring of all electrical appliances in the home
- Support of green circuit feature to maximize solar usage
- Electrical phase monitoring (3 phase, four-wire)

Figure 3.2 represents the energy measurement equipment utilized in the research for data collection.



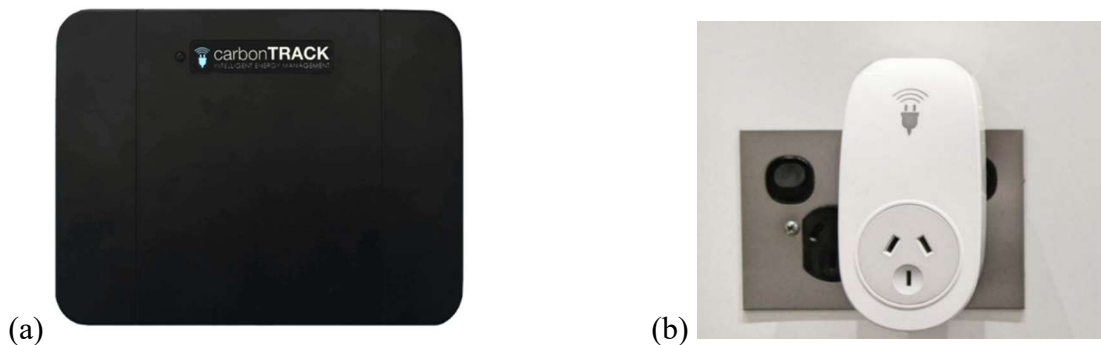(a)                                                                                   (b)

Figure 3.2: The energy measuring equipment. (a) The CT200i smart gateway and (b) Zigbee smart plug

The Smart Gateway is set up near the distribution board to connect four monitoring current clamps. The clamps can be for the four major electrical energy consumers: air conditioner, fridge, water heater, and lights. For additional current monitoring in more appliances, the carbon TRACK Smart plug can be utilized. The smart plug possesses IoT monitoring and control for electrical appliances. The smart plug is connected in-between the socket and the electrical appliances power cable. It monitors electricity consumption in intervals of 15 minutes (CarbonTRACK 2019). Electrical appliances are remotely controlled from your phone via Wi-Fi connectivity.

3.3.1.4   Metering physical design

The experimental household consists of a variety of electrical appliances. The overall electricity usage in the home will also be monitored. Below is the list of the practical instruments that will be energy monitored.

- Washing machine
- Fridge
- Lights
- 4x Air conditioners
- Miscellaneous appliances

Based on the available appliances in the household, two smart gateway devices will be required, along with two smart plugs. Below is a schematic diagram that indicates the physical layout of the installation of the metering equipment in the household. Figure 3.3 represents the installation schematic for the energy measurement equipment, and Figure 3.4 illustrates the electrical distribution board of the building in experimentation.



Figure 3.3: The installation schematic of the energy measuring equipment in the house in the experiment.

Figure 3.4: The distribution board (DB) of the house in the experiment and electrical appliances list.

### 3.3.1.5 Data collection

The energy consumption data is stored in an online dashboard. The installation company provides an application service provider (ASPs) for the data consumption information of the building in the experiment. Every 15 mins the electricity consumption information is recorded and stored online. Figure 3.5 illustrates a snapshot of the online dashboard where the energies are recorded for future usage.
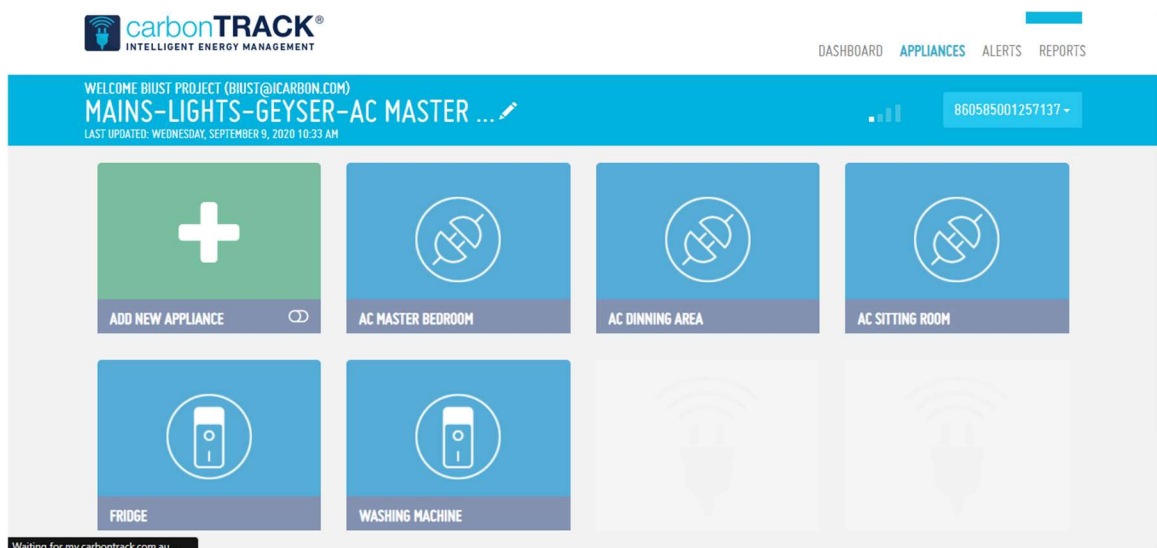


Figure 3.5: Snapshot of the online dashboard and storage center

The parameters that will be measured include electricity usage (kWh), Peak power (kW), power factor, power (kW), apparent power (VA), and Auxiliary values (voltage, grid frequency, and signal strength).

### 3.4 Descriptive and predictive analytics

The smart meter devices will be logging energy consumption in the experimental household every 15 minutes throughout the day. The 15-minute energies will reveal the peaks and valleys linked with the daily activity of the inhabitants. Data science allows for the analysis of the data for the household to show the inhabitant's characteristics and energy-saving opportunities. The software environment utilized for data science in the research includes SPSS, Microsoft excel, and Statistics & Machine learning toolbar in MATLAB with computational resources of intel Core i5 laptop with a RAM of 12 GB. Figure 3.6 depicts the various applications and techniques in smart meter data analytics.
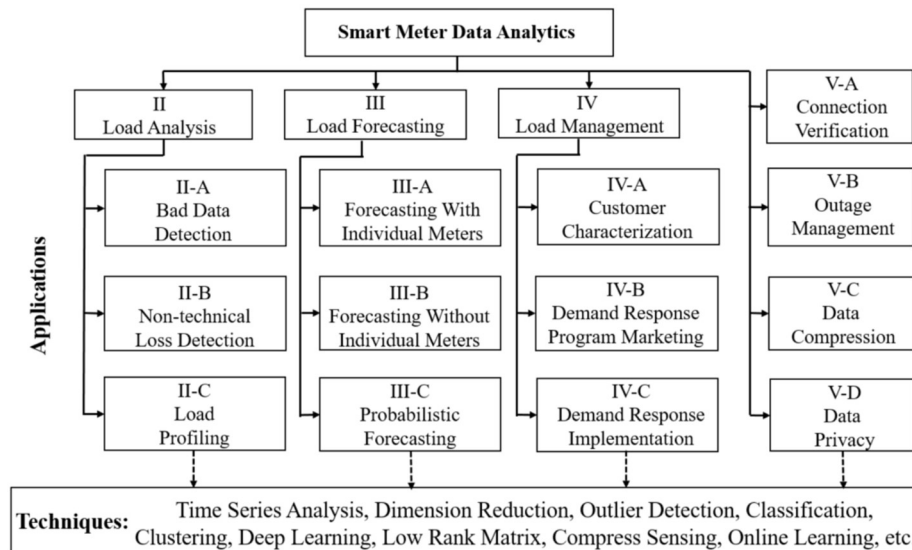


Figure 3.6: Various applications and techniques of smart meter data. SOURCE: (Yamashita et al. 2012)

Predictive analytics, prescriptive analytics, and descriptive analytics are the three types of data analytics. Descriptive analytics shows the structure and character of the data set, whereas predictive analytics uses previous data to forecast the nature of the data in the future. The central tendency and dispersion will be measured as part of the descriptive

analysis. The predictive analysis includes forecasting, regression, and clustering (Deb et al. 2017). The time series analysis will be utilized for building energy consumption forecasting. The daily load profiles of a residential household are characterized by high energy usage variability. Based on occupation and energy usage behavior, the peaks and valleys in the load profile may differ from that of another day. Graphs of daily load profiles will be generated along with the median and quartiles load profiles. The Pearson correlation (r) and Euclidean distance (d) will be utilized to identify a relationship to analyze the time-series relation of the daily load profiles. Equation 3.1 and equation 3.2 represent the mathematical expressions for Pearson correlation and Euclidean distance, respectively.

$$Pearson\ correlation\ (r) = \frac{\sum_{i=1}^{m}(L_{A,i} - \overline{L_A})(L_{B,i} - \overline{L_B})}{\sqrt{\sum_{i=1}^{m}(L_{A,i} - \overline{L_A})}\sqrt{\sum_{i=1}^{m}(L_{B,i} - \overline{L_B})^2}} \qquad 3.1$$

$$Euclidean\ distance\ (d) = \sqrt{(L_{A,i} - L_{B,i})^2} \qquad 3.2$$

Where m represents the number of 15-minute periods in the day, A and B represent the daily period symbols, $L_{A,i}$ represents the load at the i$^{th}$ 15-minute period of the day and $\overline{L_A}$ represents the average load for day A. A Pearson correlation $(r)$ of $\geq 0.5$ indicates a good relationship, while a Pearson correlation $(r)$ of $\leq 0.5$ indicates a poor relation. The Euclidean distance is a feature of energy distance that comprises the variance between distribution and probability (Rizzo and Székely 2016).

### 3.4.1   Regression analysis to identify load model parameters.

The parameters of the ZIP model ( $Z_p$ , $I_P$ , $P_P$ and $Z_q$, $I_q$, $P_q$) are identified by the least-squares method/ algorithm (Sadeghi and Abdollahi Sarvi 2009; Zhao et al. 2010). The least-squares (LS) method is an analytical algorithm that combines a set of measurements

to derive approximations of the parameters which specify the curve that best identifies with the data (Nixon and Aguado 2013). The LS method can be expressed by Equation 3.3 and Equation 3.4:

$$min_p \sum_{n=1}^{N} (y_n - px_n)^2$$

3.3

Where $y_n$ represents the group of measurements and $x_n$ represents the various parameter values.

$$\pi = \sum_{n=1}^{N} (Z_p \left(\frac{V_i}{V_o}\right)^2 + I_p \left(\frac{V_i}{V_o}\right) + P_p \left(\frac{P_i}{P_o}\right))^2$$

3.4

Where $V_i$ and $P_i$ are the input voltage and power consumption. Where $V_o$ and $P_o$ are the nominal values of voltage and power. Through the LS algorithm then identifies the three parameters through derivation. Finally, the ZIP coefficients are calculated using the reverse matrix of the electrical parameters from the house in the experiment. An X-Y scatter chart illustrates the link between power usage and voltage. Through the analytical algorithms, predicted energy consumption will be compared to the actual energy consumption. Below is an example of an incandescent model. The ZIP load demand of an incandescent model was identified as hybrid constant impedance and current model (ZI) through mathematical expression in Equation 3.5 and Equation 3.6, respectively.

$$P_{ZI} = P_o \left[ 0.6 \left(\frac{V}{V_o}\right)^2 + 0.4 \left(\frac{V}{V_o}\right)\right]$$

3.5

And the constant impedance model (Z model) is:

$$P_z = P_O \left(\frac{V}{V_o}\right)^2$$

3.6

From Equations 3.5 and 3.6, the coefficient parameters $Z_p$, $I_P$, $P_P$ were found to be 0.6, 0.4, and 0, respectively. Figure 3.7 represents a diagram of the comparisons between the actual energy usage and the predicted energy usage of the incandescent model.
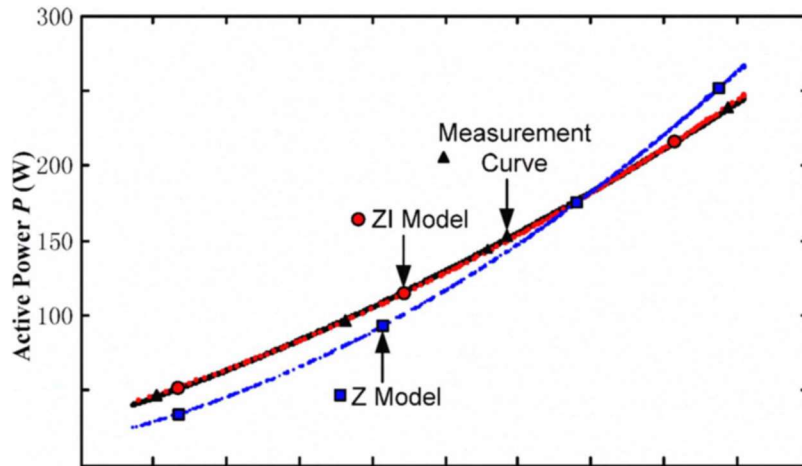
Figure 3.7: A comparison of the simulation results of incandescent models and the measurement curve. SOURCE:(Zhao et al. 2010)

The measurement curve and the ZI model curve are similar, indicating that the model accurately depicts the electrical appliance's energy usage behavior. The regression analysis reveals the best-case load model to represent the typical load profile of the electrical appliances in the residential household.

### 3.4.2   Time series analysis

The high variability of daily energy usage makes it very complex to accurately model and simulate the energy consumption data of residential households. Machine learning techniques utilizes previously recorded data to predict future energy usage (Deb et al. 2017; Gulin et al. 2014). Time series forecasting is critical to the assessment of building performance optimization. The three main components of time series analysis include:

   i.    Trend

The trend method composes a linear increase or decreases behavior of the series over time without accounting for seasonality and anomalies.

   ii.    Seasonality

A seasonal pattern in time series is dependent on factors such as day of week or month. However, seasonality patterns compose of a consistent and predictable frequency.

   iii.    Residuality

This time series pattern can depict either the trend or seasonality design or both. Data variables experience an increase and decrease without any fixed frequency.

Artificial Neural Networks (ANN), Support Vector Machines (SVM), and Autoregressive Integrated Moving Average (ARIMA) are some of the most well-known machine learning methods for time series forecasting (Kuster, Rezgui, and Mourshed 2017). The ANN algorithm is a frequently used technique for predicting short, medium, and long term. The ANN techniques employ a multi-layer neural network with a modified backpropagation learning algorithm(Deb et al. 2017; Kuster, Rezgui, and Mourshed 2017). The ARIMA algorithm is a linear equation in which the predictors are the dependent variable's lags and the prediction error (Chou and Tran 2018). The ARIMA model can be mathematically expressed in Equation 3.7.

$$Y_t = c + \emptyset Y_{t-1} + \emptyset Y_{t-2} \ldots + \epsilon_t \qquad\qquad 3.7$$

Where $Y_t$ represents the dependent variable, $c$ represents a constant, $\emptyset$ represents the magnitude of the autocorrelation and $\epsilon_t$ represents the error. Based on its own historical values, the ARIMA model forecasts a time series. A form of ARIMA, Seasonal Autoregressive Integrated Moving Average (SARIMA), uses a seasonal trend pattern in linear forecasting (Chou and Tran 2018). The SARIMA method can be expressed mathematically in Equation 3.8.

$$Y_t = c + \emptyset Y_{t-s} + \epsilon_t \qquad\qquad 3.8$$

Where subscript $s$ represents the number of lags comprising of one full period of seasonality. The SARIMA model comprises of a linear combination of seasonal past values and forecast errors (Deb et al. 2017). SVM is another time series method consisting of a hybrid of the Support Vector Regression (SVR) and the SVM, which uses element boundary variables to address function fitting problems (Zhang et al. 2019).

### 3.4.3   Load forecast through regression analysis

For load forecasting analysis of the experimental household, the linear regression techniques, namely the least-squares method (LSD), will be utilized. In addition, the short-term forecasting technique will be used to predict the energy usage of appliances in the residential home. The LSD technique calculates model regression coefficients that reduce the sum of square error between anticipated and actual observations from data collection (Fumo and Rafe Biswas 2015). Following the identification of load prediction models for a single-family, statistical programs such as SPSS and MATLAB will develop load models for additional 24 residential families to represent an urban neighborhood. Through the LSD, a relationship between the voltage and power in the ZIP load model will be analyzed. The power (P) will act as the independent variable through the analysis, and the voltage (V) will serve as the dependent variable.

#### 3.4.3.1   Linear regression

Simple linear regression is characterized by a random variable ($y$) that can be modeled as a linear function of another random variable ($x$) (Fumo and Rafe Biswas 2015; Y. Wang et al. 2019). The relationship between the variables is expressed in Equation 3.9:

$$y = \beta_o + \beta_1 x + \varepsilon \qquad\qquad 3.9$$

The response and predictor variables are denoted by $y$ and $x$ respectively. The regression coefficients are $\beta_o$ and $\beta_1$ and $\varepsilon$ is the error that accounts for the discrepancy between the forecasted and observed data.

### 3.4.3.2 Quality of model

Through the smart metering data, a linear model is generated for electricity usage in the household. A coefficient of determination ($R^2$) is utilized to analyze the effectiveness of the linear model (Fumo and Rafe Biswas 2015; Di Leo et al. 2020). $R^2$ is expressed mathematically in Equation 3.10 by:

$$R^2 = 1 - \frac{\Sigma(y_i - \hat{y}_i)^2}{\Sigma(y_i - \bar{y}_i)^2} \qquad 3.10$$

Where $(y_i - \hat{y}_i)^2$ represent the sum of the squared errors and $(y_i - \bar{y}_i)^2$ represent the total sum of squares. $R^2$ is a number between 0 and 1. The closer $R^2$ is to 1, the more accurately the model indicates that the predictor variables account for a large portion of the variability in response variables. Another way to validate a prediction model's performance is through the Root Mean Square Error ($RSME$), which is expressed mathematically in Equation 3.11 (Zhang et al. 2019).

$$RSME = \sqrt{\frac{\Sigma_{i=1}^{N}(y_i - \hat{y}_i)^2}{N}} \qquad 3.11$$

Where $y_j$ denotes the observed electricity consumption of the household j, $\hat{y}_i$ denotes the forecast electricity consumption, and N is the number of observations.

### 3.4.4 Clustering analysis

The clustering analysis involves the partitioning of a set of data objects into subsets. The purpose of clustering analysis is to perform load pattern grouping. Clustering analysis is a data mining approach used to assess residential household power use (Amri et al. 2016). The metering process's time-series power demand data will be used to group similar profiles into the same groups and determine the most common load profiles (Chicco 2012; Yildiz et al. 2017). The clustering approach identifies the key features of residential household consumption practices. The following is a systematic technique for characterizing electrical loads in an urban community using clustering (Mcloughlin, Duffy, and Conlon 2015). There are various clustering algorithms for multiple applications, but only the centroid clustering technique will be adopted for this research. The K-means algorithm, a centroid clustering technique, is capable of handling large sets of data, especially residential electricity consumption, compared to the other clustering algorithms (He et al. 2018).

#### 3.4.4.1 K-Means clustering method

The K-means algorithm poses the capability to segment data into multiple clusters according to the similarity of the data. The K-means technique utilized the Euclidean distance formula to find the relationship between two objects (Khan, Jayaweera, and Alvarez-Alvarado 2018). Several steps are undertaken to analyze big data using the K-mean algorithm, represented through a flow-chart in Figure 3.8.
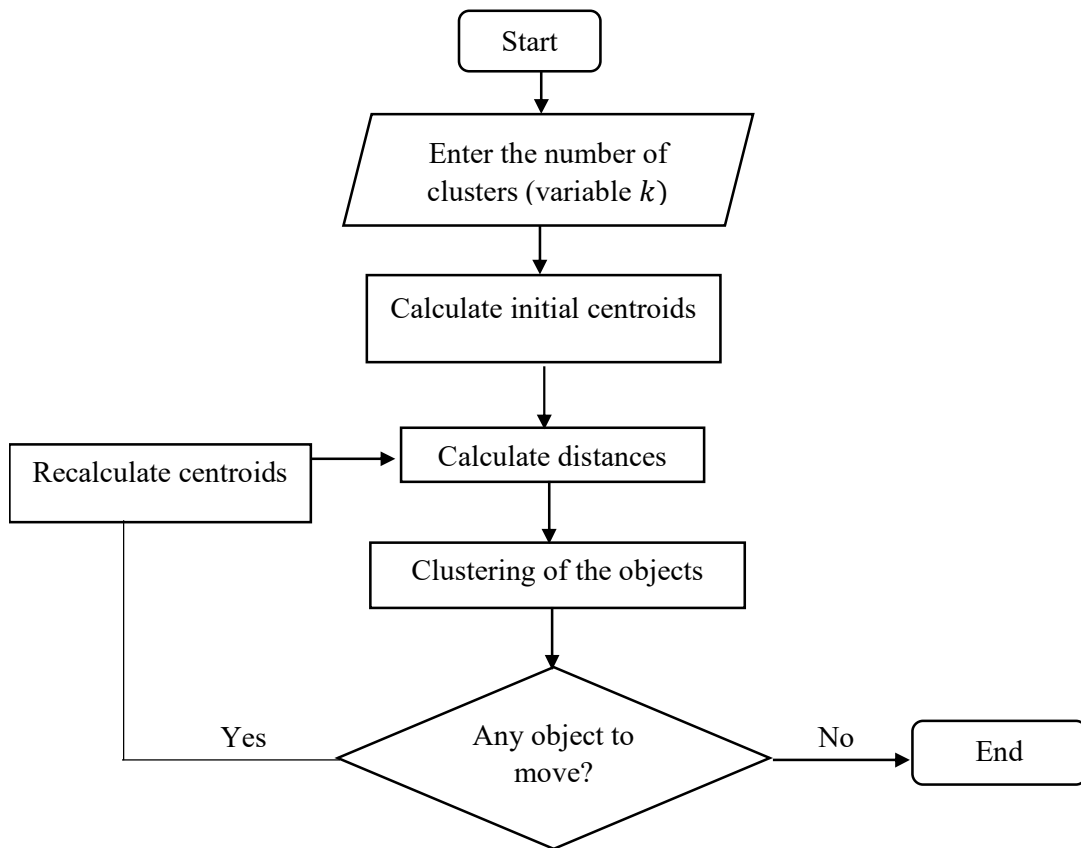
Figure 3.8: Process flow-chart of the K-means clustering algorithm. (Nepal et al. 2019)

The process flowchart will reveal the final clusters of the energy consumption data through a select number of iterations (He et al. 2018). The clustering algorithms execution will be conducted in the program SPSS.

### 3.4.5   Data preparation

The large dataset requires pre-processing to clean missing data and remove outliers for more accurate statistically significant data. The hourly dataset was cleaned through the MATLAB preprocessing algorithms. Figure 3.9 represents the flowchart for cleaning missing data.

```
┌──────────┐
│  Start   │
└──────────┘
     │
     ▼
┌──────────────┐
│ Load hourly  │
│ usage data   │
└──────────────┘
     │
     ▼
┌──────────────────────┐
│ Fill missing data    │
│ through linear       │
│ interpolation        │
└──────────────────────┘
     │
     ▼
┌──────────────────┐
│ Save interpolated│
│ data             │
└──────────────────┘
     │
     ▼
┌──────────┐
│   End    │
└──────────┘
```
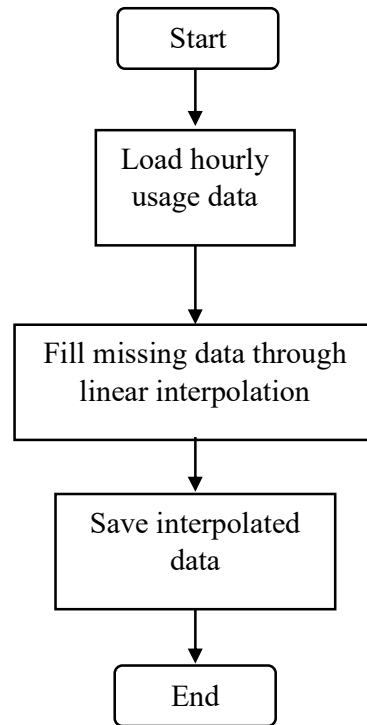
Figure 3.9: Flowchart for cleaning missing data

Missing smart metering data was corrected by linear interpolation in the MATLAB program. To eliminate processing mistakes and inadequate sampling in the hourly energy usage data, another data processing approach, outlier elimination, was used. Figure 3.10 depicts the flow diagram for the removal of outlier data.
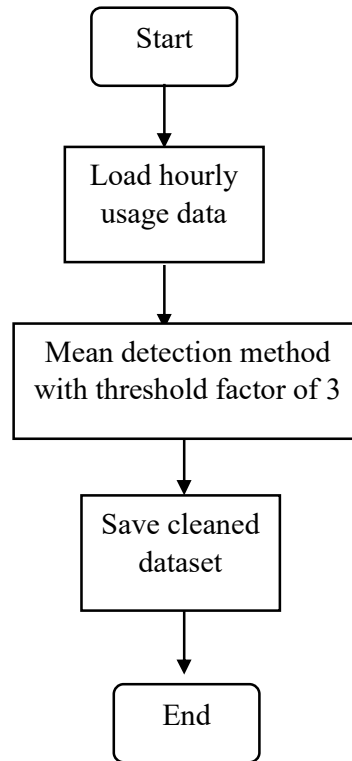
Figure 3.10: Process flow diagram for removing outlier data

Outlier data was removed from the smart metering dataset to improve accuracy in statistical analysis. As indicative in Figure 3.10, the mean detection method with a threshold factor of 3 was chosen. The mean method defines outliers as items that are more than three standard deviations from the mean.

3.5    Design and sizing of grid-connected solar PV system

The design of the single household grid-connected solar PV will be done in the simulation software PVSyst. The design of the solar PV systems is dependent on two major factors, namely the energy consumption and the solar radiation in a particular area. Figure 3.11 represents the layout design of the grid-connected solar PV system for a single household.
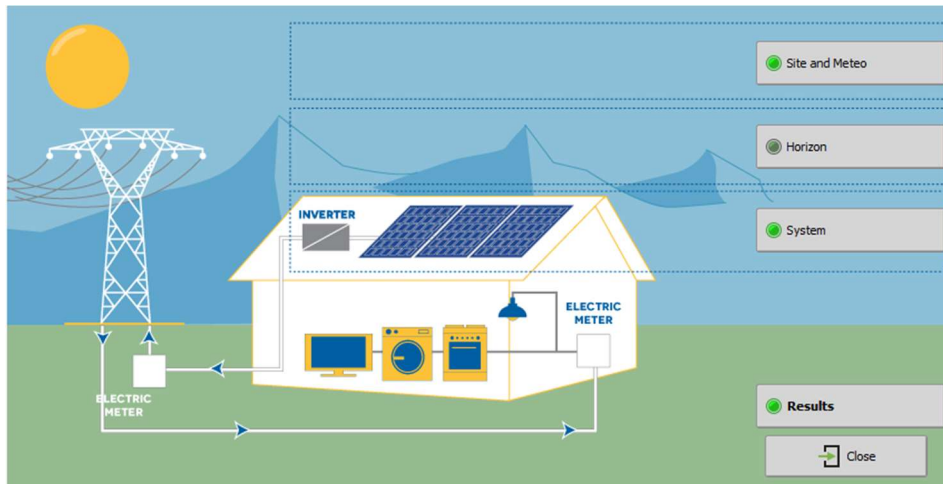


Figure 3.11: Grid-connected solar PV layout design. SOURCE: PVSyst

The design procedures of the PV system include choosing the correct number, size, and type of PV modules and inverters (Kalogirou 2009). The PVSyst simulation environment was used to examine a solar PV system with a planned power of 10 kW. The system will be connected to the grid and without battery support. The self-consumption of the house was set as the average daily electricity usage.

3.5.1    Site selection

Gaborone is the capital city of Botswana. Palapye will be the case study for the research with coordinates 22.5515° south latitude and 27.1147° east longitude. Palapye, on average from 1994 to 2018, receives approximately 6.2 kWh/m$^2$ of sunshine per day.
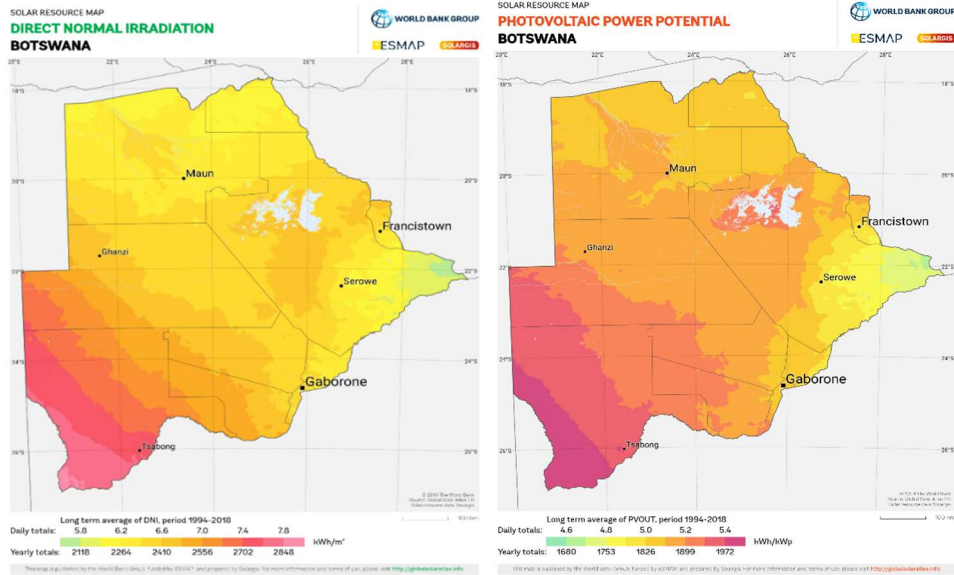
Figure 3.12: The average direct normal irradiation and PV power potential in Botswana. (Global Solar Atlas 2018)

Figure 3.12 Indicates the direct normal average irradiation between 1994 and 2018, (b) indicates the photovoltaic power potential between 1994 and 2018. The country's southwest region receives the highest amount of solar radiation ($7.4 – 7.8$ kWh/ m$^2$), with the lowest solar radiation figures (approximately $5.8$ kWh/m$^2$) experienced in the eastern region. The house in experimentation is in the east-central area with the solar radiation received set at $6.2$ kWh/m$^2$ (Global Solar Atlas 2018).

### 3.5.2    Daily load demand

A common daily load profile from the residential household in experimentation was utilized as the load demand for the simulation in PVSyst. The load profile was identified for simulation through the clustering analysis. Figure 3.13 illustrates the average daily electricity usage.
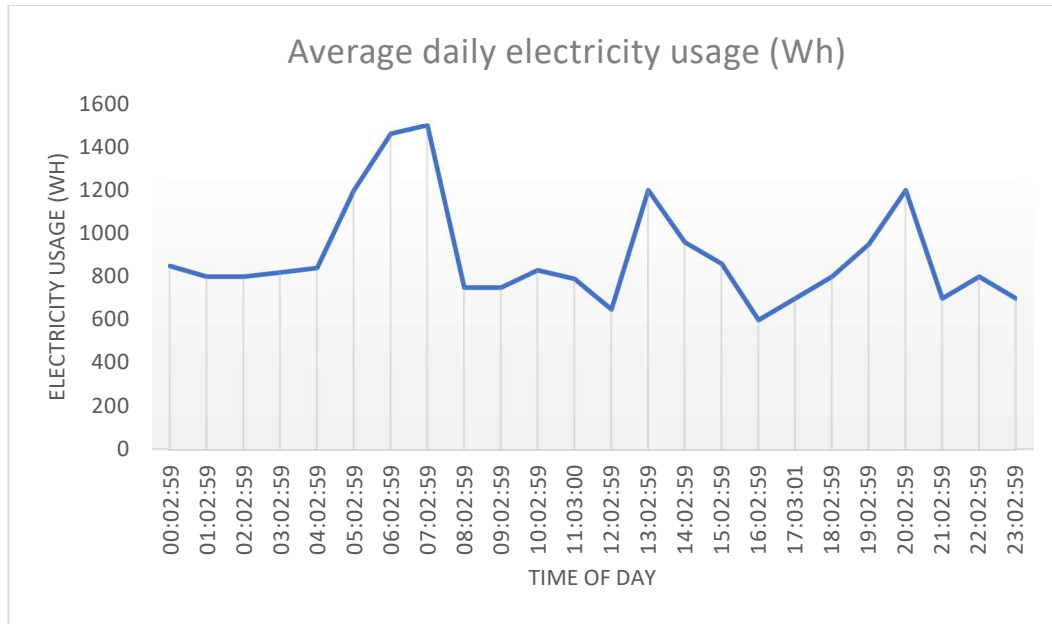
Figure 3.13: The average daily energy consumption for the house in the experiment.

### 3.5.3 PV Module

PV cells can have a single crystal, polycrystalline, or amorphous atomic structure. Mono-crystalline cells were investigated for the design, with an efficiency of roughly 20% (Alnoosani et al. 2019; Harvey 2006). The solar panel's electrical data specification is shown in Table 3.2.

Table 3.2: The PV module specifications

| Type | Mono-crystalline |
|---|---|
| No's of modules | 91 |
| Maximum power ($P_{max}$) | 110 W |
| Voltage at maximum point ($V_{mpp}$ (60 ºC) | 29.6 V |
| Open circuit voltage ($V_{oc}$ (- 10 ºC) | 42.3 V |
| Maximum Power Current ($I_{mpp}$) | 21.1 A |
| Short circuit current ($I_{SC}$) | 20.4 A |

The PV module specifications were extracted from the database in the software program PVSyst. Temperature affects crystalline cells, so that a rise in module temperature decreases the electricity output by 0.04-0.9 % (Harvey 2006).

### 3.5.4 Tilt and yield

Different regions have an optimum tilt angle which ensures maximum energy output from the PV array. For this research, the fixed tilt angle comprises two tips, namely, the collector tilts angle $\beta$ and the collector azimuth angle $Z_s$ (Chinchilla et al. 2021; Nfaoui and El-Hami 2018). Latitude tilt is whereby the PV module tilt angle is equal to the local geographic latitude. For a country such as Botswana, the slight tilt angle is incorporated to maximize energy production in the summer months. The sun is higher in the sky, and there will be less shading between adjacent modules (Kalogirou 2009). The relationship between the optimum tilt angle for annual yield and the latitude angle ($L$) is expressed mathematically in Equation 3.12.

$$\beta = 0.764\, L + 2.14°, for\ L \leq 65 \qquad\qquad 3.12$$

For the village of Palapye, the latitude angle is 22.6°, and the optimum tilt angle for the PV module is 19°. and the direction of the azimuth is south (0°).

### 3.5.5 Array specifications

The number of parallel strings of the PV generator ($N_{pg}$) relation with the maximum current of the inverter ($I_{mpp}$) and the maximum current under Standard Test Conditions at 1000 W/m$^2$ is expressed by the Equation 3.13 (Kalogirou 2009).

$$N_{pg} < {I_{max}}\big/{I_{mpp}} \qquad\qquad 3.13$$

The number of PV modules in series ($N_{sg}$) relates to the power rating of the inverter ($P_o$) and the number of parallel strings of the inverter ($N_{pg}$) by the mathematical expression in Equation 3.14.

$$N_{sg} = \frac{P_o}{N_{pg}} \qquad\qquad 3.14$$

The ten kWp planned solar PV system would require 13 PV modules connected in series on six parallel strings, resulting in approximately 78 modules. The area of the PV array is 70 m$^2$. Table 3.3 provides the list of the electrical array specifications.

Table 3.3: PV array specifications for the solar PV system design

| Type | Specifications |
|---|---|
| Voltage at maximum point ($V_{mpp}$ (60 °C) | 385 V |
| Open circuit voltage ($V_{oc}$ (- 10 °C) | 460 V |
| Maximum Power Current ($I_{mpp}$) | 21.1 A |
| Short circuit current ($I_{SC}$) | 20.4 A |
| Plane irradiance | 1103 W/m$^2$ |
| Short circuit current ($I_{sc}$) at standard test conditions (STC) | 20.4 A |

### 3.5.6   Inverters

The inverter serves to convert DC-generated power to AC power type to provide electrical energy to the AC loads in the residential household. The efficiency of the inverter is reliant on the DC output voltage (Woyte and Goy 2017). The system in design is grid-connected; thereby, the nominal array power will be equal to the inverter size rating (Kalogirou 2009). The relationship between the inverter and the grid is expressed mathematically by Equation 3.15.

$$E_{grid} = E_A n_{inv} \qquad\qquad 3.15$$

Where $E_{grid}$ is the energy available to the grid, $E_A$ represents the energy available to the electrical loads and battery and $n_{inv}$ represents the efficiency of the inverter. Table 3.4 provides the list of the inverter characteristics of the solar PV system.

Table 3.4: Inverter specifications for the solar PV system

| Type | Parameters |
|---|---|
| Inverter power | 4.2 kW with 2 MPPT |
| Operating voltage | 125-500 V |
| Input maximum voltage | 700 V |
| Number of inverters | 2 |
| Efficiency | 97% |
| Grid frequencies | 50/60 Hz |

The inverter is equipped with an MPPT to achieve the optimum PV generation on the modules.

### 3.6    Design and model of a solar PV microgrid system

This section of the research comprises the design and sizing of the solar PV microgrid system for a community of households in an urban settlement. The solar PV microgrid system includes four major components: the Solar PV system, Energy Storage System (ESS), bi-directional DC/DC converter, DC/AC inverter, DC, and AC loads. The community solar PV microgrid system design will be conducted on the MATLAB program, namely Simulink/ Simscape, by gathering components from the library block of Sim-power frameworks. The microgrid system exists in two primary states, namely, island and Grid-connected mode of operation.

### 3.6.1 Community load profile

The load profiles of residential homes represent average energy use in Botswana's metropolitan residential districts. The primary residence, where the experiments were carried out, presented the researchers with basic energy use behavior patterns in urban residential settings. The community's load profile is a yearly load profile that runs from January to December. Throughout the year, the burden on the various dwellings fluctuates. Based on the cumulative energy consumption behavior of the consumers in the community settlement, the district load profile has peaks and troughs. The residential households' total maximum load demand will be approximated at 250 kW. The simulation conducted in MATLAB is for a single day; thereby, the peak-daily profiles from the residential household in the experiment were utilized as daily load profiles for 25 residential homes in a community. The ten kWp for 25 residential families equates to a 250-kWp planned solar PV power system. The three-phase load block from the Simscape library was utilized, and the model structure type selected was constant impedance.

### 3.6.2 Solar PV system

The generic mathematical model of an ideal PV cell is expressed in Equation 3.16:

$$I = I_{PV} - I_O[\,exp\,(\frac{(N_S\,k\,T\,)V\,+\,R_sI}{q\,\alpha}) - 1\,] - \frac{V\,+\,R_sI}{R_{sh}} \qquad 3.16$$

The current created by incoming light is represented by $I_{pv}$, the diode saturation current is represented by $I_o$ and the series and equivalent shunt resistances of the array are depicted by $R_s and R_{sh}$. The ideality factor $(\alpha)$ indicates the ideality factor, which is a constant that depends on the PV cell technology used by the manufacturer (Bellia 2014; Prakash and Singh 2016). Other parameters include $N_S$ which is the number of cells in series, $k$ is the Boltzmann's constant (1.3806503 * $10^{-23}$ J/ K), T (K) which is the diode temperature, and $Q$ which represents the charge of an electron (1.60217646 * $10^{-19}$ C).

Table 3.5 provides the module parameters for the PV panel (Solar Tech Energy ASC-6P-72-300).

Table 3.5: Solar PV Module parameters

| Parameters | Values |
|---|---|
| Maximum power ($P_{max}$) | 299.9835 W |
| Voltage at maximum point ($V_{mpp}$ (60 ºC) | 36.45 V |
| Open circuit voltage ($V_{oc}$ (- 10 ºC) | 44.75 V |
| Maximum Power Current ($I_{mpp}$) | 8.23 A |
| Short circuit current ($I_{SC}$) | 8.62 A |
| Cell per module (Ncell) | 72 |

Table 3.6 presents the PV specifications for the 250 kW planned generation system

Table 3.6: Photovoltaic specifications

| Modules /string | Strings /array | Number of arrays | String voltage (V) |
|---|---|---|---|
| 15 | 4 | 13 | 546.75 |

### 3.6.2.1   DC-DC Boost converter

The community microgrid system's DG unit is an intermittent source that produces a highly variable output voltage, necessitating a DC/DC converter to reduce voltage ripples and function as a step-up or step-down voltage device depending on the energy demands of the loads. The converter connects the solar PV system to the DC microgrid system (Zammit et al. 2018). In addition, the boost converter may serve as a voltage booster for the DC bus (Farrokhabadi et al. 2018). Inductor, capacitors, and MOSFET devices with switching functions make up the converter, which controls the voltage flow according to the energy needs. Finally, the energy storage components are charged and discharged

using the bi-directional converter (Lee et al. 2011). The boost converter specs are listed in Table 3.7.

Table 3.7: DC-DC converter parameters

| Boost converter parameters | Value |
|---|---|
| String Voltage (Vin) | 546.75 V |
| Output Voltage (Vo) | 835V |
| Switching Frequency (fs) | 5 kHz |
| Converter Power (P) | 20 kW |
| Inductor current peak to peak percentage ripple | 137.17 A |
| Output voltage peak percentage ripple ($\Delta$Vo) | 27.34 V |
| Inductor Resistance (RL) | 2.064e-04 Henry |
| ESR of Capacitor (Rc) | 1.00e-03 Farads |
| Duty ratio (D) | 0.3452 |

### 3.6.2.2   Maximum PowerPoint tracking (MPPT)

A control approach known as maximum power point tracking was devised to optimize output power generation. The primary purpose of the MPPT is to achieve proper operation of the PV module (Zainal, Yusoff, and Ajisman 2016). Figure 3.14 is a flowchart algorithm for MPPT control for a solar PV system.
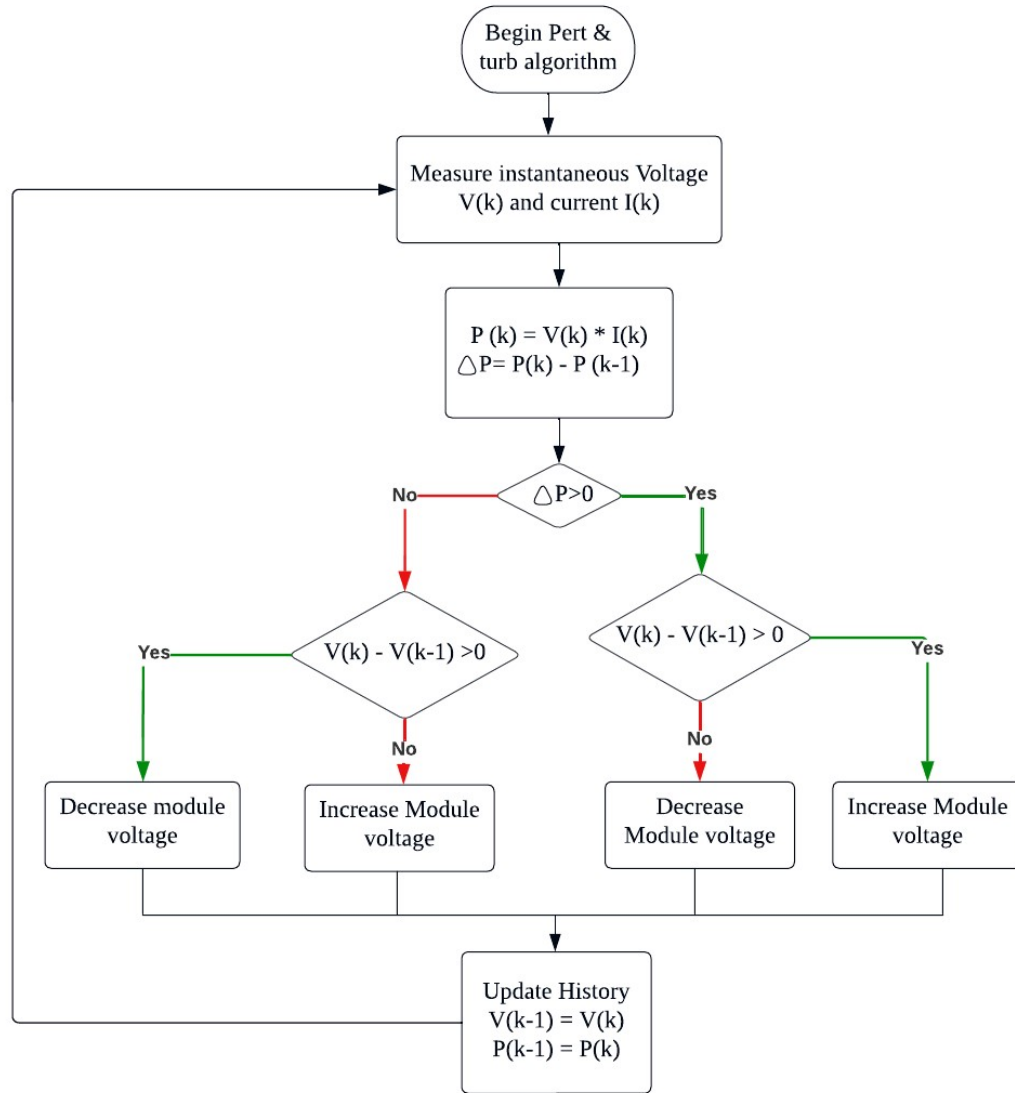
Figure 3.14: Flowchart for the pert & turb MPPT algorithm. (Nedumgatt et al. 2011)

The method involves a comparative analysis of the PV module voltage variation (Nedumgatt et al. 2011). The P & O MPPT algorithm begins with the measurement of the instantaneous voltage and current in the solar PV module as depicted in Figure 3.14. Then the instantaneous power change is evaluated using a decision tree to determine whether it is positive or negative. When the power change is positive and the voltage change is

positive, it means that the algorithm is approaching the MPPT, so a positive perturbation is needed. When the power change and the voltage change are both negative, it means that the algorithm is approaching the MPPT and therefore a positive perturbation is needed (Kordestani et al. 2018). When the power change is negative, but the voltage change is positive, a negative perturbation is required to approach MPPT. A disturbance is applied to the module voltage, and the resulting output power is compared to that of the initial disturbance cycle (Atallah, Abdelaziz, and Jumaah 2014). The perturbation's goal is to find power variations among the cycles. When the PV module's power increases due to a perturbation cycle, the cycle is preserved and repeated until the maximum power point is achieved. Further perturbation after Maximum Power Point (MPP) has been reached will result in a decrease in power.

### 3.6.3 Island mode of operation

This mode of operation comprises the solar PV system and the BESS as the only energy suppliers for the microgrid system. The required DC bus voltage is regulated through a PID controller that communicates with the BESS whether to feed voltage into the microgrid bus or charge depending on the solar PV system output. Figure 3.15 provides the simulation design for 250 kW static load on Simulink.
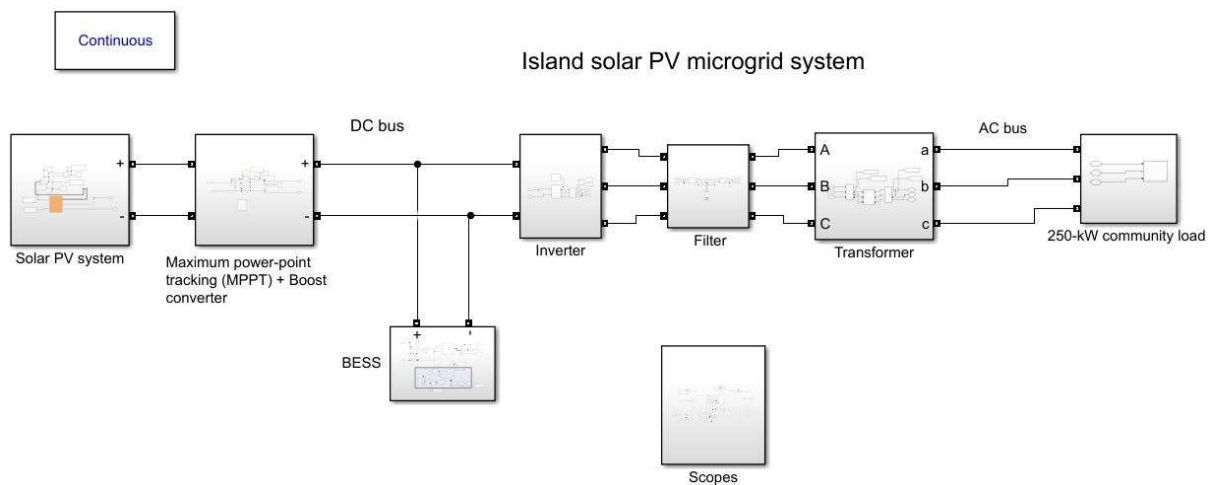


Figure 3.15: Island mode of operation MATLAB simulation design

The solar PV system block in Figure 3.15 comprises of a solar PV module with irradiance and temperature inputs. The DC bus voltage is then boosted to the desired bus voltage of 835V via the MPPT and boost converter block. The BESS block comprises of lithium-ion batteries connected across the DC bus. The DC bus is then connected to the inverter block where the DC power is converted to AC type power. The AC power has harmonics in the output waveform which are reduced by the filter block. Subsequently, the transformer lowers the voltage to that acceptable to the electrical appliances of the residential community.

The battery helps to balance electricity in a microgrid by acting as a load or generator during the charging and discharging phases. Lithium-Ion batteries are widely utilized in solar community microgrids. They display a higher depth of discharge (DoD) than other battery types such as lead-acid and nickel-hydride batteries (Bila, Opathella, and Venkatesh 2016; Farrokhabadi et al. 2018; Vetter and Rohr 2014). Factors such as DoD, state of charge (SOC), and temperature affect capacity and life (Alvarez et al. 2018). A buck-boost converter topology was utilized to serve the function roles of discharging and charging the BESS in the microgrid. Figure 3.16 is the BESS model design and control in MATLAB/Simulink.
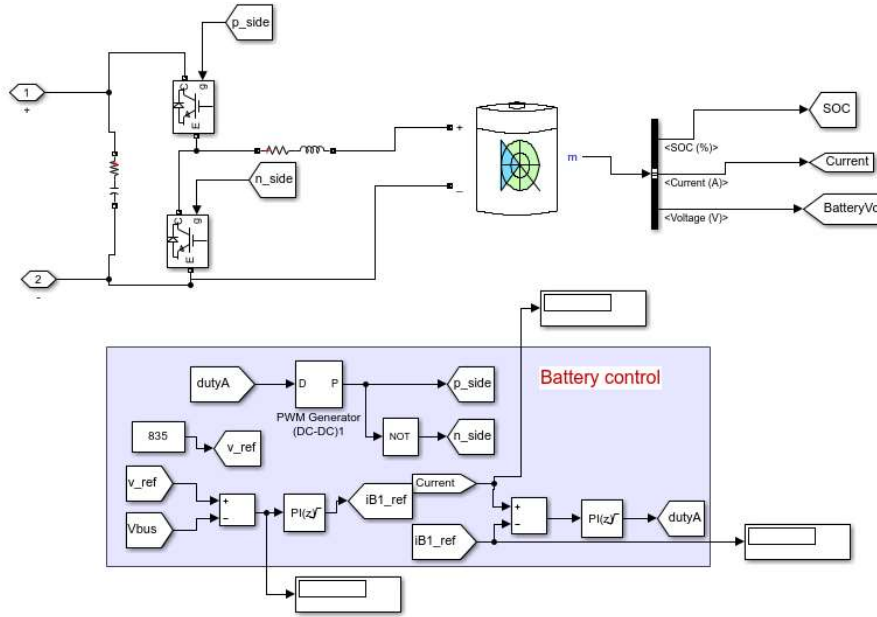
Figure 3.16: BESS model design and control scheme

The BESS comprises a lithium-ion battery model, a MOSFET driven circuit to enable the charging and discharge of the battery depending on the available power in the DC bus of the microgrid system. A voltage reference (v_ref) of 835 V is set as the DC bus voltage. It also comprises a control scheme that utilizes PI controllers and PWM DC-DC generators that incorporate the boost converter's output and the desired load voltage level in the microgrid system. The actual voltage in the bus and the v_ref was compared, and the error signal was compensated by the PI controllers to generate a current reference (iB1_ref). The current reference is then compared to the current in the battery and the resulting error is compensated by the PI controller to generate a signal for the boost converter. The voltage is subsequently increased by the boost converter to the target bus voltage of 835 V. Table 3.8 presents the parameters of the lithium-ion battery.

Table 3.8: Parameters of the lithium-ion battery

| Description | Value |
| --- | --- |
| Initial SOC | 50% |
| Nominal voltage | 550 V |
| Rated capacity | 200 Ah |

The battery was rated at 550 V due to the Vmpp of the solar PV module being stated at 546 V; thereby, during periods of low solar radiation, the battery capacity will be able to meet the desired DC bus voltage of 835 V. The aggregate configuration for the battery packs will be utilized whereby all the lithium-ion battery units will be stored in a central location (D. W. Gao 2015b). The system design calculations dictate that approximately 40% of the daily energy usage is utilized in the night; thus, estimates for a 100 kWh battery system were designed. Table 3.9 provides the battery array specifications.

Table 3.9: The specifications of the BESS

| Number of batteries/ strings | Number of strings/arrays | Number of arrays | String voltage (V) | Energy stored /array (kWh) |
| --- | --- | --- | --- | --- |
| 3 | 3 | 2 | 72 V | 43.2 kWh |

### 3.6.4   Grid-connected mode of operation

The grid-connected mode of operation comprises the island mode of operation components alongside the utility grid. An inverter was generated from an analog circuitry composed of a two-level converter consisting of switching devices that change the waveform of DC voltage to AC voltage. The converter is connected to an inductor-capacitor-inductor (LCL) filter, removing harmonics in the output waveforms and yielding a pure sine wave (Pan et al. 2017). Figure 3.17 depicts the MATLAB design of the grid-connected mode of operation.
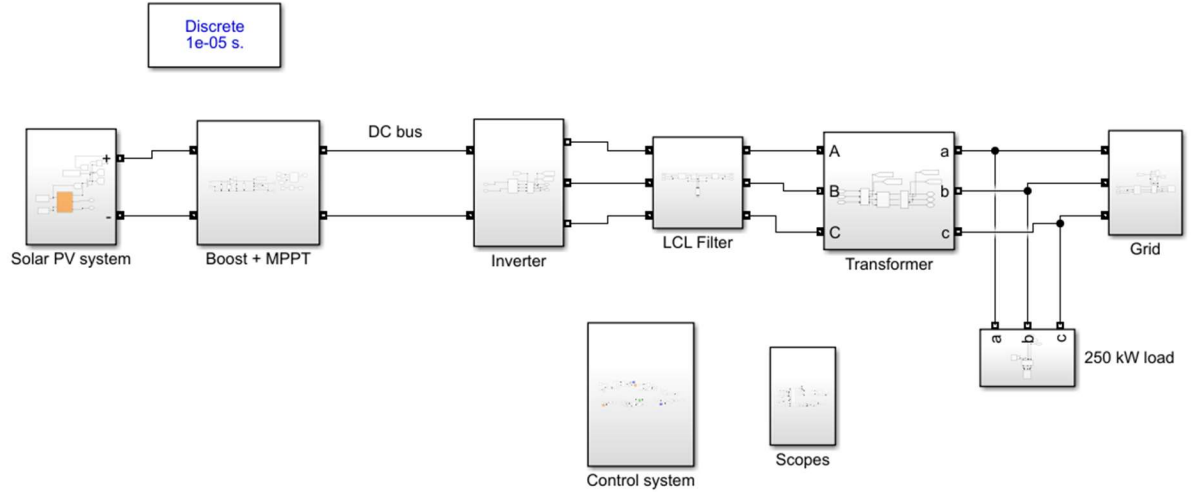
Figure 3.17: Grid-connected mode MATLAB simulation design

The simulation design comprises of the solar PV system block connected to the boost and MPPT block. The boosted voltage in the DC bus is then converted into AC power type via the inverter block as depicted in Figure 3.17. The LCL filter block then filters out harmonics from the output voltage waveforms. The voltage is then stepped down in the transformer block before being directed to the community residential load. As the microgrid system is connected to the utility grid, the control system regulates the power flow based on the energy requirements. Figure 3.18 expands on the control mechanism of the grid-connected microgrid system.

### 3.6.4.1 Inner control loop

To synchronize the frequency and allow the desired currents to inject the requested levels of active and reactive power for specific measured grid voltages, a VSI control system between the inverter and the grid is required (Kabiri, Holmes, and McGrath 2013). Equation 3.17 can be used to express the grid-connected inverter's mathematical control model:

$$\begin{bmatrix} u_d \\ u_q \end{bmatrix} = L \frac{d}{dt} \begin{bmatrix} i_d \\ i_q \end{bmatrix} + R \begin{bmatrix} i_d \\ i_q \end{bmatrix} + \omega L \begin{bmatrix} -i_q \\ i_d \end{bmatrix} + \begin{bmatrix} e_d \\ e_q \end{bmatrix} \qquad 3.17$$

The grid voltage park conversion component is represented by $e_d$ and $e_q$. And the elements of the park transformation of the inverter output are represented by $u_d$ and $u_q$. The active and reactive transformation components of the inverter current are represented by $i_d$ and $i_q$ respectively. $\omega$ and L represents the angular grid frequency and inductance between the grid-connected inverter and grid, respectively. A closed-loop current regulator powers a high-frequency PWM switching controller. A closed-loop current regulator drives a is powered by a closed-loop current regulator. The dq0 transformation control is utilized as it can operate near unity power factor to any magnitude of solar radiation (Abdalrahman, Zekry, and Alshazly 2012; Schonardie et al. 2012). Figure 3.18 depicts the inner control loops for the three-phase VSI.
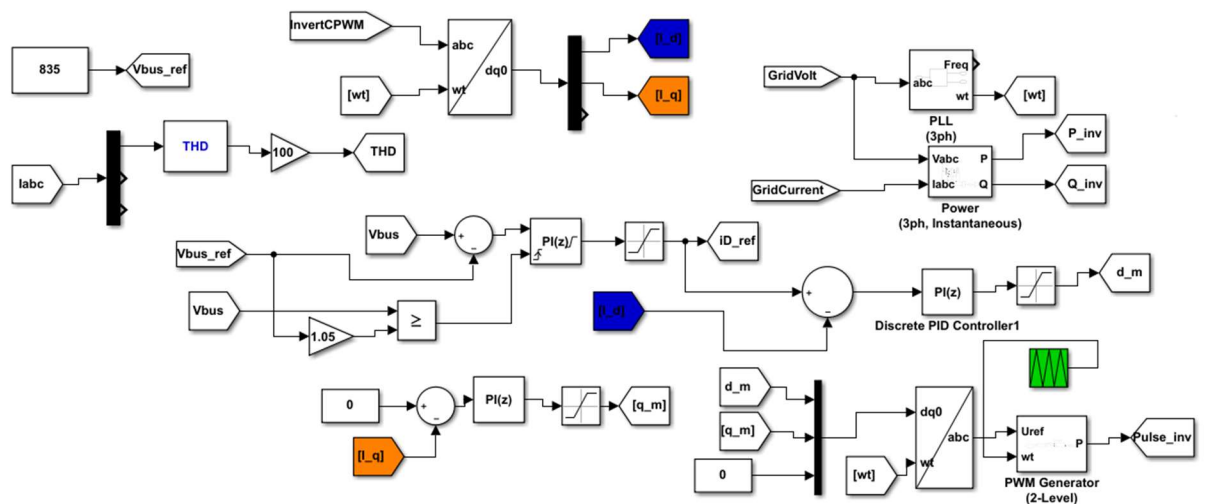


Figure 3.18: Inner control loops for a three-phase VSI.

The inner control loops comprise of current and voltage control strategies. PID and PLL controllers are included in the DQ control, and they are capable of regulating DC variables and extracting the phase angle of the grid voltage, respectively (Phuong, Dzung, and Huy 2012). The primary purpose of the inverter side control is to extract the maximum amount of electricity from the solar PV system. The active and reactive inverter currents can be removed using the DQ transformation. The phase angle of the grid voltage (wt) and the inverter current were fed into a DQ transformation to generate the inverter current's active

(I_d) and reactive (I_q) transformation components as depicted in Figure 3.18. An error signal is formed by comparing the desired reference voltage (Vbus_ref) with the voltage in the capacitor, and it is sent through the voltage controller to generate the reference current signal (iD ref). Following that, iD_ref is compared to I_d, and the resulting current error is adjusted for by PI controllers to generate a signal (d_m). To produce a reference current for the PWM generator, the corrected signals d_m and q_m are passed through an inverse DQ transformation together with the grid voltage's phase angle. The PWM generator controls the active and reactive current components that are provided to the utility grid (Abdalrahman, Zekry, and Alshazly 2012). Grid side control includes regulating the amount of power fed into the grid as well as grid synchronization. Table 3.10 is the inverter specification.

Table 3.10: Inverter specifications

| # of inverters | 5 |
|---|---|
| Input voltage (Vi) | 835 |
| Power rating (kW) | 50 |
| Output voltage (Vac) | 460 |
| Amplitude modulation (Ma) | 0.9 |
| Frequency modulation index (Mf) | 166.6666667 |

### 3.6.4.2   LCL Filter design

The LCL filters are widely favored to serve as the link between grid-connected inverters and the grid as they serve their primary purpose of removing harmonics in the output, presenting a resonant frequency while also providing a better fading of the ripple currents in the grid current (Judewicz et al. 2018; Sahoo et al. 2014). The maximum allowed total harmonic distortion (THD) from the grid side current should be within 5% according to IEEE-519 standard (Hamizah et al. 2014). Table 3.11 provides the parameters for the filter design.

Table 3.11: Filter design parameters

| Parameters | Magnitude |
|---|---|
| Resonant frequency (fres) | 5000 Hz |
| Grid current (Ig) | 181.2 A |
| Ripple grid current (Igsw) | 0.544 A |
| Inverter inductor (L1) | 8.0825e-04 H |
| Capacitor (C) | 6.2679e-05 F |
| Grid inductor (L2) | 8.0825e-04 H |

3.7 Conclusion

The purpose of the research was to analyze residential load pattern flow through smart meter data analytics. A measurement device was installed in a residential household in a typical urban neighborhood to record the load usage for 12 months. The data collected was then subjected to descriptive and predictive analytics to find relations and draw conclusions from various parameters such as voltage, peak power, active and reactive power. Through the maximum peak load of 10 kW recorded in the residential household in experimentation, a grid-connected solar PV system was sized and designed through the application PV Syst. Afterward, a community PV microgrid system with a maximum demand load of 250 kW is designed on the program application, MATLAB/Simulink. The system design will be based on two operation states, namely grid-connected and island mode. Through the island mode of operation, the DG units and the battery will be serving as the primary energy suppliers in the DC microgrid system, with the DG unit as the primary supplier. The grid-connected mode will comprise three energy suppliers: the DG unit, battery, and utility grid. A three-phase closed-loop control will be utilized to regulate the DC grid bus voltage and dictate when to charge and discharge the BESS as per the energy requirements of the microgrid bus. The loop control system includes a primary control that utilizes droop and impedance loops that enables a parallel connection of VSIs that share active and reactive powers. The secondary control enables synchronization of voltage and frequency between the DGs unit, BESS, and the utility grid. The desired bus voltage was set at 835 V, and the control system enables the communication between the microgrid components to achieve the desired voltage bus level. The PWM control ensures the reduction of the voltage noise ripples in the output waveforms.

## 4    CHAPTER 4: RESULTS AND ANALYSIS

### 4.1    Overview

This chapter presents the energy metering assessment in a typical urban household and the simulation results of the single household solar PV and the community solar PV microgrid systems. It also provides an overview of the 12 months energy usage of the house in experimentation through data analytics. Descriptive and predictive analysis was conducted on the dataset, and load models of the typical urban household energy profile in Palapye, Botswana, were identified.

### 4.2    Introduction

Through linear regression analysis, the information from the metering enables the development of the electrical appliance forecast energy usage.  The energy demand forecast is necessary to generate demand-side management (DSM) techniques and alternative energy generation activities. Activities such as load scheduling and load management are essential to establishing an effective solar microgrid system. A time series analysis was also developed to predict energy usage in the household through smart metering data. Through synthetic load profile generation, the load profile of the community will be generated and subjected to data analytics to identify the load demand patterns. Twenty-five daily load profiles from the house in experimentation will be utilized to simulate a community of 25 residential households. A solar PV system for the home in the experiment was also designed with no battery support in the PVSyst environment. The average peak power demand was identified as 10 kW of which is frequently experienced in the morning. A grid-connected solar PV system of the nominal power of ten kWp was designed in a PV system, and the results are discussed below. The following work is developing a 250-kW community solar PV microgrid system executed in MATLAB/Simulink.

### 4.3    Metering results

Through the online dashboard, the metering results were extracted and summarized in the Microsoft Excel program. Graphs and tables were formulated from the data. Monthly, weekly, daily, and hourly electricity consumption graphs were prepared.

#### 4.3.1    Overall load profiles

The average daily electricity usage (kWh) of the house in experimentation is 27.39991 kWh. The statistic is extracted from the period between August 2020 and August 2021. Below are the graphs for the 15-minute intervals, hourly and daily intervals. Figure 4.1 provides a schematic diagram of the 15-minute interval energies record for the 21$^{st}$ of August 2020.
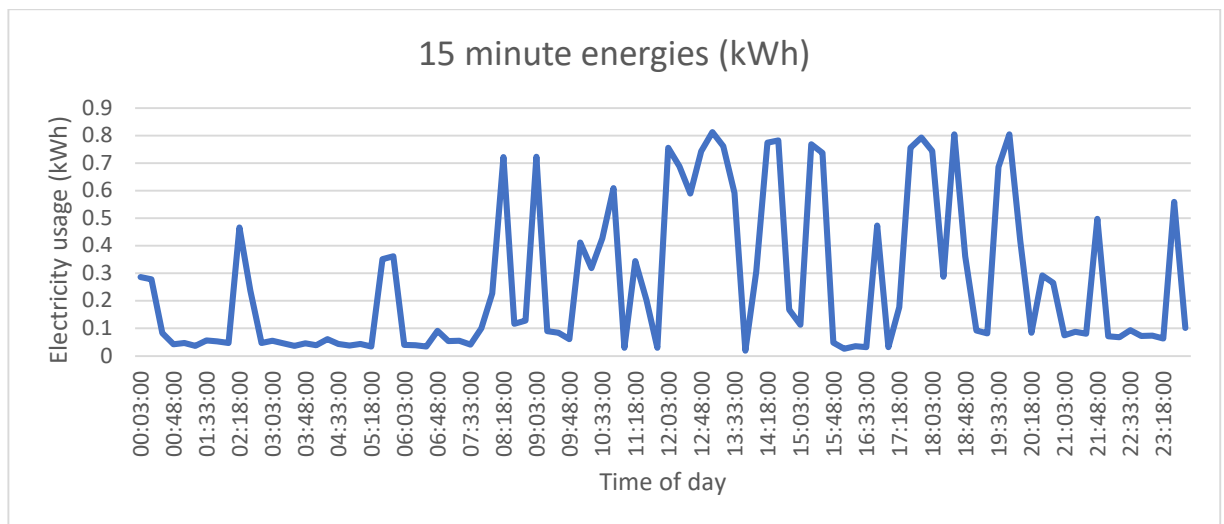


Figure 4.1: The 15-minute energies

From Figure 4.1, the peak energy demand occurs around 2300 hrs. The peaks and valleys across the day result from the instantaneous energy usage behavior of the inhabitants in the residential home. Therefore, the peak energy demand varies daily and depends on the inhabitants' energy usage behavior in the residential household. Figure 4.2 provides a weekly load profile for the house in experimentation.
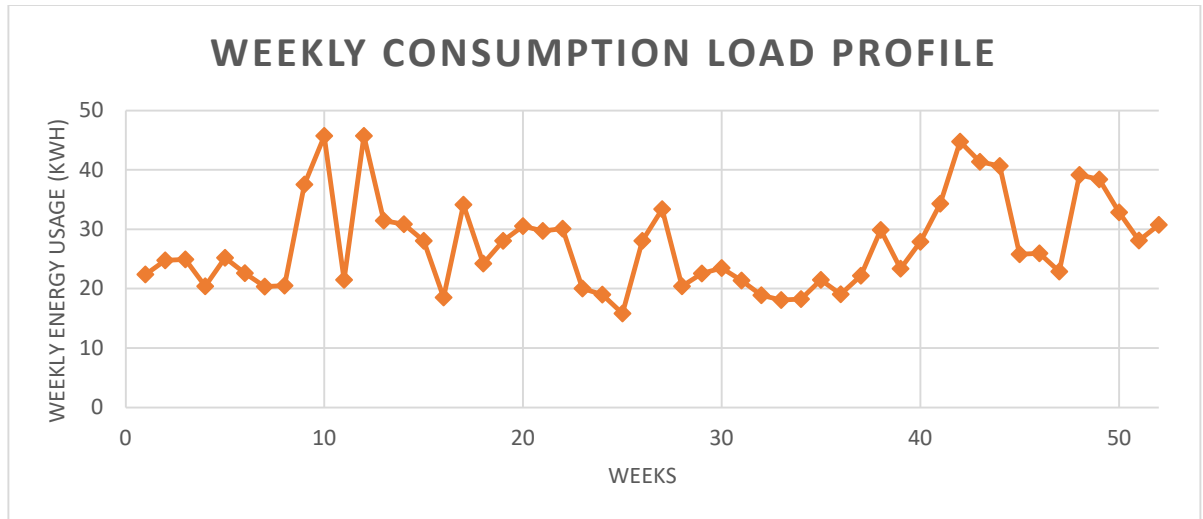
Figure 4.2: Weekly energy consumption (kWh)

The average weekly analysis reveals an average electricity usage of 27.28 kWh. From Figure 4.2, a steep rise was identified between week eight and week 13, indicating the increased Air Conditioner (AC) usage in the residential household. Another steep climb occurred between week 40 and week 45. The maximum and minimum weekly energy usage was recorded at 45.7 kWh and 15.84 kWh. Figure 4.3 and Figure 4.4 represent the daily electricity usage and peak power, respectively, for the residential household in experimentation.
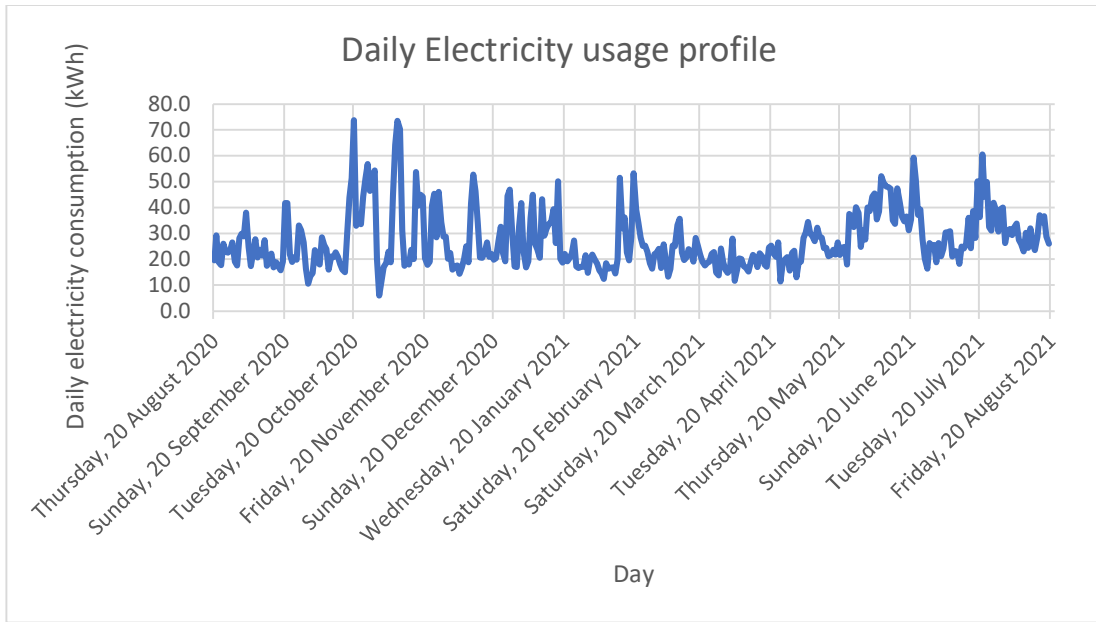
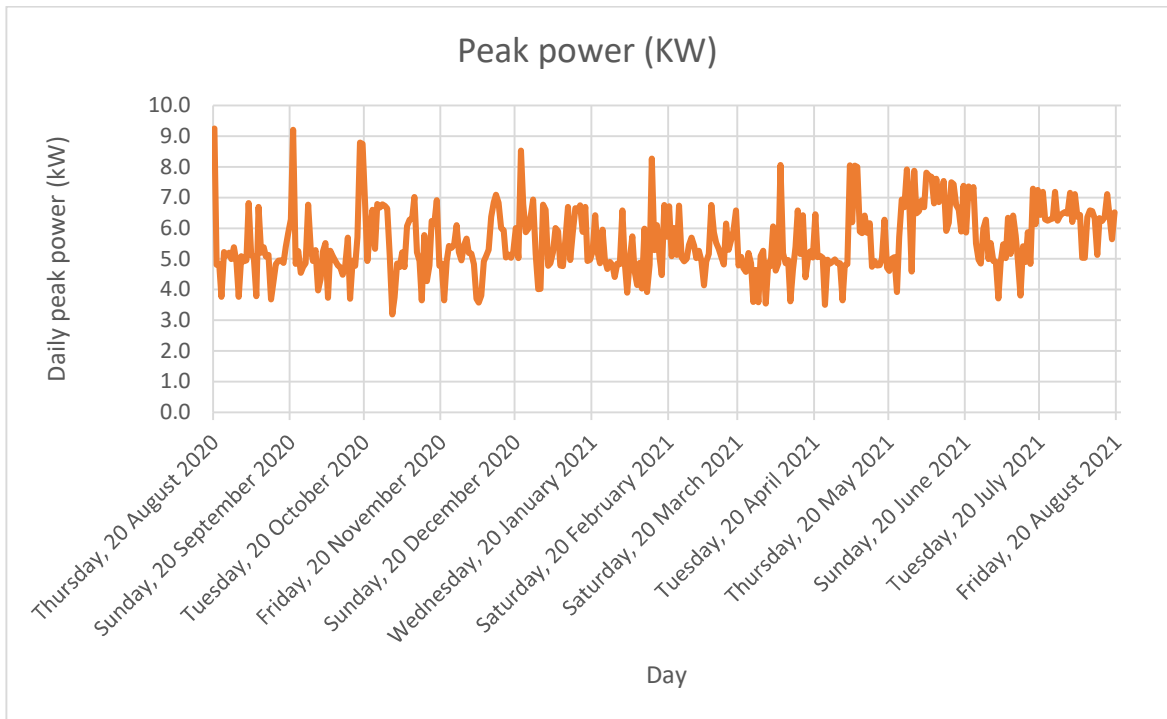Figure 4.3: Daily electricity usage (kWh)



Figure 4.4: Daily peak power

From Figure 4.3 and Figure 4.4, it can be concluded that high peaks are experienced during the week, and low peaks occur during the weekends. The daily average electricity usage was 27.4 kWh from the experimental recordings, while the daily peak power usage was recorded at 5.575 kW. The maximum daily electricity usage and peak power was recorded at 73.797 kWh and 9.249 kW, respectively.

### 4.3.2   Seasonal analysis

The yearly metered data was sampled through the year's four seasons, namely summer, autumn, spring, and winter. The y-axis is the electricity consumption in kW and the x-axis is the days/ months of the respective seasons. In addition, daily usage graphs of peak days of the seasons experienced in Botswana were prepared. A semi-arid climate throughout the year characterizes Botswana's weather; thus, it generally experiences summer and winter seasons. The summer period is from November to March and the winter period is from May to August. Figure 4.5 and Figure 4.6 depict the peak load profiles for summer and winter period, respectively.
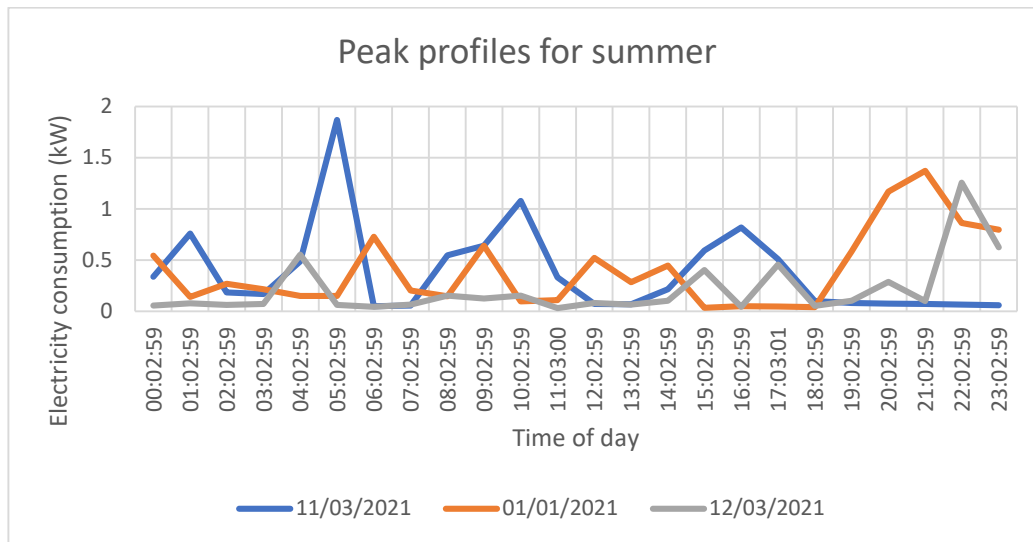


Figure 4.5: Peak hourly profiles during the summer period
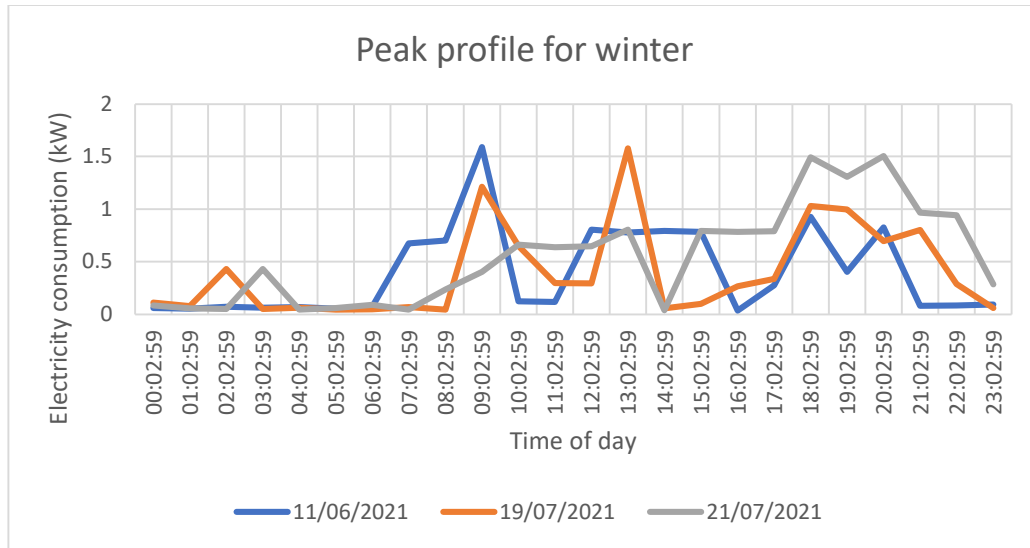
Figure 4.6: Peak hourly profiles during the winter season

The highest hourly peak electricity usage was recorded during the summer season, followed by the season winter. From Figure 4.5, the peak hourly usages are in the early mornings and late evenings. The winter season from Figure 4.6 indicates that the energy peaks occur late morning, early afternoon, and evening. Figure 4.7 provides a graphic description of the seasonal electricity usage by month in Botswana.



Figure 4.7: Seasonal electricity usage by months

The dataset was analyzed, and it revealed the following:

- The mean electricity consumption was recorded at 0.229563 kW in the summer season, with the maximum and minimum hourly usage at 1.87773 kW and 0.0144 kW, respectively. The total electricity consumption recor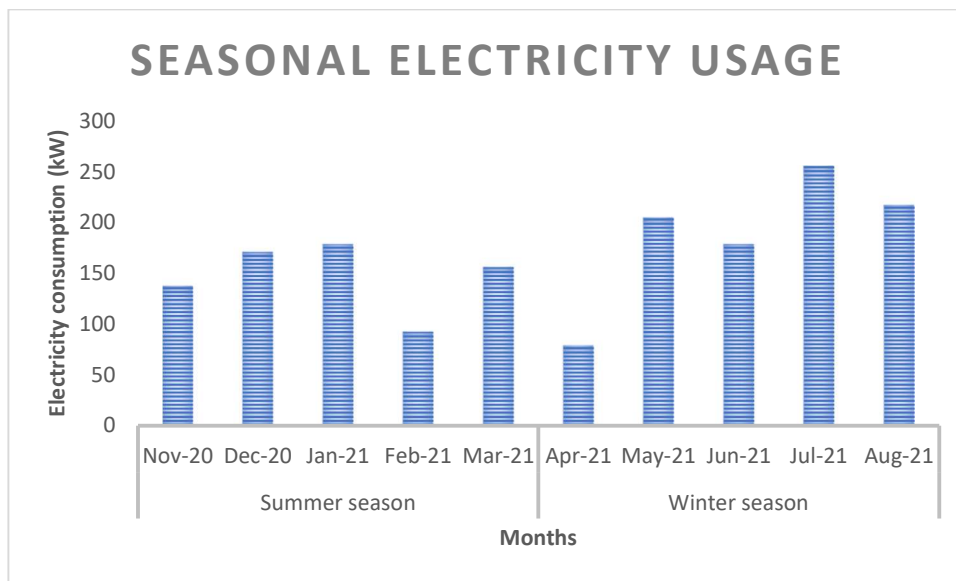ded was 831.9379 kW. Descriptive statistics reveal that the standard deviation and variance of the hourly metered data were found to be 0.233701 and 0.054616.

- In the winter season, the mean electricity was recorded at 0.281758 kW, with the maximum and minimum hourly usage was recorded at 2.88389 kW and 0.00975 kW, respectively. The total electricity consumption recorded was 966.992 kW. Descriptive statistics reveal that the standard deviation and variance of the hourly metered data were found to be 0.297272 and 0.08837.

The summer season was the highest amongst the other seasons regarding the total electricity usage per season in Botswana. High temperatures and rainfall characterize it, thus the increased use of air-conditioners during those months. In addition, the smart metering observation revealed a steep rise in the energy usage of air-conditioners during the summer period.

### 4.3.3    Electrical appliance profiles

The house in experimental study comprises a variety of electrical appliances. Still, due to budget constraints, energy measuring equipment was utilized for the significant energy-consuming devices, including the six air conditioners, lights, fridges, and washing machines. Below are the energy consumption profiles of the appliances.

### 4.3.3.1    Lights

The load profile of the lights in the residential household illustrates peaks in the late night and early morning, and troughs occur during daylight hours. Figure 4.8 is the typical daily profile (11th of March 2021) for the lights in the residential household.
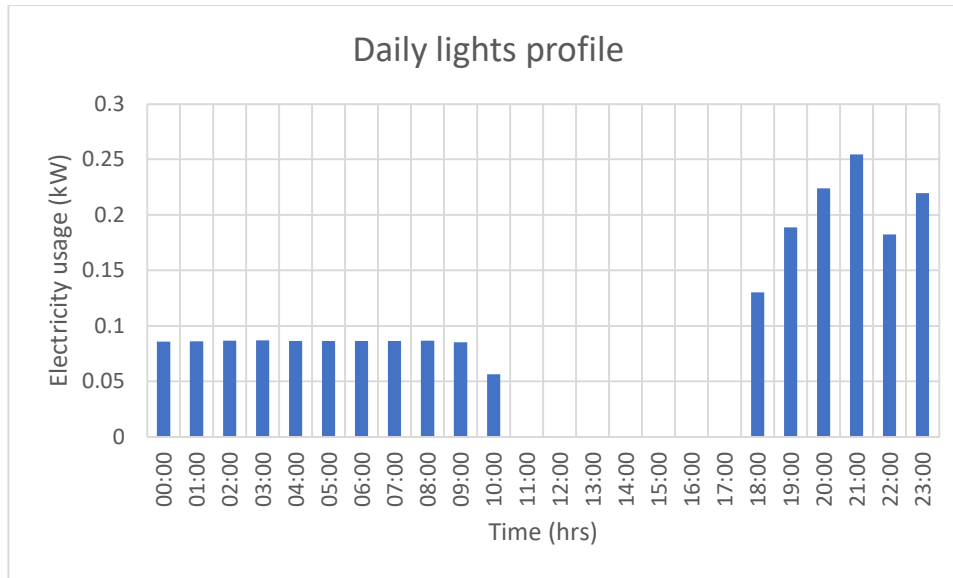
Figure 4.8: The energy load profile of the lights in the residential household

The load profile of the lights in the household reveals high usage at night and early morning. The more effective use was identified at night and the least between 733am and 1800pm due to daylight.


### 4.3.3.2   Geyser


The geyser is connected to a solar water heater with the electric heater as a backup. The usage in metering is electric hence the low electricity usage in the recording. Figure 4.9 is the typical daily load profile for the electrical appliance geyser.
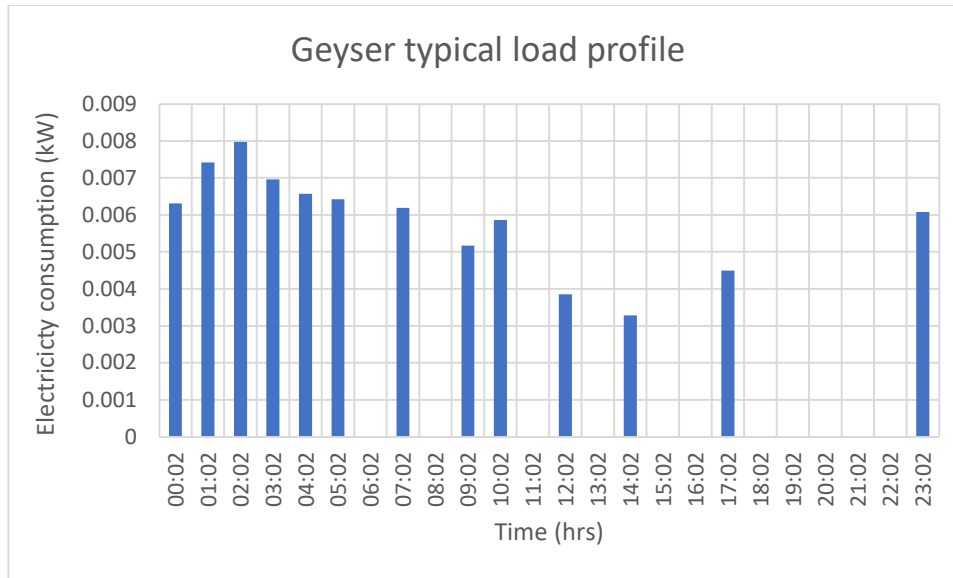
Figure 4.9: Typical load profile for the geyser

When the energy from the sun is low, the geyser extracts electrical energy through the home electrical wiring. The peaks have been seldom identified during midnight.

### 4.3.3.3    AC 1 (Sitting room)

The AC is in the sitting room hence the low usage because of factors such as daylight heating. Figure 4.10 represents a typical daily load profile for the AC situated in the sitting room.
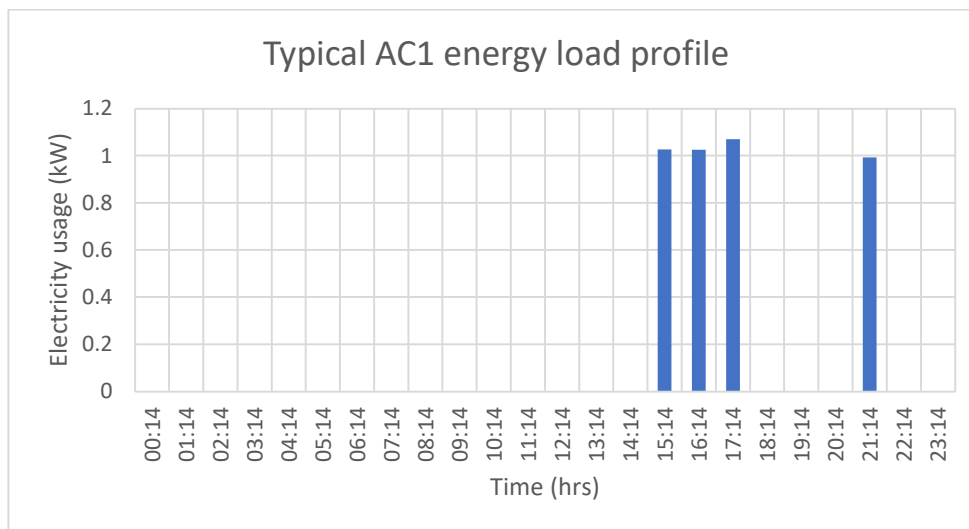


Figure 4.10: Typical load profile of AC1 situated in the sitting room

The profile is for the date 26$^{th}$ of December 2020, which is a summer month, thereby justifying the increased energy usage in the afternoon and late in the night.

### 4.3.3.4   AC 2 (Sitting room)
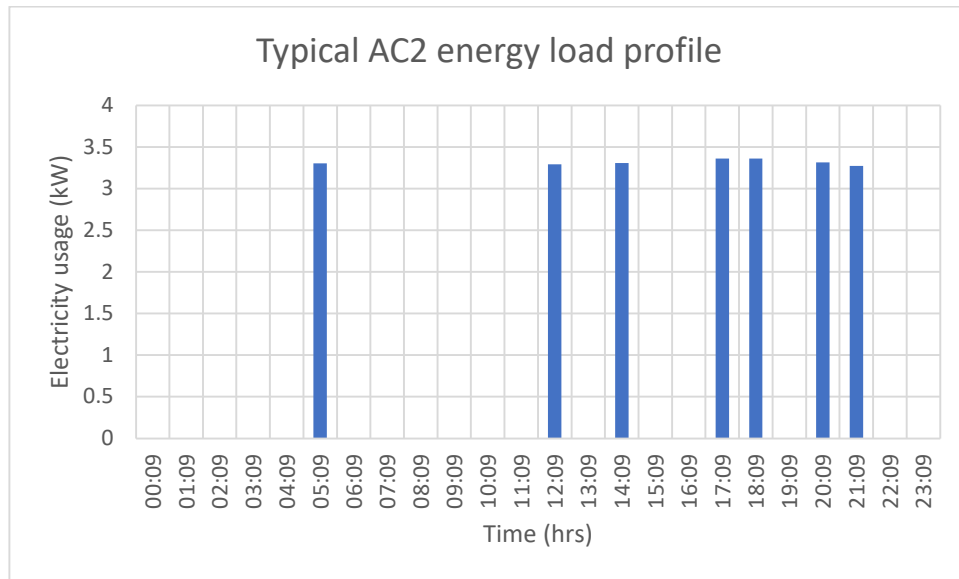


Figure 4.11: Typical load profile for AC2 situated in the sitting room

AC 2 is frequently utilized hence the continuous energy usage over time. The AC constitutes a significant percentage of the overall daily energy usage in the residential household. Figure 4.11 is a typical load profile for the date 12$^{th}$ of October 2020.

### 4.3.3.5   AC 3 (Master bedroom)

Figure 4.12 represents the daily load profile for the AC located in the master bedroom for the residential house in experimentation.
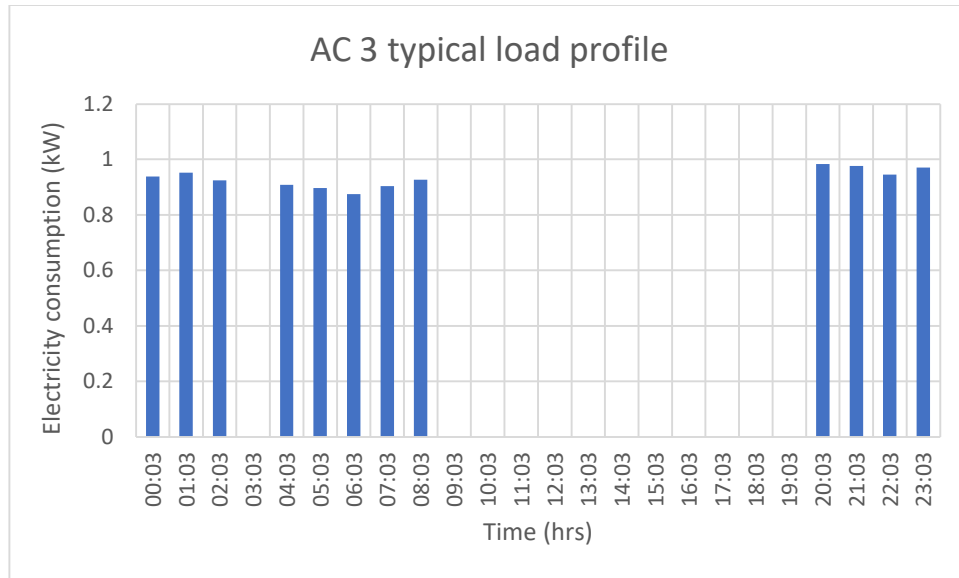
Figure 4.12: Typical energy load profile for AC3 situated in the Master bedroom

The typical energy usage by AC3 is defined by more significant energy peaks in the late evening toward midnight and lesser, more consistent peaks during the early mornings. The energy load profile extracted is for the 27th of September 2020.

### 4.3.3.6   Fridge and Washing machine

The measuring equipment attached to the fridge and washing machine is the two wireless ZigBee smart plugs. The recorded energy consumption data available on the dashboard indicates the total. The refrigerator runs throughout the day and weekly, while the washing machine is used sparingly throughout the week.
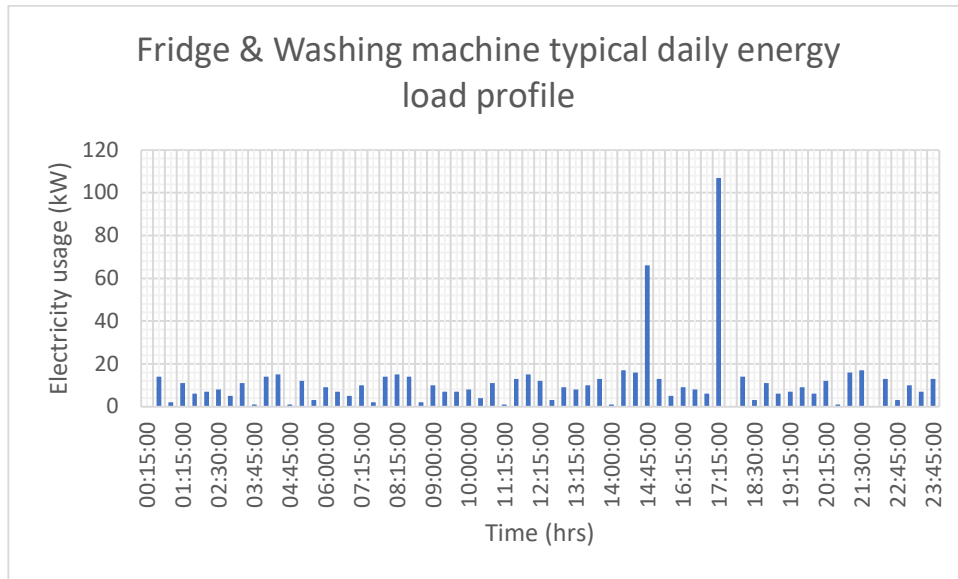
Figure 4.13: Load profile for the fridge and washing machine

The energy usage of the two appliances was combined in the output report. Figure 4.13 shows that the high energy spikes result from the use of the washing machine. The constant load during all the hours of the day indicates the energy usage of the fridge.

### 4.4    Descriptive and predictive analysis

The smart metering data was fed through descriptive and predictive analytics software programs to identify energy relationships through data science. The data analysis techniques include correlation, regression, and time series. Another technique for analyzing household load profiles through an unsupervised technique is clustering, which makes subsets of similar daily load profile households (Yildiz et al., 2017).

### 4.4.1    Clustering analysis

The purpose of clustering analysis is to perform load pattern grouping. The clustering analysis is a data mining technique used to characterize electricity consumption in

residential households (Amri et al. 2016). For the clustering analysis, the dataset was subjected under the following scenarios in Table 4.1:

Table 4.1: Methods of clustering classification

| Method | Number of clusters, iterations | Smallest MSE |
|---|---|---|
| 1. Iterate and classify with outliers | 3,10 | 0.364 |
| 2. Iterate and classify without outliers | 3,10 | 0.383 |
| 3. Iterate and classify with outliers | 5,20 | 0.466 |
| 4. Iterate and classify without outliers | 5,20 | 0.421 |

The dataset was fed through various k-means clustering methods to identify the best strategies that yielded the best load pattern grouping, representing a typical load of the house in the experiment. The hourly usage annual values were converted into variables for standardization before being fed into the clustering algorithm. The Z-score method of standardization involves subtracting the mean value for a field of values and dividing by the standard deviation. The Z-score indicates each score's position within the distribution of all scores. Method 4 yielded the best final cluster results in terms of the overall months of the year as the values were in the high positives. The other four methods yielded a similar MSE value with and without outliers. The optimum cluster number after various trails was identified to be three at an iteration figure of 10. The clusters displayed a good relationship between the 12 months of the year. Figure 4.14 depicts the final clustering centers of the monthly energy usage.
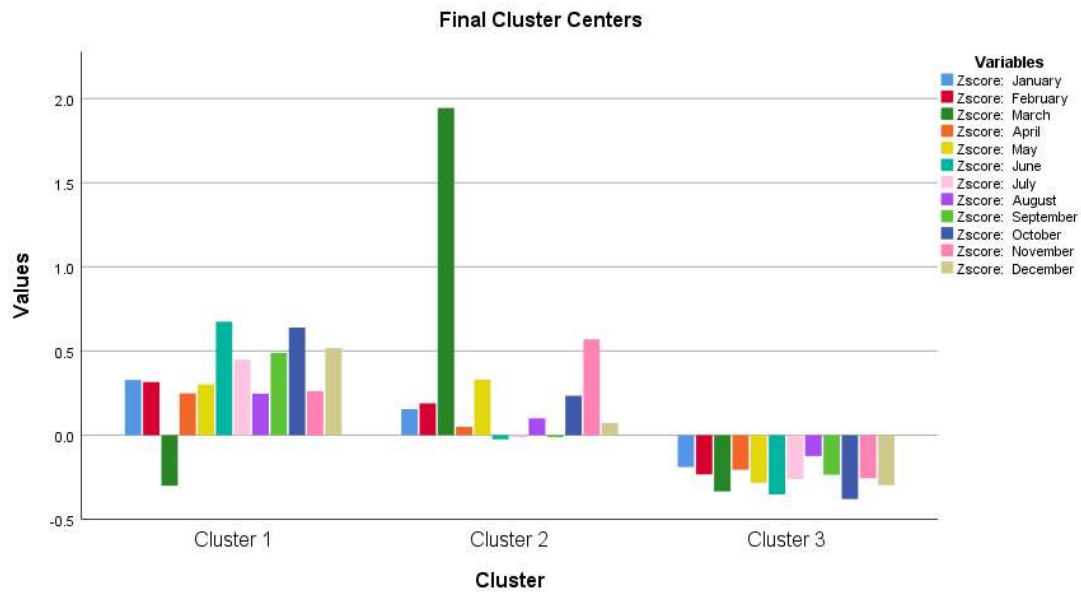
Figure 4.14: Final clustering centers of the monthly energy usage

Cluster 1 revealed the positive Z-score on the energy usage of 11 months of the year instead of the month of March. Cluster 2 revealed relatively low Z-scores amongst the most months of the year instead of the month of March. A distribution scale revealed a raw score for the month of March in cluster 2 of 1.8, which is around two Standard Deviations (SD) above the mean. The high Z-score indicates a strong correlation in March's hourly energy consumption. The dataset for that month can be used for additional data analysis approaches because the high correlation displays the most consistent daily energy usage patterns and has the potential for very accurate analysis. The mean square error was least for March at 0.364 amongst all the other months of the year. Cluster 3 reported negative Z-scores on hourly energy usage for the entire year. All the data for the months have significant value towards the cluster centers. The Euclidean distance between the three final cluster centers was minimal, thus displaying a high correlation between the individual data units. Figure 4.15 is a boxplot graph of the spread of cluster centers to the number of each cluster case.
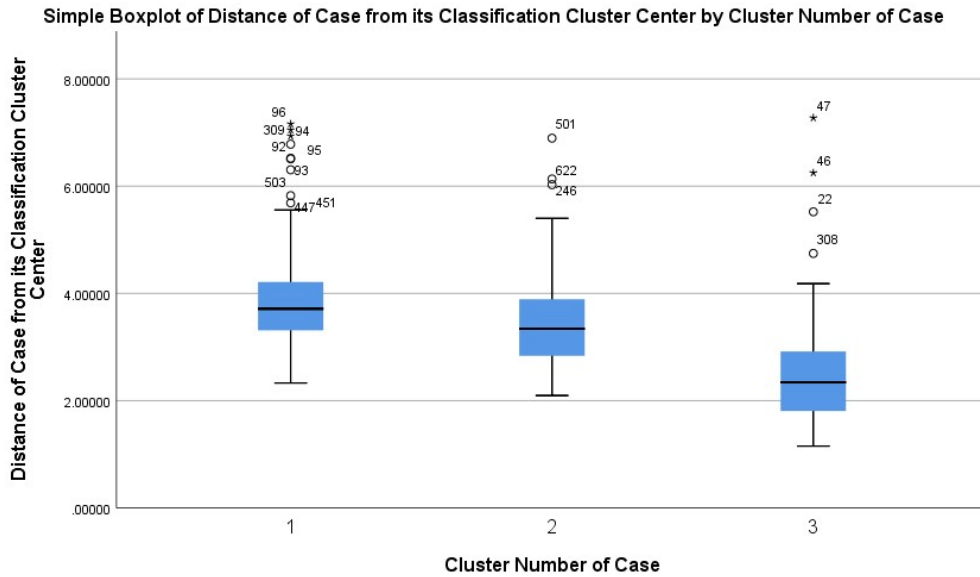
Figure 4.15: Boxplot of the cluster centers to the number of each cluster number case

From Figure 4.15, the outliers in cluster number case 1 were more prevalent than those followed by cluster 3 and, lastly, cluster 2. The similarity is low between the cluster number cases, and thereby the high cluster centers indicate high significance in the individual month's energy usage.

### 4.4.2 Time series analysis

The dataset of the annual energy usage was fed through a time-series modeler in the program SPSS. Figure 4.16 is the total daily and predicted energy usage for the whole year.
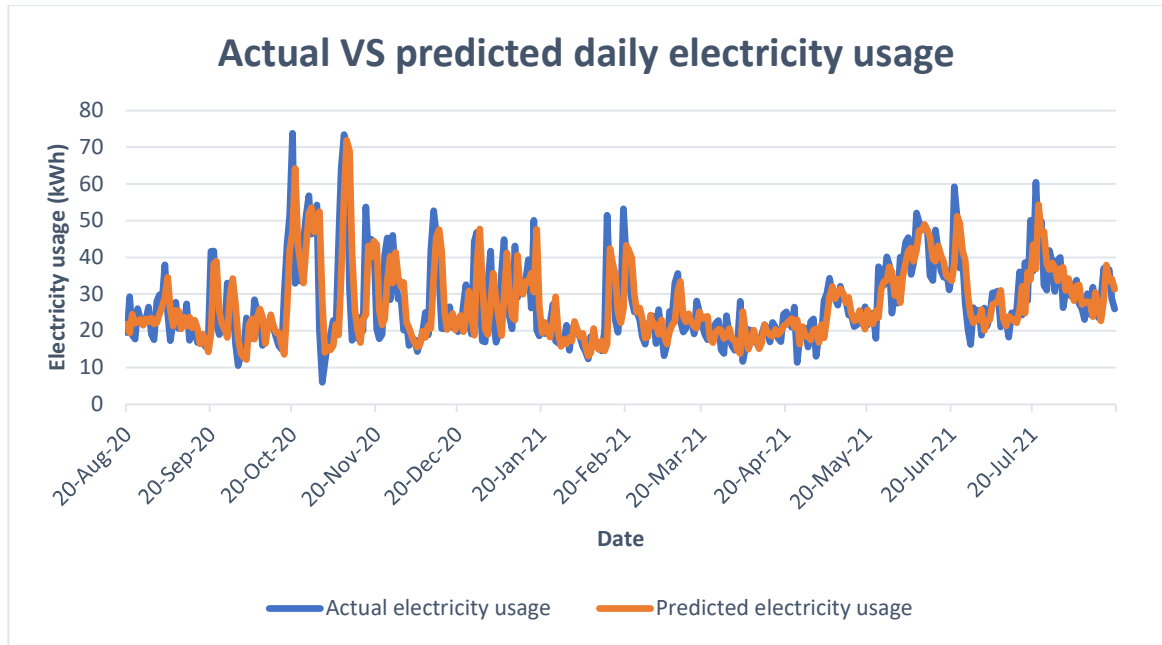
Figure 4.16: Observed vs. predicted electricity consumption

The dataset revealed a repeating cycle or trend in the daily electricity usage in the residential household. Analysis of the SPSS program revealed that the SARIMA model is the most accurate model for the dataset. The model statistics reveal that the RSME, MAPE, and $R^2$ were found at 8.432, 23.338, and 0.515. Furthermore, the descriptive statistics of the observed data indicate that the mean, maximum and minimum include 27.422 kWh, 73.80 kWh, and 6.08 kWh, respectively. On the other hand, the forecasted model statistics reveal the mean, top, and minimum energy usage as 27.34 kWh, 71.92 kWh, and 12.24 kWh, respectively. Therefore, the difference between the observed and the forecasted mean electricity usage was determined at approximately 0.3%, which is infinitesimal.

### 4.4.3    Linear regression

The linear regression analysis was utilized to identify the relationship between the parameters such as electricity usage and peak energy usage. The total daily energy usage and the peak daily usage were fed through a regression modeler to identify a relationship between the two parameters. The daily peak power is the predictor value, and the daily

electricity usage is the response variable. Table 4.2 represents the polynomial degree and their respective goodness of fit.

Table 4.2: Polynomial degree and goodness of fit

| Polynomial degree | R-square | RSME |
|---|---|---|
| 1 | 0.4427 | 8.33 |
| 2 | 0.4498 | 8.288 |
| 3 | 0.4847 | 8.032 |
| 4 | 0.4856 | 8.036 |
| 5 | 0.5005 | 7.93 |

Linear model Poly5:

$$f(x) = p1*x^5 + p2*x^4 + p3*x^3 + p4*x^2 + p5*x + p6 \qquad\qquad 4.1$$

Coefficients (with 95% confidence bounds):
    p1 =    0.2242 (0.08935, 0.359)
    p2 =     -6.9 (-11.11, -2.694)
    p3 =    82.27 (30.85, 133.7)
    p4 =    -474.6 (-782, -167.2)
    p5 =     1331 (433.5, 2230)
    p6 =    -1441 (-2465, -417.4)

Where p1, p2, p3, p4, p5, p6 represent the regression coefficients. From Table 4.2, it can be determined that the greater the polynomial degree, the greater the goodness of fit between the daily electricity usage and peak power. Figure 4.17 indicates a linear regression fit between electricity usage and peak power.
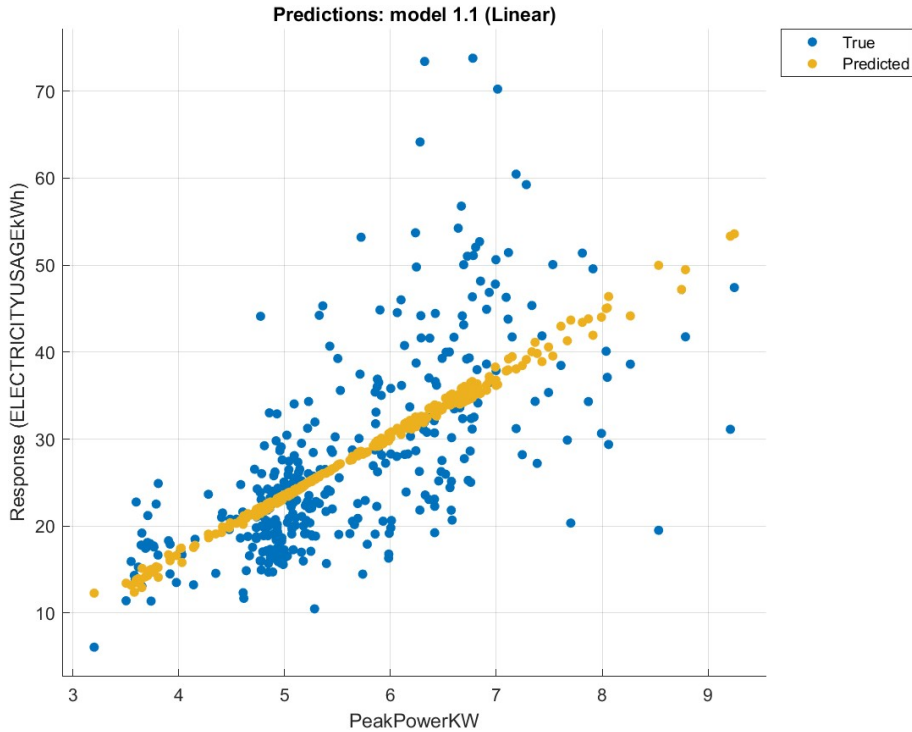
Figure 4.17: Linear prediction model utilizing electricity usage and peak power.

The dataset was imported into the Regression Modeler tool in the MATLAB modeling environment. The results of the trained model in the regression modeler tool revealed that the linear predictor was the best accurate model for the dataset. From Figure 4.17, there is a positive correlation between the daily electricity usage and the daily peak power. A linear model was used to estimate the response graph of the association between power usage and peak. Therefore, the prediction model fit can be utilized to forecast electricity usage. Furthermore, the model fit results indicate an RSME of 8.3442, which is reasonably low, thus informing the model's accuracy.

### 4.5    Single household PV system design on PVSyst

A 10 kW nominal power solar PV system was designed on the simulation environment; PV Syst. Simulation results of daily and annual generation were extracted

### 4.5.1   Design layout

The type of solar PV system is grid-connected with no battery support. The energy flow from the PV array travels through the inverter to the user, and excess power generated is stored in the utility grid for later usage. Figure 4.18 provides a system design schematic for a grid-connected solar PV system for a single household.



Figure 4.18:System design of the solar PV system

### 4.5.2   Energy yield production

The simulation was computed on the platform PVsyst for the annual energy yield of the planned 10 kW solar PV system. The maximum peak power recorded in the residential household was 9.212 kW; thus, a 10-kW peak solar PV system was designed. Table 4.3 represents the overall yearly PVSyst simulation results.

Table 4.3: PVSyst yearly simulation results

**New simulation variant**

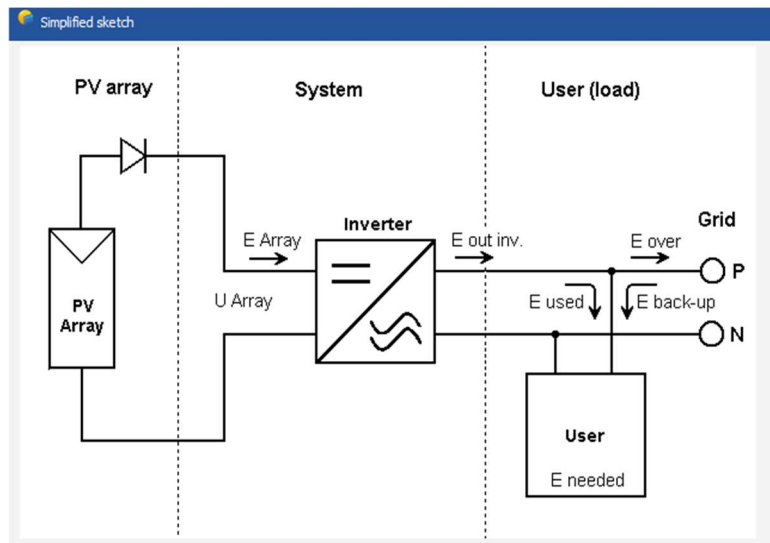| | GlobHor | DiffHor | T_Amb | GlobInc | GlobEff | EArray | E_User | E_Solar | E_Grid | EFrGrid |
|---|---|---|---|---|---|---|---|---|---|---|
| | kWh/m² | kWh/m² | °C | kWh/m² | kWh/m² | kWh | kWh | kWh | kWh | kWh |
| January | 190.2 | 78.65 | 25.83 | 242.7 | 225.1 | 1832 | 666.8 | 311.4 | 1457 | 355.4 |
| February | 164.6 | 74.53 | 25.11 | 209.2 | 194.7 | 1600 | 602.3 | 260.1 | 1285 | 342.2 |
| March | 177.5 | 66.14 | 23.93 | 235.2 | 217.1 | 1799 | 666.8 | 282.9 | 1455 | 383.9 |
| April | 160.4 | 47.54 | 21.51 | 221.6 | 203.3 | 1714 | 645.3 | 265.0 | 1392 | 380.3 |
| May | 153.5 | 30.03 | 18.05 | 223.7 | 202.2 | 1756 | 666.8 | 274.6 | 1425 | 392.2 |
| June | 136.4 | 25.04 | 15.13 | 203.0 | 180.6 | 1602 | 645.3 | 264.8 | 1286 | 380.5 |
| July | 146.0 | 25.74 | 14.48 | 215.3 | 192.2 | 1697 | 666.8 | 272.3 | 1370 | 394.5 |
| August | 167.8 | 34.43 | 18.58 | 235.4 | 217.1 | 1860 | 666.8 | 275.0 | 1524 | 391.8 |
| September | 184.9 | 47.91 | 22.14 | 255.7 | 234.5 | 1948 | 645.3 | 283.2 | 1599 | 362.1 |
| October | 187.9 | 58.64 | 25.60 | 257.3 | 234.7 | 1896 | 666.8 | 308.8 | 1522 | 358.0 |
| November | 185.4 | 84.55 | 25.22 | 235.8 | 218.8 | 1801 | 645.3 | 311.9 | 1429 | 333.4 |
| December | 189.1 | 86.03 | 25.54 | 237.1 | 221.7 | 1821 | 666.8 | 320.5 | 1439 | 346.3 |
| Year | 2043.7 | 659.22 | 21.74 | 2771.9 | 2542.0 | 21325 | 7851.1 | 3430.4 | 17184 | 4420.7 |

From Table 4.3, it can be identified that the highest energy solar yield was recorded from the months January, October, November, and December, which coincides with the highest monthly Global horizontal irradiation (GHI). Figure 4.19 depicts the reference incident energy received on the solar collector plane.
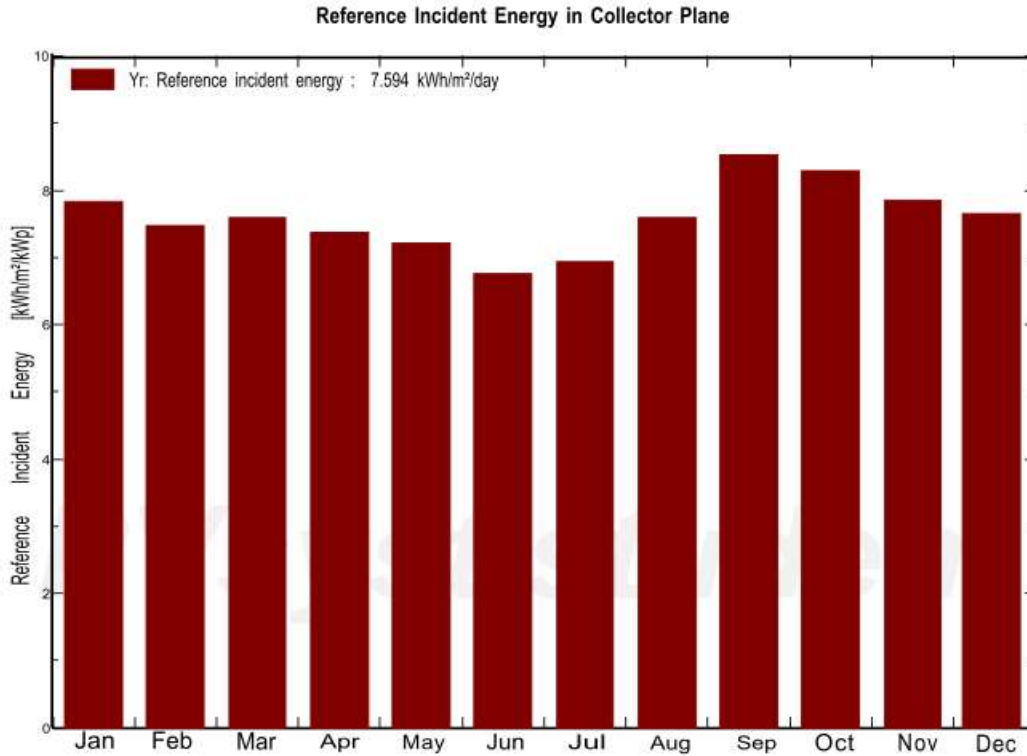
Figure 4.19: Reference incident energy on the solar collector plane

On a 10-kW solar PV system with scheduled electricity generation, the system produces an average monthly yield of 7.594 kWh/m2/day. The lowest outcomes were recorded during the winter months, when the monthly GHI was at its lowest. Of the solar PV system's normalized production (per installed kWp). The normalized energy production is depicted in Figure 4.20 (per installed kWp).
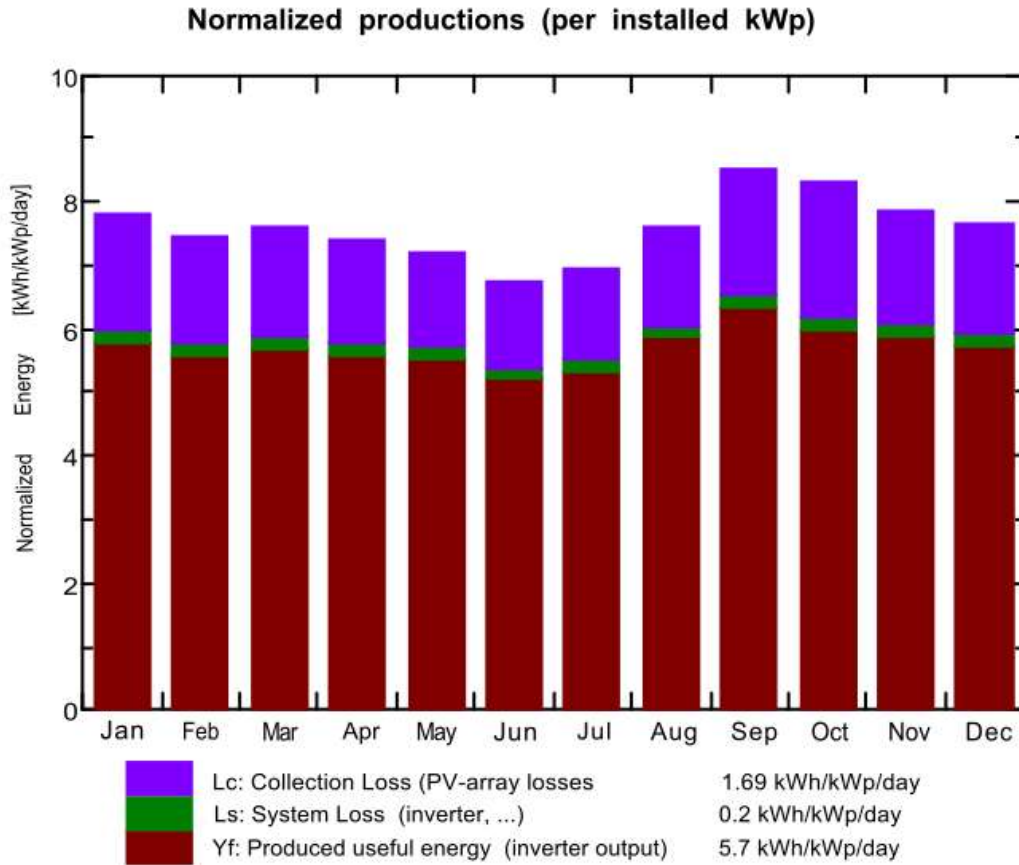
Figure 4.20: The normalized energy production (per installed kWp)

The system generates 5.7 kWh/kWp/day of peak usable energy. The PV array and system losses accounted for 1.69 kWh/kWp/day and 0.2 kWh/kWp/day, respectively, of the energy losses. The summer months which experience a higher GHI generate the higher solar PV power as compared to the winter months which receive a lesser GHI. Figure 4.21 represents the average monthly performance ratio for the solar PV system.
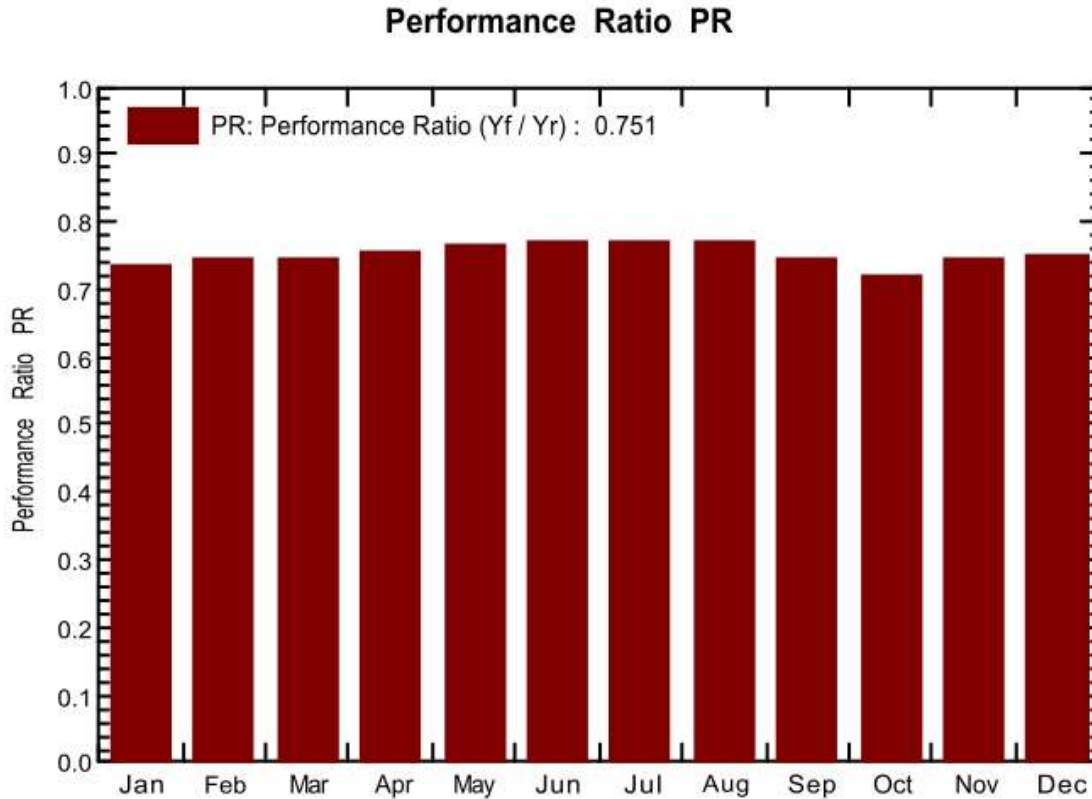
Figure 4.21: Performance ratio of the solar PV system

The solar PV system design achieves an average performance ratio of 75.1% across the monthly performance. The system performed best during the winter months compared to the summer months. Summer months in Botswana are characterized by very high temperatures, which affect the PV module efficiency, thus the lower performance of the solar PV system.

### 4.5.3   Energy losses

There are energy losses experienced in a solar PV system through individual components. Figure 4.22 shows the energy losses diagram for the solar PV system.

**Loss diagram for "New simulation variant"  -  year**

| | |
|---|---|
| 2044 kWh/m² | **Global horizontal irradiation** |
| +35.6% | **Global incident in coll. plane** |
| -7.5% | Near Shadings: irradiance loss |
| -0.9% | IAM factor on global |
| 2542 kWh/m² * 65 m² coll. | **Effective irradiation on collectors** |
| efficiency at STC = 15.15% | PV conversion |
| 25198 kWh | **Array nominal energy (at STC effic.)** |
| -0.1% | PV loss due to irradiance level |
| -13.0% | PV loss due to temperature |
| +0.8% | Module quality loss |
| -2.1% | Mismatch loss, modules and strings |
| -1.4% | Ohmic wiring loss |
| 21326 kWh | **Array virtual energy at MPP** |
| -3.3% | Inverter Loss during operation (efficiency) |
| 0.0% | Inverter Loss over nominal inv. power |
| 0.0% | Inverter Loss due to max. input current |
| 0.0% | Inverter Loss over nominal inv. voltage |
| 0.0% | Inverter Loss due to power threshold |
| 0.0% | Inverter Loss due to voltage threshold |
| 20614 kWh | **Available Energy at Inverter Output** |
| 17184 kWh | **Energy injected into grid** |

grid consumption

4421 kWh   3430 kWh   17184 kWh

to user          to user          to grid
from grid      from solar

Figure 4.22: Energy loss diagram of the solar PV system

The annual energy losses of the solar PV system are depicted in Figure 4.22. Inverter losses account for 3.3% during the standard operation of the solar PV system. The high temperatures experienced in Botswana led to PV power losses accounting for up to 13%.

## 4.6    Community solar PV microgrid system

The 250-kW planned power DC microgrid was designed on the software environment MATLAB/Simulink for both the island mode and grid-connected mode of operation. The

simulation was conducted for a single day to identify key performance parameters of the components of the microgrid system.

### 4.6.1    Island solar PV microgrid

The design of the island microgrid model includes a static load of 250 kW with sources as the solar PV system and the BESS. The load behavior of the loads was set to constant impedance.

#### 4.6.1.1    Solar irradiation profile

$W/m^2$ denotes the y-axis of the irradiation profile, and the x-axis is represented by time (hrs.).
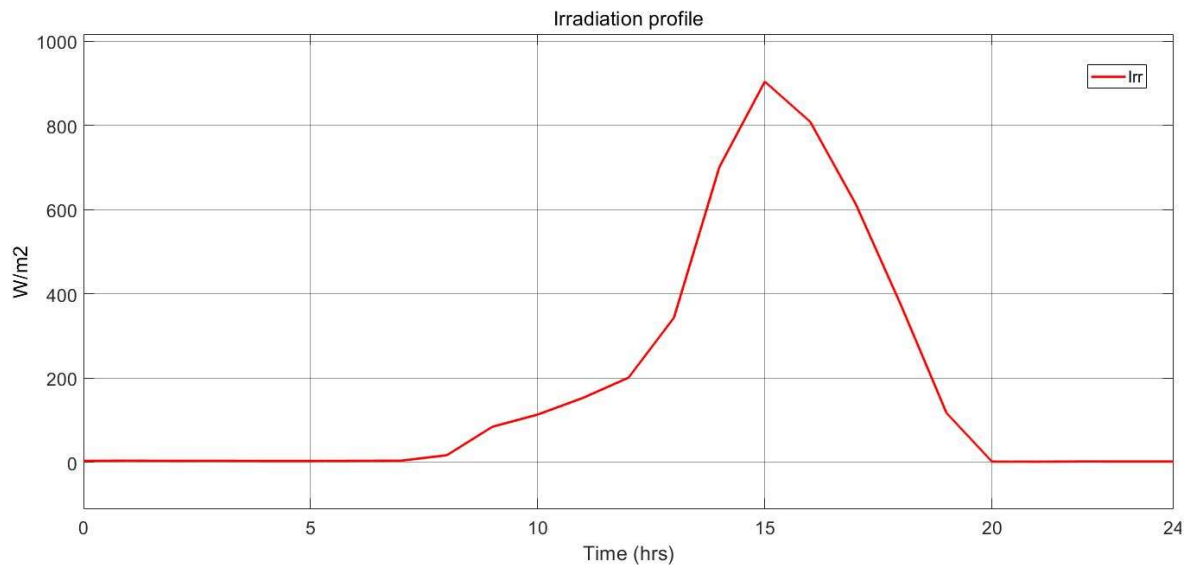


Figure 4.23: Solar irradiation profile

Figure 4.23 shows the irradiation profile for the village of Palapye, and the peak daily irradiation is experienced at 1500hrs. The daylight times are between the hours 0600hrs and 1900hrs.

### 4.6.1.2   DC bus voltage

The key objectives of the microgrid system design are to maintain a DC constant bus voltage of 835 V to meet the 250-kW static load demand. The system generated a maximum power of 224-kW during the peak solar radiation hours. Therefore, the y-axis of Figure 4.24 is denoted by Voltage (V), and the x-axis is indicated by time (hrs.).
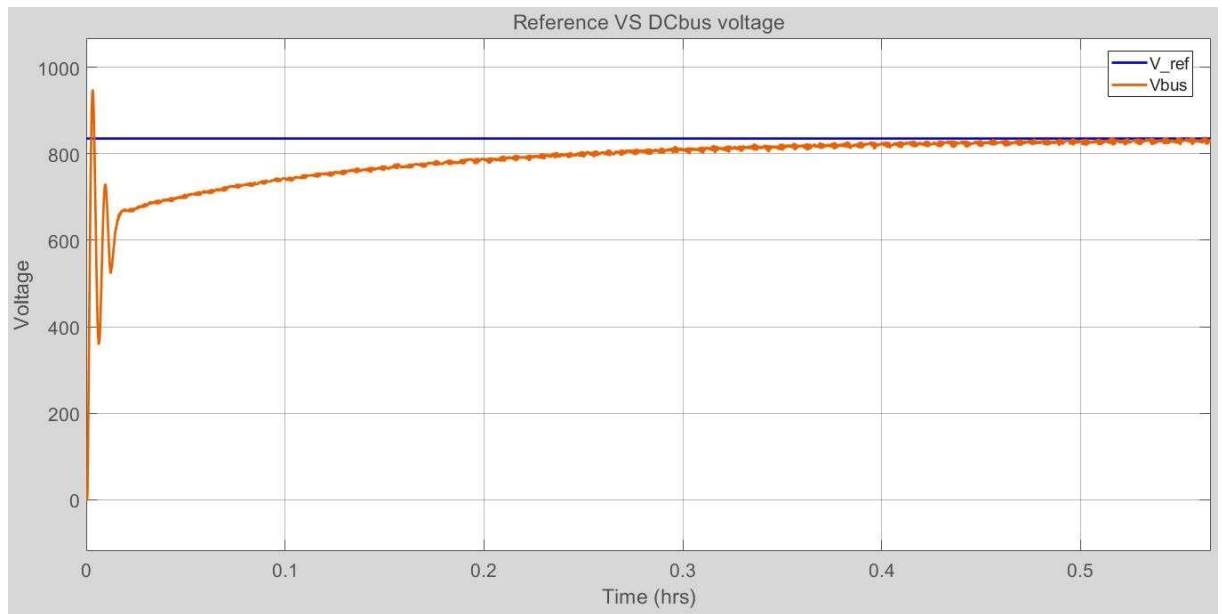


Figure 4.24: Microgrid DC bus voltage and the reference voltage

Figure 4.24 indicates that the PID control stabilized the system within approximately 0.4 hrs. and generated a constant DC bus voltage of 835 V.

### 4.6.1.3   Battery SOC

The y-axis in Figure 4.25 is represented by the battery SOC (%), and the x-axis is denoted by time (hrs.).
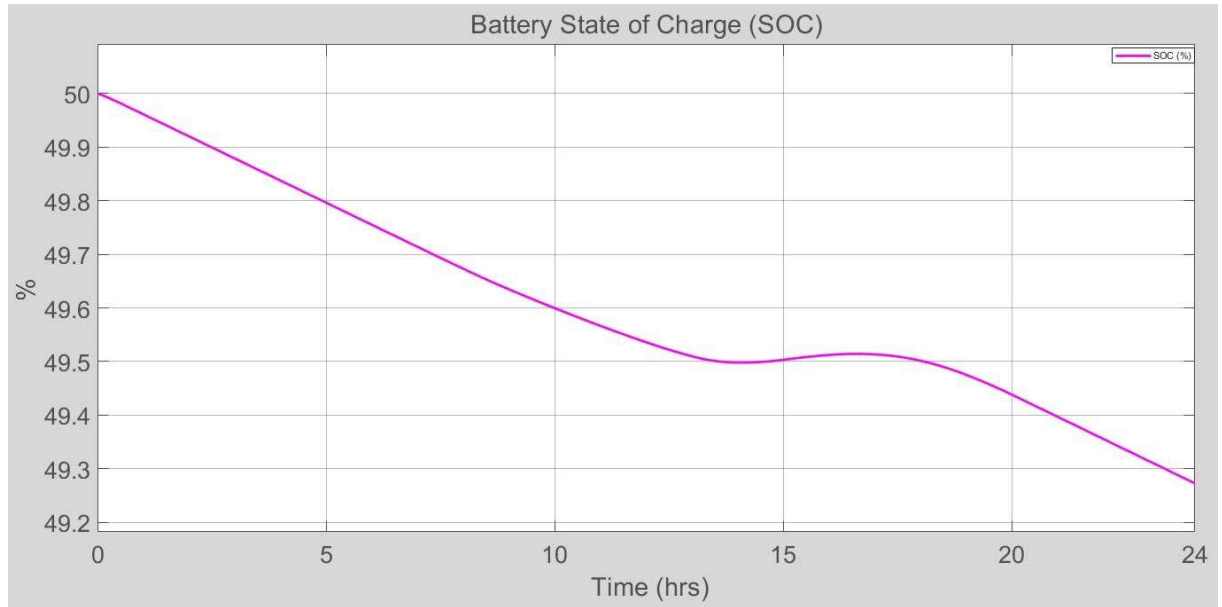
Figure 4.25: Battery SOC

From Figure 4.25, there is very minimal solar PV power generation during the early times of between 0000hrs and 0900hrs. Thereby, the battery discharges to maintain a constant DC bus voltage of 835 V. The hourly increase in sun irradiation received in the area causes a sharp increase in solar PV power generation between 0900 and 1500. The battery will not be depleted between 1400 and 1700 hours since the energy supply from the solar PV system meets the conditions of a required DC bus voltage of 835 V. Between the hours of 1700 and 2359, the battery begins to deplete again, which corresponds to a decrease in the power produced by the solar PV system.

### 4.6.1.4   Solar PV power generation

A graph of the ideal solar PV power generated, and the actual solar PV power generated was prepared. The y-axis of the Pideal and Ppv graph is represented by kW, and the x-axis is denoted by time (hrs.).
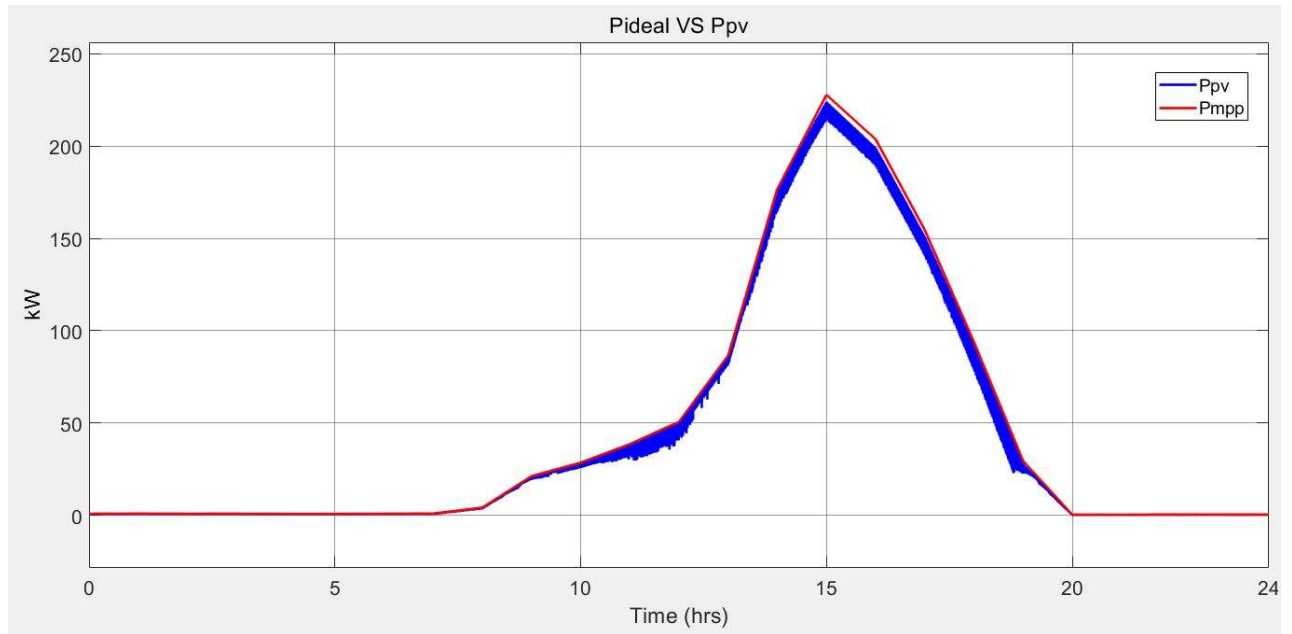
Figure 4.26: Ideal PV power versus actual PV power

Figure 4.26 indicates the correlation between the ideal solar PV power and the true PV power generated. The peak of the ideal PV and real PV power was determined at 222.5293 kW and 222.2798 kW during the peak solar irradiation time (1500hrs).

### 4.6.2    Grid-connected mode

The microgrid system was then simulated connected to the grid. The simulation was running for a single day (24hrs).

### 4.6.2.1    Power generation

During times of low solar power generation, the utility grid was supplying power to the electrical loads. Figure 4.27 provides a schematic of the PV power generated and the inverter's power along the y-axis as kW, and the x-axis is time (hrs).
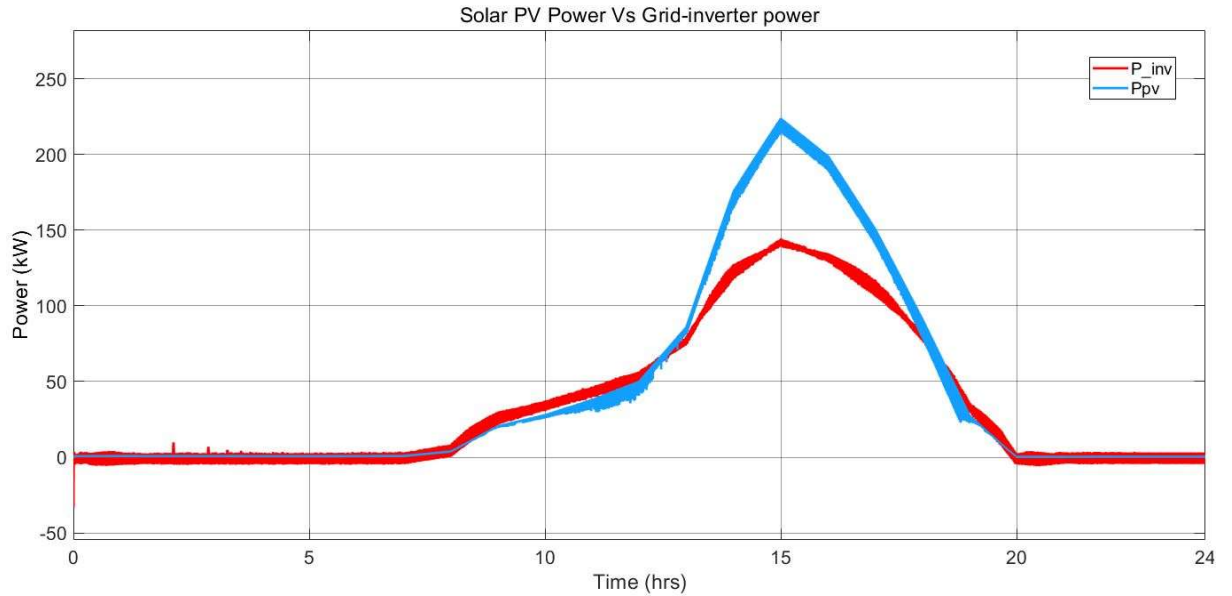
Figure 4.27: Graph of solar PV power produced and the active power of the inverter

From Figure 4.27, it can be identified that during high solar peak PV power generation, the solar PV system will be supplying power to the electrical loads without the assistance of the utility grid. Excess solar PV power generated is stored in the lithium-ion batteries. Between the hours 1100hrs and 1500hrs, there is a steep rise in solar PV power generation. Figure 4.28 depicts the DC bus voltage, and the PWM output waveforms of the inverter voltage with the y-axis as Voltage and the x-axis is time (hrs.).
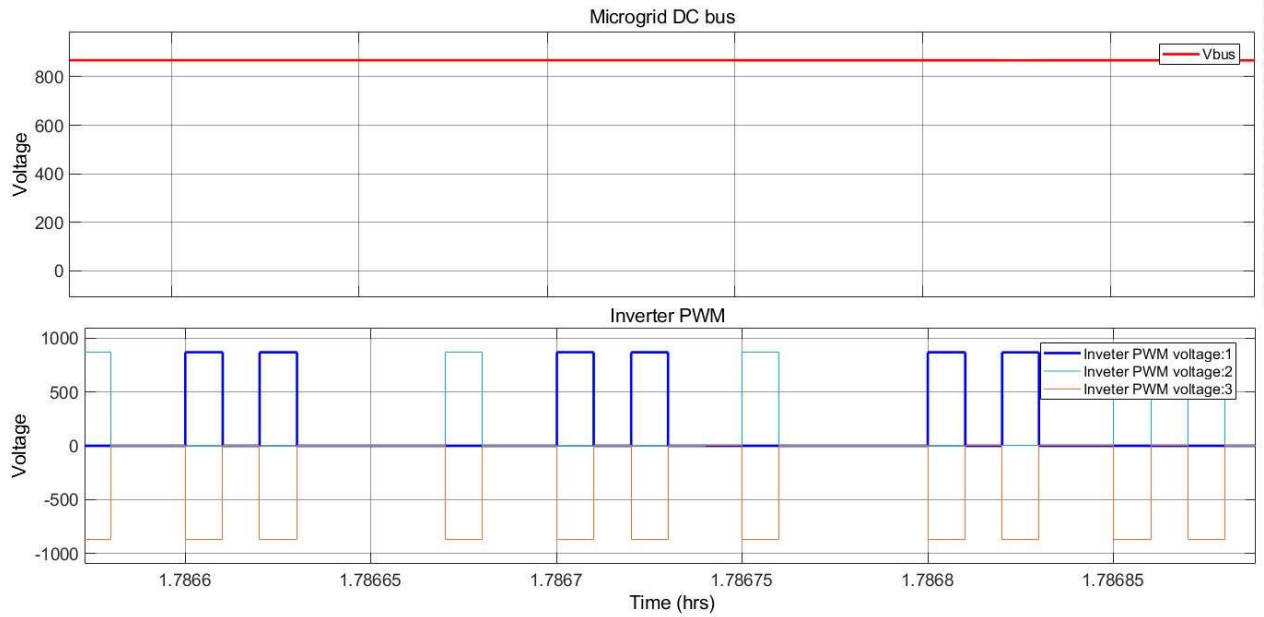
Figure 4.28: Snapshot of the DC bus voltage and the inverter PWM voltage

The solar PV system generated a DC-type power supply of 835 V. With a modulation index of 0.9, an output waveform was developed through the VSI with a peak of 835 V and a low of -835V.

### 4.6.2.2   Total harmonic distortion (THD)

Figure 4.29 depicts the THD experienced in the inverter-grid side current with % as the y-axis and time (hrs) as the x-axis.
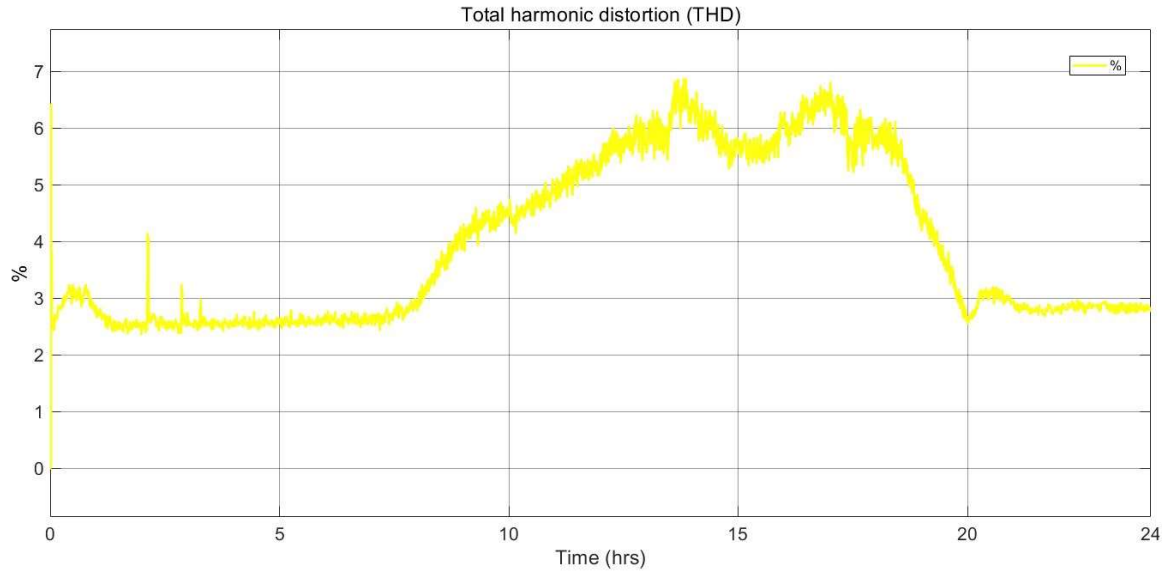
Figure 4.29: Total Harmonic distortion

From Figure 4.29, it can be identified that the THD generated peak was recorded at approximately 6.5% and the trough at 2.5%.

### 4.6.2.3   Inverter voltage

The grid and inverter output voltages are in phase. The LCL filter achieved the function of removing ripples in the output waveforms of the inverter voltage. Figure 4.30 shows a graph of the grid and inverter voltage waveforms with the y-axis as the Voltage (V) and the x-axis as the time (hrs.).
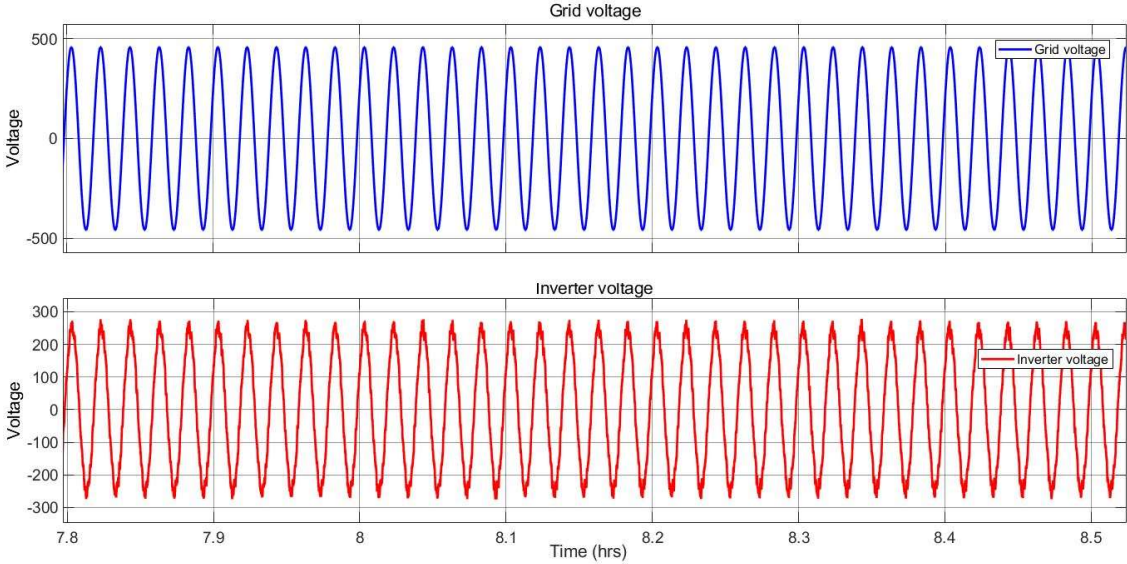
Figure 4.30: Snapshot of the grid and inverter voltage

4.7     Conclusion

Data analytics can infer the residential household energy characteristics. They reveal the behavior of occupants in a household throughout the year. The 12-month study was conducted during COVID-19; thus, a typical standard daily profile was not accurately identified. The frequent lockdowns impacted the energy usage behaviors of the working personnel and the school children. The K-means clustering analysis provided insights that 3 clusters with 20 iterations algorithm technique revealed the best electricity usage relationship between the 12 months of the year. The model fit could have been more accurate when the previous year's electricity consumption data was provided. The peak daily energy usage was utilized to size a grid-connected solar PV system for the metered house on the simulation platform PVSyst. The results from the simulation revealed that an average monthly yield of 7.594 kWh/m2/day. The simulation results showed an average monthly performance ratio of 75.1%, with the winter months generating a higher output than the summer months. The disparity is mainly due to the high temperatures experienced during the summer months that result in energy losses in the PV array. Simulations on MATLAB were conducted for a particular day to reveal the daily performance of the 250-kW community load solar PV microgrid system. The DG unit, solar PV system of the microgrid system generated a daily peak load of 224-kW during the peak solar irradiation hours. Through the support of the battery, the system could supply continuous power to the 250-kW load in the microgrid system. During the grid-connected mode of operation, the THD-generated peak was identified as approximately 7% and the least of 3%.

## 5 CHAPTER 5: MICROGRID SYSTEM OPTIMIZATION

### 5.1 Overview

This chapter outlines the control algorithms and techniques that ensure the efficient usage of power within the microgrid structure. The nature of solar as an intermittent source requires a smart energy management system to provide a constant supply of power to electrical loads in a microgrid community structure. Optimization of the microgrid system includes utilizing the fuzzy logic control (FLC) system to achieve the economic operation through the two microgrid operation modes and at a minimum required cost.

### 5.2 Introduction

Microgrid systems utilize an additional DG unit or an ESS to maintain the power balance supply in the microgrid system. A rapidly rising technique used in the optimization of a microgrid is machine learning. Machine learning through linear programming, effective energy management within the microgrid is accomplished through the scheduled economic dispatch and unit commitments of the microgrid components (Shrivastwa et al. 2019). Optimization models such as DER-CAM have been utilized to encompass mixed-integer linear programming (MILP) for microgrids with various energy types. Authors (Mashayekh et al. 2017), through MILP, use multi-modeling nodes for optimal siting of electrical and heating/cooling networks. Through linear programming, the community's standard and forecast load profiles will aid in the microgrid system's adequate sizing and design techniques through control algorithms. Another machine learning technique for the optimization model of microgrid energy management is dynamic programming. The FLC system is an alternative technique to utilize for energy management in microgrids instead of PID controllers. The FLC system can effectively manage the power flow between the components of the microgrid system through a set of governing rules (Al-Sakkaf et al. 2019). Multi-parameter dynamic programming can be utilized to optimize microgrids by addressing issues of non-linear loads and power supply intermittency of DG units (X. Wang et al. 2020). Through technology advancement, projections indicate that by 2050,

solar PV will be the cheapest source of power, with costs estimated at USD 0.014- 0.05/ kWh (IRENA 2019a). Solar PV microgrids are promising energy solution avenues for developing countries considering the high Global Horizontal Irradiation (GHI) values received in certain countries (Yekini et al. 2013).

### 5.3    Energy flow in microgrid system through fuzzy logic control

The solar PV system in the microgrid system plays the role of the primary energy provider to the electrical loads. The secondary is the surplus energy provider alongside the utility grid. A control system is utilized to manage the power flow of the microgrid system. The core aim of the control system is to maintain the desired DC bus voltage necessary for the continuous power supply to the electrical loads in a settlement. The energy flow in a grid-connected microgrid system occurs between the solar PV system, BESS, and the utility grid. Therefore, the primary energy supplier to the microgrid system is the solar PV system. The fuzzy logic control (FLC) algorithm was utilized to maintain power between the PV unit, battery, and utility grid. The FLC operates as a supervisory control to inform the charging and discharging of the battery depending on the amount of solar PV power generated (Anitha and Krishna 2015). Control systems are characterized by using one physical component to change another so that it exhibits desired attributes. The basic components of the FLC framework are a fuzzifier, a fuzzy inference engine in which the ruleset runs, and a defuzzifier. The FLC structure consists of crisp input quantities with either a value of 0 or 1 (Reyes-Garcia and Torres-Garcia 2022). The crispy quantities are transformed into fuzzy quantities throughout the fuzzification process. The elements of fuzzy quantities have a degree of membership in a set. The fuzzy logic utilizes a set of if-then rules to execute commands. The defuzzification process then converts the fuzzy quantities into crisps quantities. The defuzzification technique converts the fuzzy sets' membership degree into real values (Nebey 2020). The deffuzified values present as action commands in a control system. The FLC structure also comprises of input and output variables. Figure 5.1 shows a process flowchart of the fuzzy logic control structure.
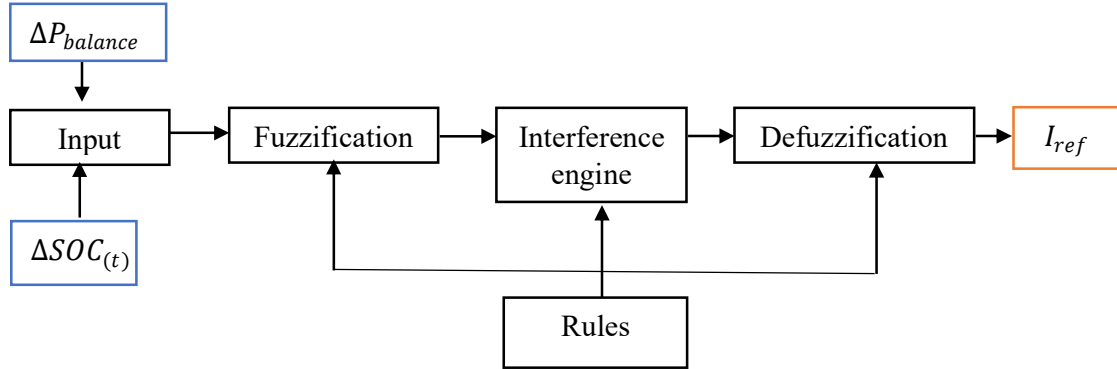
Figure 5.1: FLC structure

The input variables for the fuzzy logic will be the change in power and the change in battery SOC, while the output will be a current reference ($I_{ref}$). The current reference generated informs the grid-connected inverter to discharge power from the grid and when to charge the grid with the excess solar PV power produced. The primary purpose of the FLC is to maintain the desired DC bus voltage of 835V required by the loads. The current reference generated by the FLC sends a control signal to the components of the microgrid, such as a solar photovoltaic system, a battery, or an electric grid to discharge or charge power in the microgrid bus to achieve the desired bus voltage. The data range of the SOC of the battery is set as the input range of the desired. Equations 5.1 and 5.2 show the mathematical expressions for the input SOC.

$$SOC_{min} \leq SOC_{(t)} \leq SOC_{max} \qquad\qquad 5.1$$

$$\Delta SOC_{(t)} = SOC_{original(t)} - SOC_{now(t)} \qquad\qquad 5.2$$

Where $SOC_{min}$ and $SOC_{max}$ represent the minimum and maximum SOC of the battery. The charging and discharging of the battery are relative to the time of day. During night hours, when the solar PV generation is very minimal, the battery will supply the desired voltage of the DC microgrid. To determine the change in SOC ($\Delta SOC_{(t)}$), the difference

between the original SOC and the actual SOC of the battery is computed. Then, the power balance Equation is expressed mathematically in Equation 5.3:

$$\Delta P_{balance} = P_{pv} - P_{load} \qquad\qquad 5.3$$

Where $P_{pv}$ and $P_{load}$ represent the solar PV power generated and the load demand power, respectively. Where $\Delta P_{balance}$ represents the power balance in the microgrid system. When the $\Delta P_{balance}$ is positive, excess solar PV power is used to charge the battery. The extra electricity generated by the solar PV system is fed into the grid once the battery is fully charged. The fuzzification process involves converting a crips input into a linguistic variable as per the assigned membership functions. The range of values of the inputs was given membership function terms to enable the rules execution of the logic algorithm.

Table 5.1: Membership functions of fuzzy variables

| Membership function terms | Meaning |
|---|---|
| NB | Negative big |
| NS | Negative small |
| ZO | Zero |
| PS | Positive small |
| PB | Positive big |

### 5.3.1 Rules

The interference engine is instructed by a list of rules that occur based on IF statements between the two inputs being $\Delta P_{balance}$ & $\Delta SOC_{(t)}$. Table 5.2 illustrates the list of rules for the FLC algorithm.

Table 5.2: List of the 25 rules for the FLC

| Rule# | $\Delta P_{balance}$ & $\Delta SOC_{(t)}$ | $I_{ref}$ |
|---|---|---|
| 1 | If $\Delta P_{balance}$ is NB & $\Delta SOC_{(t)}$ is NB | Then Iref is PB |
| 2 | If $\Delta P_{balance}$ is NB & $\Delta SOC_{(t)}$ is NS | Then Iref is PB |
| 3 | If $\Delta P_{balance}$ is NB & $\Delta SOC_{(t)}$ is ZO | Then Iref is ZO |
| 4 | If $\Delta P_{balance}$ is NB & $\Delta SOC_{(t)}$ is PS | Then Iref is NS |
| 5 | If $\Delta P_{balance}$ is NB & $\Delta SOC_{(t)}$ is PB | Then Iref is NB |
| 6 | If $\Delta P_{balance}$ is NS & $\Delta SOC_{(t)}$ is NB | Then Iref is PB |
| 7 | If $\Delta P_{balance}$ is NS & $\Delta SOC_{(t)}$ is NS | Then Iref is PB |
| 8 | If $\Delta P_{balance}$ is NS & $\Delta SOC_{(t)}$ is ZO | Then Iref is ZO |
| 9 | If $\Delta P_{balance}$ is NS & $\Delta SOC_{(t)}$ is PS | Then Iref is NS |
| 10 | If $\Delta P_{balance}$ is NS & $\Delta SOC_{(t)}$ is PB | Then Iref is NB |
| 11 | If $\Delta P_{balance}$ is ZO & $\Delta SOC_{(t)}$ is NB | Then Iref is PB |
| 12 | If $\Delta P_{balance}$ is ZO & $\Delta SOC_{(t)}$ is NS | Then Iref is PS |
| 13 | If $\Delta P_{balance}$ is ZO & $\Delta SOC_{(t)}$ is ZO | Then Iref is ZO |
| 14 | If $\Delta P_{balance}$ is ZO & $\Delta SOC_{(t)}$ is PS | Then Iref is NS |
| 15 | If $\Delta P_{balance}$ is ZO & $\Delta SOC_{(t)}$ is PB | Then Iref is NB |
| 16 | If $\Delta P_{balance}$ is PS & $\Delta SOC_{(t)}$ is NB | Then Iref is PB |
| 17 | If $\Delta P_{balance}$ is PS & $\Delta SOC_{(t)}$ is NS | Then Iref is PS |
| 18 | If $\Delta P_{balance}$ is PS & $\Delta SOC_{(t)}$ is ZO | Then Iref is PS |
| 19 | If $\Delta P_{balance}$ is PS & $\Delta SOC_{(t)}$ is PS | Then Iref is NS |
| 20 | If $\Delta P_{balance}$ is PS & $\Delta SOC_{(t)}$ is PB | Then Iref is NB |
| 21 | If $\Delta P_{balance}$ is PB & $\Delta SOC_{(t)}$ is NB | Then Iref is PB |
| 22 | If $\Delta P_{balance}$ is PB & $\Delta SOC_{(t)}$ is NS | Then Iref is PB |
| 23 | If $\Delta P_{balance}$ is PB & $\Delta SOC_{(t)}$ is ZO | Then Iref is PB |
| 24 | If $\Delta P_{balance}$ is PB & $\Delta SOC_{(t)}$ is PS | Then Iref is PB |
| 25 | If $\Delta P_{balance}$ is PB & $\Delta SOC_{(t)}$ is PB | Then Iref is PB |

The result of the $\Delta P_{balance}$ and $\Delta SOC_{(t)}$ generates a signal to the grid-connected inverter to relay the power exchange between the microgrid and the grid. As a result, during high peak solar generation hours, the battery SOC increases, and the PCC is disconnected. Still, during low solar generation hours, the grid supplies energy to the electrical loads while charging the battery.

### 5.4    Simulation Overview

The y-axis of Figure 5.2 in the battery SOC graph is denoted by % (percentage) and the x-axis as the time (hrs.). Likewise, the y-axis of Figure 5.2 of the solar PV generation (Ppv) is denoted by kW, and the x-axis is represented by time(hrs.).
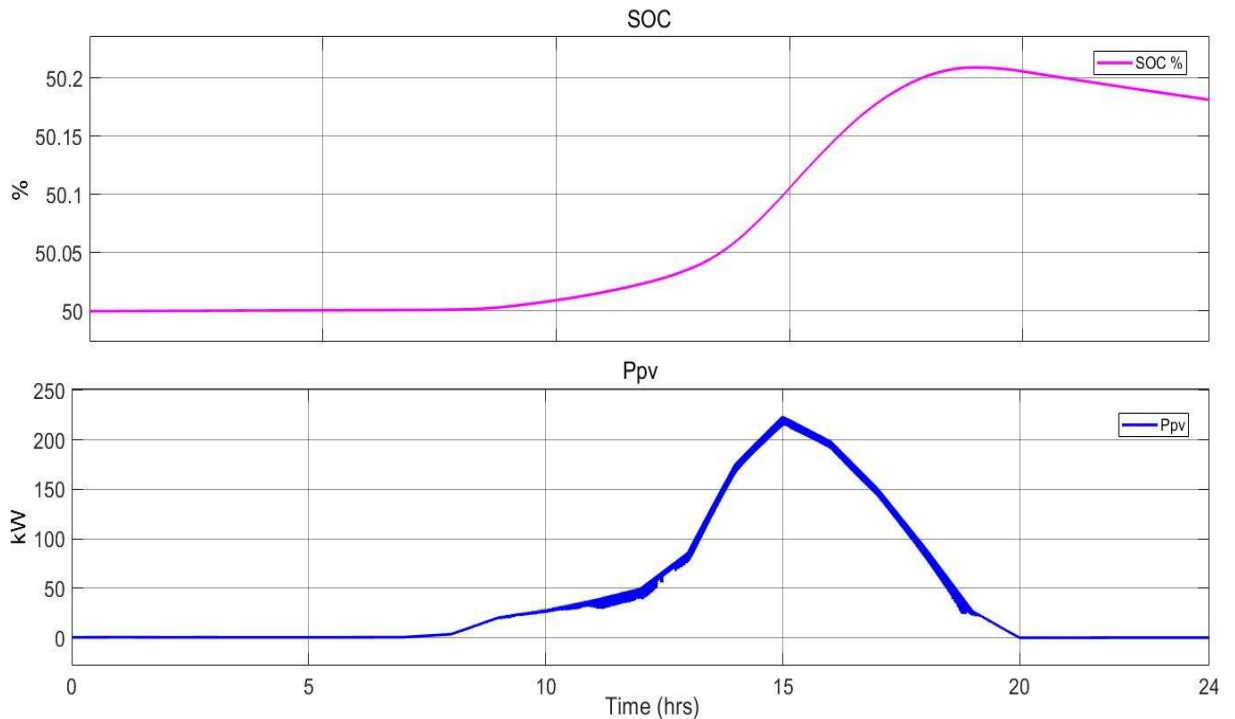


Figure 5.2: Daily PV power generated and the battery SOC

From Figure 5.2, the FLC algorithm is designed. During low solar PV power generation, the utility grid provides power to the electrical loads while charging the battery. The battery serves the function of stabilizing the DC bus voltage during the transition from

island mode and grid-connected mode for the microgrid system. Between the time 1400hrs and 1600hrs, the microgrid system will be operating in island mode with battery support. From 1600hrs, when the solar PV power generation decreases, the battery provides auxiliary power to the electrical loads as the connection to the utility grid is re-established. The y-axis of Figure 5.3 is denoted by Current (C), and the x-axis is represented by time(hrs.).
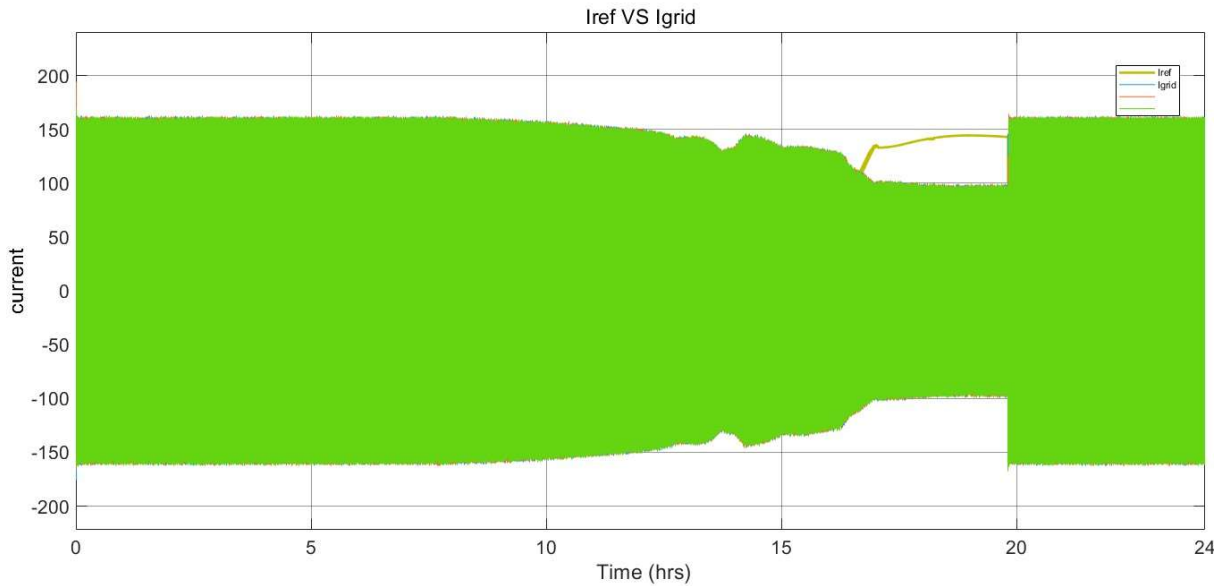


Figure 5.3: Grid-connected inverter current and reference current signal

From Figure 5.3, there are periods of the day when the grid-connected inverter current was the same as the load current, meaning that the microgrid system was operating in the grid-connected mode. The system was in island mode between 1000hrs and 2000hrs because the times of day corresponded with the peak solar irradiation hours. Therefore, the y-axis of Figure 5.4 is denoted by Power (kW), and the x-axis is represented by time (hrs.).
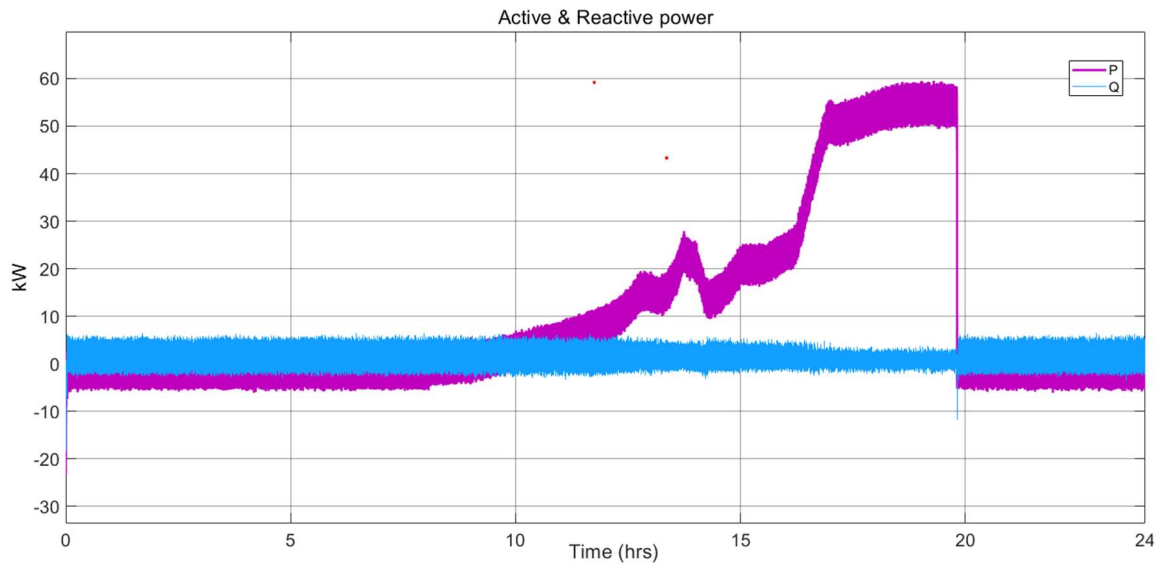
Figure 5.4: The active and reactive power of the grid-connected inverter

From Figure 5.4, there is an uptake of power into the grid during periods when the solar PV generation was high. Excess power generated from the solar PV system was fed into the grid. The steep rise active power at 1600hrs is a combination of the solar PV power and battery power discharge into the grid-inverter. Thereafter at 2000hrs when the solar PV power generation was least, the microgrid system began to operate in grid-connected mode of operation. The y-axis of Figure 5.5 is denoted by percentage (%), and the x-axis is represented by time (hrs.).
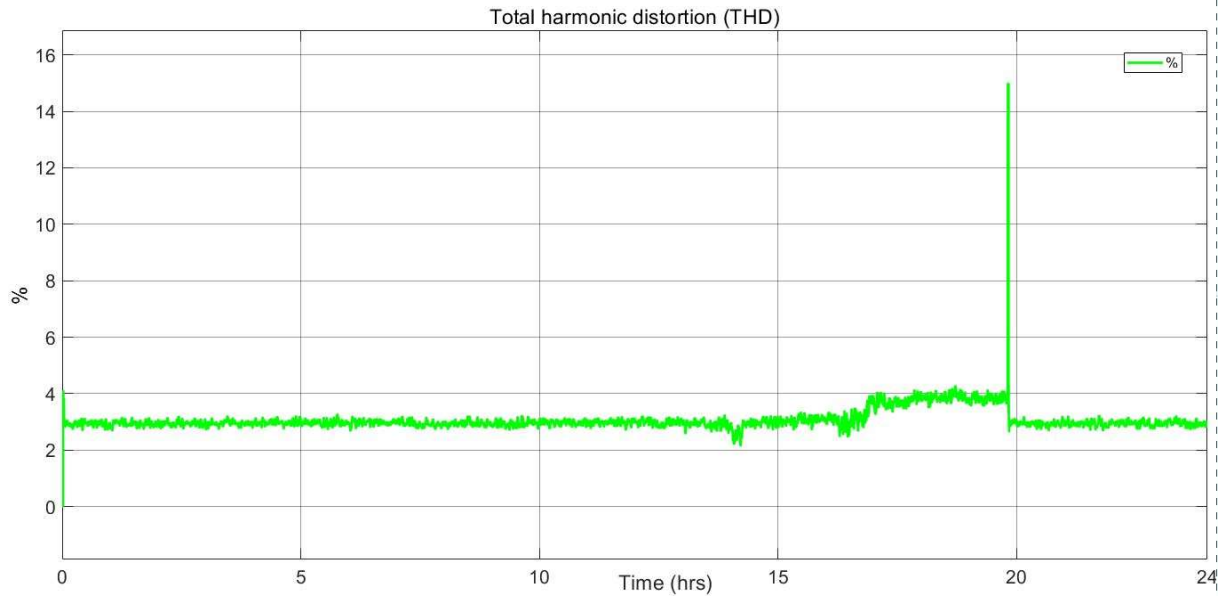
Figure 5.5: THD of the solar PV microgrid system

Figure 5.5 provides a schematic of the THD of the inverter-side current with the average percentages recorded at approximately 3%. By optimizing the microgrid system through FLC, the generated THD was more stable and closer to the allowable THD within 5% as per IEEE-519 standard.

## 5.5    Conclusion

The optimization technique for a grid-connected solar PV microgrid with battery storage is described in this chapter. The strategy incorporates the usage of the fuzzy logic system to perform energy management functions in the microgrid structure. The inputs of the FLC are changes in SOC and power balance in the microgrid system. The simulation analysis shows that the microgrid system operates in the grid-connected mode during low solar PV power generation. The battery provides stability to the DC microgrid voltage during the transition between the two modes of operation. However, during periods of the day when the solar PV power generation is high, the microgrid system will be operating in an island model. Based on the availability of electricity in the system for electrical loads, the FLC algorithm may provide a current reference signal that instructs when the microgrid system will run in either island or grid-connected mode. The optimization through FLC revealed a more stable THD with minimal spikes; thus, it enhanced the stability of the microgrid system.

# 6    CHAPTER 6: ECONOMIC ANALYSIS IN HOMERPRO

## 6.1    Overview

The simulation of the designed solar PV microgrid on the software environment HOMERPro is included in this chapter. A cost summary of the 250-kW planned microgrid system is prepared.

## 6.2    Introduction

The components of the microgrid system, which include the solar PV system and battery, have initial capital costs. Therefore, the system sizing and design were fed through the software environment HOMERPro to analyze the cost analysis of the proposed system. HOMERPro is an industry-leading software in the design and optimization modeling of microgrid systems. It also examines the economic feasibility design by conducting a cost analysis of the microgrid system in design.

## 6.3    System design

The system comprises a 250-kW planned power solar PV system, a 100-kWh lithium-ion battery
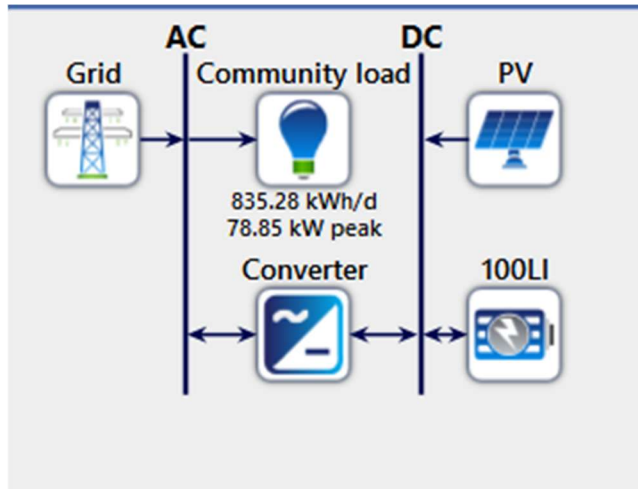
Figure 6.1: Microgrid system design

## 6.4    Initial capital costs

The costs of a solar PV system have significantly depreciated over the past decade by improving technology and competitive supply chains (IRENA 2019b).

### 6.4.1    Solar PV system

The total installed costs for solar PV systems are USD 995/ kW. The fee includes solar PV modules, charge controllers, and boost converters (IRENA 2019b).

Table 6.1: Cost specifications for a 250-kW solar PV system

| Architecture/PV (kW) | PV/Capital Cost ($) | Cost/Initial capital ($) | PV/Capital Cost ($) |
|---|---|---|---|
| 249.3906308 | 3274.807 | 551229.3 | 249390.6 |

### 6.4.2    Battery

The average capital cost of a 4hr lithium-Ion battery is estimated at USD 400/kWh (Cole, Frazier, and Augistine 2021). Therefore, the total costs for a 100-kWh lithium-Ion battery will be calculated at USD 40,000.00.

Table 6.2: Battery usage specification

| 100LI/Autonomy (hr) | 100LI/Nominal Capacity (kWh) | 100LI/Usable Nominal Capacity (kWh) |
|---|---|---|
| 2.298639 | 100.0002 | 80.00016 |

From Table *6.2*, it can be identified that the usable nominal capacity of the 100-kWh lithium-Ion battery was set at 80.00016 kWh. Therefore, the battery system is operated for 2.298639 hr. in a single day.

### 6.5    Energy calculations

Table 6.3: Energy purchased and energy sold to the grid

| Grid/Energy Purchased (kWh) | Grid/Energy Sold (kWh) | Energy balance (kWh) |
|---|---|---|
| 168197.3 | 267445.9 | 99248.6 |
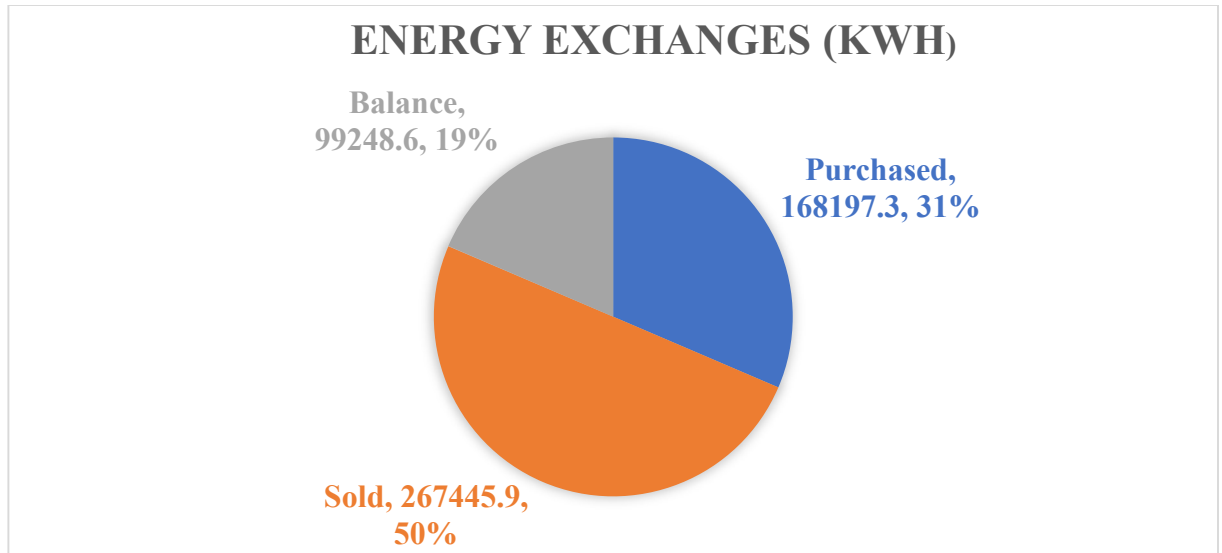
Figure 6.2: Energy exchanges between the grid and microgrid

### 6.6    Levelized Cost of Electricity (LCOE)

Based on how much energy is generated and sold to the utility grid, a cost analysis component is determined, namely the Levelized Cost of Energy (LCOE). Equation 6.1 represents the expression for the LCOE.

$$LCOE = \frac{Total\ life\ cycle\ cost}{Total\ lifetime\ power\ produced} \qquad 6.1$$

$$LCOE = \frac{\$10.90}{kWh}(base\ cost)$$

### 6.7    Net present cost

A net present cost is an economic tool representing the installation and operation expenses of a project throughout the project deficient of the current value of the revenues the project

earns over its lifetime duration. Equation 6.2 represents the mathematical expression for the net present cost.

$$NPC = \sum_{t=0}^{n} \frac{R_{(t)}}{(1+i)^t}$$ 6.2

Where $R_{(t)}$ represents the net cash flow during a single period $t$, $i$ represents the discount rate and $t$ represents the number of timer periods. Using Equation 6.2, HOMERPro revealed the results in Table 6.4.

Table 6.4: The NPC of the microgrid system

| Base case | Lowest system cost |
|-----------|--------------------|
| USD 317,235 | USD 284,430 |

## 6.8    Conclusion

This chapter of the research revealed the cost analysis of the 250-kW planned power solar microgrid system. The initial capital costs of the solar PV system were calculated at USD 249,390.6, while the lithium-ion battery's initial capital costs were calculated to be USD 40,000.00. Annual analysis reveals that excess energy stored on the grid was estimated at 99,248.6 kWh. The LCOE and NPC of the microgrid system were determined to be USD 10.90/kWh and USD 317,235, respectively.

## 7    CHAPTER 7: CONCLUSION AND FUTURE WORK

### 7.1    Overview

This chapter presents a conclusion derived from the study effort per the research objectives and questions.

### 7.2    Load metering analysis

One of the objectives of the research was to measure the electricity consumption of a residential household in Botswana over a period of one year. The load metering was successfully completed in a residential home for 12 months between 20th August 2020 and 20th August 2021. The data collected from the residential household was presented in Chapter 4, sub-section 4.3. The data analysis revealed critical data such as the daily peak power usage and daily electricity usage. Another objective of the research was to execute smart meter data analytics. The smart meter analysis was successfully carried out using techniques such as regression analysis, time series analysis, and clustering analysis, as described fully in Chapter 4, sub-heading 4.4. The smart meter analysis revealed the characteristics of energy usage behavior in urban residential households. However, due to high variability in the daily energy usage, the linear regression analysis revealed a low RSME, thus indicating the low model accuracy of the analyzed dataset as per the analysis technique.

On the other hand, the clustering analysis revealed high model accuracy in the monthly energy usage analysis among the other analytics methods. In addition, the load profiling assessment revealed the clustering analysis as an accurate technique to identify typical load profiles for long-term energy planning. A challenge of the smart metering analysis was the lack of previous energy usage data, which could have improved the accuracy in both the linear regression and time series analysis. Another challenge was the lack of data recording due to power cuts and equipment malfunction.

### 7.3 Single household solar PV system simulation

Another objective of the research was to design a single household solar PV system. Following the load metering analysis, the time series energy usage of the residential house was fed into the solar PV system design in PVSyst simulation software as the load. The metering analysis revealed a daily peak load of 9.2 kW, thereby informing the design and simulation of a ten kWp planned solar PV power system. The simulation analysis incorporated the solar irradiation and temperature profiles of the residential households as inputs of the solar PV system. The average daily hourly load profile of the residential house was utilized as the daily self-consumption profile on PVSyst. The simulation results revealed an average monthly reference incident energy of 7.594 kWh/kWp/day. The performance of the solar PV system was only recorded at 75.1%, thus indicating the substantial energy losses from PV modules due to temperature. Modern monocrystalline solar cells need to be incorporated as they possess a higher efficiency and can withstand high temperatures. The primary goal of the objective was met through the design of the solar PV system in the PVSyst simulation environment.

### 7.4 Community solar PV microgrid

A significant section of the research included the simulation analysis of the designed solar PV microgrid. Another goal of the research was to model and simulate the solar PV microgrid in both the island and grid-connected modes. The design and simulation of the microgrid system were carried out in the MATLAB/Simulink simulation environment. The load in the microgrid system was a 250-kW community load block in MATLAB/Simulink, with the model structure being constant impedance. The assumption is that the residential household has similar load profiles; hence, the 10-kWp of each house was utilized, so the cumulative community load accounted for 250-kWp. Bidirectional converters were used to ensure bidirectional power flow amongst the other components. SPWM inverters were incorporated to reduce harmonics in the output waveforms, and their performance was assessed in the simulation analysis. The control of the microgrid system was through PID controllers, and for optimization, fuzzy logic control was incorporated. The goal of the objective was successfully achieved through the design of a

250-kW microgrid system built in the MATLAB/Simulink software environment for both island and grid-connected operation. Daily irradiation and temperature profiles of Palapye were utilized for the solar PV microgrid.

### 7.4.1   Island mode

The microgrid system's design and simulation under the island mode of operation was successful. The simulation's critical results demonstrated that the usage of PID controllers achieved power management in the microgrid system.  Periods of the day when the solar PV system was low, the battery was supplying power to the DC microgrid, while when the solar PV power generated was in excess, the battery was charged. The primary function of the battery control method was to maintain the desired DC voltage level in the microgrid system. The lithium-ion battery operated as the load or generator to ensure the optimum operation of the microgrid system.

### 7.4.2   Grid-connected mode

The model design and simulation of the microgrid system in grid connected mode was successfully performed in the MATLAB / Simulink simulation environment. The desired DC voltage bus level was achieved through power management between the solar PV system and the grid through the grid-connected mode. Periods of the day when the solar PV power generated was low and energy was discharged from the grid into the microgrid system. The performance of the grid-inverter current revealed a THD between 3 and 7%, which is similar to the allowable THD of the grid-side current of approximately 5% (IEEE-519 standard) (Hamizah et al. 2014).

### 7.5   Optimization and economic analysis

Another objective of research included the optimization and sensitivity analysis of the solar PV microgrid system. A fuzzy logic control was implemented for the grid-connected microgrid with battery backup to optimize the microgrid system. The FLC's main goal

was to switch between the island and grid-connected modes dependent on the amount of solar PV power available. The simulations were successful since the microgrid system operated in grid-connected mode during low solar PV power generation times and island mode during high solar PV power generation periods. The battery served as an auxiliary power supply during the transitions between the two modes of operation. By utilizing the FLC, a more stable THD of approximately 3% was achieved throughout the day. The optimization analysis was successful due to the improved power quality of the solar PV microgrid system. The transition from island to grid-connected mode revealed a temporary high THD, thereby indicating the need for further analysis of the impact of the FLC on the microgrid system. The simulations of the microgrid could only be conducted for a single day in Simulink due to the lack of advanced computer processing equipment. The economic analysis was successfully conducted in the HOMERPRO simulation environment and critical results revealed the LCOE and NPC of USD 10.90/kWh and USD 317,235.

## 7.6    Research contributions

The research achieved the following as per the stated research objectives:

I.    Carried out smart energy metering in a residential household in Botswana.

II.    The residential characteristics and energy behavior usage trends were identified through smart meter data analytics.

III.    The sizing and simulation analysis of a grid-connected solar PV system was done for the metered residential household.

IV.    The design and simulation assessment of the solar PV microgrid system was done for a community.

V.    The economic analysis was done to determine the feasibility of the proposed solar PV microgrid for residential communities in Botswana.

### 7.7   Published work

The research author performed a presentation at a conference and has also submitted other work done to journals.

- Conference

Authors: Tumelo B Seane, Professor Ravi Samikannu

Title: Energy management of solar PV microgrids through fuzzy logic control: A review

Presented at: 3rd International Conference on Engineering Facilities Maintenance and Management Technologies (2021), 28th – 29th October 2021, Botswana International University of Science & Technology (BIUST), Botswana

Submitted two other papers which are in review:

1. Assessment of residential building energy usage through regression and clustering techniques (Applied Energy journal)
2. Solar Photovoltaic Community Based Microgrids: A Review (Technology and Economics of Smart Grids and Sustainable Energy journal)

### 7.8   Future work

Through the research analysis, more future work on solar PV microgrids can be continued in the following areas:

- Microgrid stability analysis which incorporates load demand predictions
- Increased accuracy of load prediction models that account for changes in human energy use behavior
- Microgrid synchronization with the utility grid (voltage, phase, and frequency)
- Reduction of harmonics in inverter output waveforms through multiple switching on the pulse width modulation (PWM)

## 7.9    Conclusion

In conclusion, despite the problems experienced, the research study was able to accomplish the specified objectives. However, further research work requires to be conducted on the model optimization of the solar PV microgrid to improve performance, thereby affecting system economics.

# 8    REFERENCES

Abdalrahman, Ahmed, Abdalhalim Zekry, and Ahmed Alshazly. 2012. "Simulation and Implementation of Grid-Connected Inverters." *International Journal of Computer Applications* 60(4): 41–49.

Abdelsalam, Abdelazeem A., Hossam A. Gabbar, Farayi Musharavati, and Shaligram Pokharel. 2014. "Dynamic Aggregated Building Electricity Load Modeling and Simulation." *Simulation Modelling Practice and Theory* 42: 336.

Abdi, Hamdi, Behnam Mohammadi-ivatloo, and Saeid Javadi. 2017. Distributed Generation Systems *Energy Storage Systems*. Elsevier Inc. http://dx.doi.org/10.1016/B978-0-12-804208-3.00007-8.

Adhikari, Sarina, and Fangxing Li. 2014. "Coordinated V-f and P-Q Control of Solar Photovoltaic Generators with MPPT and Battery Storage in Microgrids." *IEEE Transactions on Smart Grid* 5(3): 1270–81.

Adrees, Atia, Hooman Andami, and Jovica V. Milanovic. 2016. "Comparison of Dynamic Models of Battery Energy Storage for Frequency Regulation in Power System." *Proceedings of the 18th Mediterranean Electrotechnical Conference: Intelligent and Efficient Technologies and Services for the Citizen, MELECON 2016*.

Aguilera, Ricardo P et al. 2018. Control of Power Electronic Converters and Systems *Basic Control Principles in Power Electronics*. Elsevier Inc. http://dx.doi.org/10.1016/B978-0-12-805245-7.00002-0.

Ahlawat, Aarti, Diksha Gupta, and S. K. Gupta. 2017. "Modeling of a Pv Array and Implementation of an Efficient Mppt Based Control Mechanism in Stand-Alone Photovoltaic Systems." *i-manager's Journal on Circuits and Systems* 5(2): 51.

Al-Sakkaf, Shehab, Mahmoud Kassas, Muhammad Khalid, and Mohammad A. Abido. 2019. "An Energy Management System for Residential Autonomous DC Microgrid Using Optimized Fuzzy Logic Controller Considering Economic Dispatch." *Energies* 12(8).

Alnoosani, Ahmed et al. 2019. "Design of 100MW Solar PV On-Grid Connected Power Plant Using ( PVsyst ) in Umm Al-Qura University." *International Journal of Science and Research (IJSR)* 8(11): 356–63.

Alvarez, Genesis, Hadis Moradi, Mathew Smith, and Ali Zilouchian. 2018. "Modeling a Grid-Connected PV/Battery Microgrid System with MPPT Controller." : 2941–46.

Alzahrani, Ahmad, Mehdi Ferdowsi, Pourya Shamsi, and Cihan H. Dagli. 2017. "Modeling and Simulation of Microgrid." *Procedia Computer Science* 114: 392–400. https://doi.org/10.1016/j.procs.2017.09.053.

Amri, Yasirli et al. 2016. "Analysis Clustering of Electricity Usage Profile Using K-Means Algorithm." *IOP Conference Series: Materials Science and Engineering* 105(1).

Anitha, M, and Raji Krishna. 2015. "A Fuzzy Logic Based Energy Management System for a Microgrid." *ARPN Journal of Engineering and Applied Sciences* 10(6): 2663–69.

Arif, Anmar et al. 2018. "Load Modeling - A Review." *IEEE Transactions on Smart Grid* 9(6): 5986–99.

Ashabani, Seyed Mahdi, and Yasser Abdel Rady I. Mohamed. 2014. "New Family of Microgrid Control and Management Strategies in Smart Distribution Grids-Analysis, Comparison and Testing." *IEEE Transactions on Power Systems* 29(5): 2257–69.

Atallah, Ahmed M, Almoataz Y Abdelaziz, and Raihan S Jumaah. 2014. "Implementation of Pertub and Observe MPPT of PV System with Direct Control Methods Using Buck Nd Buck-Boost Converter." *Emerging Trends in Electrical & Instrumentation Engineering: An international Journal (EEIEJ)* 1(1): 31–44.

Baran, M, and Mahajan. 2003. "Distribution for Industrial System: Opportunities and Challenges." *IEEE Transactions on Industrial Informatics* 39(9): 1596–1601.

Basak, Prasenjit, S. Chowdhury, S. Halder Nee Dey, and S. P. Chowdhury. 2012. "A Literature Review on Integration of Distributed Energy Resources in the Perspective of Control, Protection and Stability of Microgrid." *Renewable and Sustainable Energy Reviews* 16(8): 5545–56. http://dx.doi.org/10.1016/j.rser.2012.05.043.

Bellia, Habbati. 2014. "A Detailed Modeling of Photovoltaic Module Using MATLAB." *NRIAG Journal of Astronomy and Geophysics* 3(1): 53–61. http://dx.doi.org/10.1016/j.nrjag.2014.04.001.

Bhuvaneswari, G., and R. Annamalai. 2011. "Development of a Solar Cell Model in MATLAB for PV Based Generation System." *Proceedings - 2011 Annual IEEE India Conference: Engineering Sustainable Solutions, INDICON-2011*.

Bifaretti, S. et al. 2017. "Grid-Connected Microgrids to Support Renewable Energy Sources Penetration." In *Energy Procedia*, , 2910–15.

Bila, M., C. Opathella, and B. Venkatesh. 2016. "Grid Connected Performance of a Household Lithium-Ion Battery Energy Storage System." *Journal of Energy Storage* 6: 178–85.

Bokhari, Abdullah et al. 2014. "Experimental Determination of the ZIP Coefficients for Modern Residential, Commercial, and Industrial Loads." *IEEE Transactions on Power Delivery* 29(3): 1372–81.

Borer, Edward Ted. 2013. *Princeton University Campus Microgrid*.

Botswana Power Corporation (BPC). 2019. *Botswana Power Corporation Annual Report*.

Breeze, Paul. 2018. "Large-Scale Batteries." *Power System Energy Storage Technologies*: 33–45.

Cagnano, A, E De Tuglie, and P Mancarella. 2020. "Microgrids : Overview and Guidelines for Practical Implementations and Operation." *Applied Energy* 258(May 2019): 114039. https://doi.org/10.1016/j.apenergy.2019.114039.

Capasso, A, W Grattieri, R Lamedica, and A Prudenzi. 1994. "A Bottom-up Approach to Residential Load Modeling." *IEE Transactions on Power Systems* 9(2): 957–64. https://ieeexplore.ieee.org/abstract/document/317650.

CarbonTRACK. 2019. *Smart Gateway (Energy Management & IoT Gateway)*.

Carneiro, Aurea S. et al. 2017. "Static Load Modeling Based on Field Measurements." *2017 IEEE Manchester PowerTech, Powertech 2017* (6).

Chicco, Gianfranco. 2012. "Overview and Performance Assessment of the Clustering Methods for Electrical Load Pattern Grouping." *Energy* 42(1): 68–80. http://dx.doi.org/10.1016/j.energy.2011.12.031.

Chinchilla, Monica, David Santos-Martin, Miguel Carpintero-Renteria, and Scott Lemon. 2021. "Worldwide Annual Optimum Tilt Angle Model for Solar Collectors and Photovoltaic Systems in the Absence of Site Meteorological Data." *Applied Energy* 281: 116056.

Chou, Jui Sheng, and Duc Son Tran. 2018. "Forecasting Energy Consumption Time Series Using Machine Learning Techniques Based on Usage Patterns of Residential Householders." *Energy* 165: 709–26.

Cole, Wesley, A Will Frazier, and Chad Augistine. 2021. "Cost Projections for Utility-Scale Battery Storage: 2021 Update." *National Renewable Energy Laboratory (NREL)* (June): 21.

Collin, Adam J., George Tsagarakis, Aristides E. Kiprakis, and Stephen McLaughlin. 2014. "Development of Low-Voltage Load Models for the Residential Load Sector." *IEEE Transactions on Power Systems* 29(5): 2180–88.

Deb, Chirag et al. 2017. "A Review on Time Series Forecasting Techniques for Building Energy Consumption." *Renewable and Sustainable Energy Reviews* 74(November): 902–24. http://dx.doi.org/10.1016/j.rser.2017.02.085.

Debela, Tamiru, Ginbar Ensermu, and Avik Bhattacharya. 2017. "Design, Control and Simulation of Grid Connected DC/AC Microgrid for Residential Applications." *Proceedings of the 2017 2nd IEEE International Conference on Electrical, Computer and Communication Technologies, ICECCT 2017*: 6–11.

Dey, Bijit Kumar, Imran Khan, Mandal Nirabhra Abhinav, and Ankur Bhattacharjee. 2016. "Mathematical Modelling and Characteristic Analysis of Solar PV Cell." *7th IEEE Annual Information Technology, Electronics and Mobile Communication Conference, IEEE IEMCON 2016*.

Donahue, Edward. J. 2019. i IntechOpen *Microgrids: Applications, Solutions, Case Studies and Demonstratons*. https://www.intechopen.com/chapters/65253.

E Silva, Felipe S.F., Luiz A. Luiz, and José Gomes De Matos. 2014. "Bidirectional DC-

AC Converter for Isolated Microgrids with Voltage Unbalance Reduction Capabilities." *2014 IEEE Energy Conversion Congress and Exposition, ECCE 2014*: 4985–91.

EL-Shimy, M. et al. 2018. "Impact of Load Models on the Static and Dynamic Performances of Grid-Connected Wind Power Plants: A Comparative Analysis." *Mathematics and Computers in Simulation* 149: 91–108. https://doi.org/10.1016/j.matcom.2018.02.003.

Essah, Emmanuel A, and Eng L Ofetotse. 2014. "Energy Supply , Consumption and Access Dynamics in Botswana." *Sustainable Cities and Society* 12: 76–84. http://dx.doi.org/10.1016/j.scs.2014.01.006.

Fahim, Muhammad, and Alberto Sillitti. 2019. "Analyzing Load Profiles of Energy Consumption to Infer Household Characteristics Using Smart Meters." *Energies* 12(773).

Farrokhabadi, Mostafa et al. 2018. "Battery Energy Storage System Models for Microgrid Stability Analysis and Dynamic Simulation." *IEEE Transactions on Power Systems* 33(2): 2301–12.

Faure, Maeva et al. 2017. *Urban Microgrids :Overview, Challenges and Opportunities*. http://www.enea-consulting.com/wp-content/uploads/2017/02/Urban-Microgrids-Public-report_VF3.pdf.

Fumo, Nelson, and M. A. Rafe Biswas. 2015. "Regression Analysis for Prediction of Residential Energy Consumption." *Renewable and Sustainable Energy Reviews* 47: 332–43. http://dx.doi.org/10.1016/j.rser.2015.03.035.

Fusheng, Li, Li Ruisheng, and Zhou Fengquan. 2016. "Composition and Classification of the Microgrid." In *Microgrid Technology and Engineering Application*, , 11–27.

Gao, David Wenzhong. 2015a. "Applications of ESS in Renewable Energy Microgrids." In *Energy Storage for Sustainable Microgrid*, , 36–76.

———. 2015b. "Interfacing Between an ESS and a Microgrid." In *Energy Storage for Sustainable Microgrid*, , 80–116.

Gao, David Zhiwei, and Kai Sun. 2016. "DC–AC Inverters." In *Electric Renewable Energy Systems*, , 355–81.

Gašparović, Goran, Siir Kilkis, Goran Krajačić, and Neven Duić. 2016. "Campus and Community Micro Grids Integration of Building Integrated Photovoltaic Renewable Energy Sources: Case Study of Split 3 Area, Croatia - Part A." *Thermal Science* 20(4): 1135–45.

Global Solar Atlas. 2018. "Botswana Solar Information." https://worldbank-atlas.s3.amazonaws.com/download/Botswana/Botswana_PVOUT_mid-size-map_156x210mm-300dpi_v20191015.png?AWSAccessKeyId=ASIAS2HACIWTPQRGMEUY&Expires=1600938296&Signature=NrNai5x4%2FedBsUtrtYnqRS0cGKs%3D&x-amz-security-token=IQoJb3JpZ2luX2VjEK.

Gray, M., and W. G. Morsi. 2015. "New Power Quantities Definition for Low and High Order Harmonic Distortion." *Electric Power Systems Research* 119: 11–18.

Gu, Cheng-hong, Qian Ai, and Jiayi Wu. 2005. "A Study of Effect of Different Static Load Models and System Operating Constrains on Static Voltage Stability." 2005: 44–49.

Gulin, Marko, Mario Vasak, Goran Banjac, and Tomislav Tomisa. 2014. "Load Forecast of a University Building for Application in Microgrid Power Flow Optimization." *ENERGYCON 2014 - IEEE International Energy Conference*: 1223–27.

Halu, Arda, Antonio Scala, Abdulaziz Khiyami, and Marta C. González. 2016. "Data-Driven Modeling of Solar-Powered Urban Microgrids." *Science Advances* 2(1): 1–10.

Hamizah, Atiqah, Mohd Nordin, Ahmad Maliki Omar, and Hedzlin Zainuddin. 2014. "Modeling and Simulation of Grid Inverter in Grid- Connected Photovoltaic System." 4(4).

Harvey, L.D Danny. 2006. *Low-Energy Buildings and District Energy Systems*.

Hasan, M Asif, and M Saad Bin Arif. 2018. "Microgrid Architecture, Control, and Operation." In *Hybrid-Renewable Energy Systems in Microgrids*, , 24–36.

He, Yongxiu et al. 2018. "Residential Power User Segmentation Based on K-Means Clustering Method in the Context of Big Data." *E3S Web of Conferences* 53: 1–4.

Hossain, Alamgir, Hemanshu Roy, Jahangir Hossain, and Frede Blaabjerg. 2019. "Evolution of Microgrids with Converter-Interfaced Generations : Challenges and Opportunities." *Electrical Power and Energy Systems* 109(December 2018): 160–86. https://doi.org/10.1016/j.ijepes.2019.01.038.

Howell, Shaun et al. 2017. "Towards the next Generation of Smart Grids: Semantic and Holonic Multi-Agent Management of Distributed Energy Resources." *Renewable and Sustainable Energy Reviews* 77: 193–214.

IEA. 2014. *Africa Energy Outlook*.

———. 2019. *World Energy Balances Overview*.

Ihbal, A M, H S Rajamani, and M K Jalboub. 2011. "Statistical Predictions of Electric Load Profiles in the UK Domestic Buildings." 7(2): 151–56.

IRENA. 2019a. November *Future of Solar Photovoltaic:Deployment, Investment, Technology, Grid Integration and Socio-Economic Aspects*. https://www.irena.org/-/media/Files/IRENA/Agency/Publication/2019/Oct/IRENA_Future_of_wind_2019.pdf.

———. 2019b. *RENEWABLE POWER GENERATION COSTS IN 2019*.

Issi, Fatih, and Orhan Kaplan. 2018. "The Determination of Load Profiles and Power Consumptions of Home Appliances." *Energies* 11.

Jain, Trapti, and E S N P Raju. 2013. "Hybrid AC / DC Micro Grid : An Overview." In *Fifth International Conference on Power and Energy Systems, Kathmandu,* , 1–7.

Jiang, Yuncong, Student Member, Jaber A Abu Qahouq, and Senior Member. 2011. "Matlab / Pspice Hybrid Simulation Modeling of Solar PV Cell / Module." : 1244–50.

Jin, Ling et al. 2017. "Comparison of Clustering Techniques for Residential Energy Behavior Using Smart Meter Data." In *Artificial Intelligence for Smart Grids and Smart Buildings*, , 260–66.

Jin, Ma, He Renmu, and David J. Hill. 2006. "Composite Load Modeling via Measurement Approach." *2006 IEEE Power Engineering Society General Meeting, PES* 21(2): 663–72.

Ju, Ping et al. 2018. "Modeling Methods for Electric Loads in a Real Power Grid." *2018 5th International Conference on Electrical and Electronics Engineering, ICEEE 2018*: 166–72.

Judewicz, Marcos Gabriel et al. 2018. "Inverter-Side Current Control of Grid-Connected Voltage Source Inverters with LCL Filter Based on Generalized Predictive Control." *IEEE Journal of Emerging and Selected Topics in Power Electronics* 6(4): 1732–43.

Justo, Jackson John, Francis Mwasilu, Ju Lee, and Jin Woo Jung. 2013. "AC-Microgrids versus DC-Microgrids with Distributed Energy Resources: A Review." *Renewable and Sustainable Energy Reviews* 24: 387–405. http://dx.doi.org/10.1016/j.rser.2013.03.067.

Kabiri, Roozbeh, D. G. Holmes, and B. P. McGrath. 2013. "Inverter Control Modelling for Distributed Generation Feeding into a Utility Network." *2013 Australasian Universities Power Engineering Conference, AUPEC 2013* (March 2015).

Kalogirou, Soteris A. 2009. Academic Press *Solar Energy Engineering*.

Khalil, Ashraf, and Khalid Ateea. 2015. "Modelling and Control of Photovoltaic-Based Microgrid." 5(3).

Khan, Zafar A., Dilan Jayaweera, and Manuel S. Alvarez-Alvarado. 2018. "A Novel Approach for Load Profiling in Smart Power Grids Using Smart Meter Data." *Electric Power Systems Research* 165(August): 191–98. https://doi.org/10.1016/j.epsr.2018.09.013.

Kharjule, Saurabh. 2015. "Voltage Source Inverter." *2015 International Conference on Energy Systems and Applications* (Icesa): 537–42.

Kim, Sang-Hoon. 2017. Electric Motor Control *Pulse Width Modulation Inverters*.

Kook, Kyung Soo, Keith J. McKenzie, Yilu Liu, and Stan Atcitty. 2006. "A Study on Applications of Energy Storage for the Wind Power Operation in Power Systems." *2006 IEEE Power Engineering Society General Meeting, PES*: 1–5.

Kordestani, Mojtaba et al. 2018. "Maximum Power Point Tracker ( MPPT ) for Photovoltaic Power Systems-A Systematic Literature Review." *2018 European Control Conference (ECC)*: 40–45.

Kounev, Velin, David Tipper, Brandon M. Grainger, and Gregory Reed. 2014. "Analysis of an Offshore Medium Voltage DC Microgrid Environment - Part II: Communication Network Architecture." *Proceedings of the IEEE Power Engineering Society Transmission and Distribution Conference*.

Kularatna, Nihal. 2015. "Rechargeable Battery Technologies." In *Energy Storage Devices for Electronic Systems*,.

Kulkarni, Vikas, and Rajesh Nehete. 2014. "Simulation and Analysis of Photo-Voltaic ( PV ) Based Solar Inverter System." In *International Journal of Soft Computing and Engineering (IJSCE)*, , 114–20.

Kumar, Y. V.Pavan, and Bhimasingu Ravikumar. 2016. "Integrating Renewable Energy Sources to an Urban Building in India: Challenges, Opportunities, and Techno-Economic Feasibility Simulation." *Technology and Economics of Smart Grids and Sustainable Energy* 1(1). http://dx.doi.org/10.1007/s40866-015-0001-y.

Kuster, Corentin, Yacine Rezgui, and Monjur Mourshed. 2017. "Electrical Load Forecasting Models: A Critical Systematic Review." *Sustainable Cities and Society* 35(June): 257–70. http://dx.doi.org/10.1016/j.scs.2017.08.009.

Labeeuw, Wouter, and Geert Deconinck. 2016. "Residential Electrical Load Model Based on Mixture Model Clustering and Markov Models." *IEEE Transactions on Industrial Informatics* (January).

Lee, Ji Heon et al. 2011. "DC Micro-Grid Operational Analysis with a Detailed Simulation Model for Distributed Generation." *Journal of Power Electronics* 11(3): 350–59.

Di Leo, Senatro, Pietro Caramuta, Paola Curci, and Carmelina Cosmi. 2020. "Regression Analysis for Energy Demand Projection: An Application to TIMES-Basilicata and TIMES-Italy Energy Models." *Energy* 196.

Li, Wei, and Géza Joós. 2007. "Performance Comparison of Aggregated and Distributed Energy Storage Systems in a Wind Farm for Wind Power Fluctuation Suppression." *2007 IEEE Power Engineering Society General Meeting, PES*: 1–6.

Liu, Xiong, Peng Wang, and Poh Chiang Loh. 2011. "A Hybrid AC/DC Microgrid and Its Coordination Control." *IEEE Transactions on Smart Grid* 2(2): 278–86.

Manias, Stefanos N. 2017. "Inverters (DC - AC Converters)." In *Power Electronics and Motor Drive Systems*,.

Da Marcello, S. Neves et al. 2017. "Advantages of Grid-Tied DC Microgrid." *14th Brazilian Power Electronics Conference, COBEP 2017* 2018-Janua: 1–6.

Mariam, Lubna, Malabika Basu, and Michael F. Conlon. 2016. "Microgrid: Architecture, Policy and Future Trends." *Renewable and Sustainable Energy*

*Reviews* 64: 477–89.

Mashayekh, Salman, Michael Stadler, Gonçalo Cardoso, and Miguel Heleno. 2017. "A Mixed Integer Linear Programming Approach for Optimal DER Portfolio, Sizing, and Placement in Multi-Energy Microgrids." *Applied Energy* 187: 154–68.

Mayer, Johannes N et al. 2015. "Current and Future Cost of Photovoltaics Long-Term Scenarios for Market Development." : 82.

Mcloughlin, Fintan, Aidan Duffy, and Michael Conlon. 2013. "Evaluation of Time Series Techniques to Characterise Domestic Electricity Demand." *Energy* 50(1): 120–30.

———. 2015. "A Clustering Approach to Domestic Electricity Load Profile Characterisation Using Smart Metering Data." *Applied Energy* 141: 190–99. http://dx.doi.org/10.1016/j.apenergy.2014.12.039.

Meng, Lexuan et al. 2016. "Microgrid Supervisory Controllers and Energy Management Systems: A Literature Review." *Renewable and Sustainable Energy Reviews* 60: 1263–73. http://dx.doi.org/10.1016/j.rser.2016.03.003.

Miveh, Mohammad Reza, Majid Gandomkar, Sohrab Mirsaeidi, and Mohammad Reza Gharibdoost. 2012. "A Review on Protection Challenges in Microgrids." *2012 Proceedings of 17th Conference on Electrical Power Distribution, EPDC 2012*: 1–5.

Moncecchi, Matteo et al. 2018. "Battery Modeling for Microgrid Design: A Comparison between Lithium-Ion and Lead Acid Technologies." *SPEEDAM 2018 - Proceedings: International Symposium on Power Electronics, Electrical Drives, Automation and Motion*: 1215–20.

Morgan, E. R. et al. 2016. "Boston Community Energy Study – Zonal Analysis for Urban Microgrids." *Massachusetts Institute of Technology Lincoln Laboratory*.

Narayanan, Vivek, Seema, and Bhim Singh. 2018. "Solar PV - BES Based Microgrid System with Multifunctional VSC." *2018 5th IEEE Uttar Pradesh Section International Conference on Electrical, Electronics and Computer Engineering, UPCON 2018*: 1–6.

Nebey, Abraham Hizkiel. 2020. "Energy Management System for Grid-Connected Solar Photovoltaic with Battery Using MATLAB Simulation Tool Energy Management System for Grid-Con - Nected Solar Photovoltaic with Battery Using MATLAB Simulation Tool." *Cogent Engineering*.

Nedumgatt, Jacob James, K B Jayakrishnan, S Umashankar, and D Vijayakumar. 2011. "Perturb and Observe MPPT Algorithm for Solar PV Systems-Modeling and Simulation." *2011 Annual IEEE India Conference* 19(1): 1–6.

Nepal, Bishnu, Motoi Yamaha, Hiroya Sahashi, and Aya Yokoe. 2019. "Analysis of Building Electricity Use Pattern Using K-Means Clustering Algorithm by Determination of Better Initial Centroids and Number of Clusters." *Energies* 12(12).

Nfaoui, Mohamed, and Khalil El-Hami. 2018. "Extracting the Maximum Energy from Solar Panels." *Energy Reports* 4: 536–45.

Nguyen, Xuan Hieu, and Minh Phuong Nguyen. 2015. "Mathematical Modeling of Photovoltaic Cell/Module/Arrays with Tags in Matlab/Simulink." *Environmental Systems Research* 4(1).

Nisha Kondrath. 2018. "An Overview of Bidirectional DC-DC Converter Topologies and Control Strategies for Interfacing Energy Storage Systems in Microgrids." *J. of Electrical Engineering* 6(1): 11–17.

Nixon, Mark S., and Alberto Aguado. 2013. "Least Squares Analysis." In *Feature Extraction & Image Processing for Computer Vision*, , 519–23.

Ofetotse, E., Essah, E. and Yao, R. 2015. "Trends in Domestic Electricity Consumption in Botswana." *TMC Academic Journal* 9(2): 83–104.

Palaniappan, Karthik, Swachala Veerapeneni, Robert Cuzner, and Yue Zhao. 2017. "Assessment of the Feasibility of Interconnected Smart DC Homes in a DC Microgrid to Reduce Utility Costs of Low Income Households." *2017 IEEE 2nd International Conference on Direct Current Microgrids, ICDCM 2017*: 467–73.

Pan, Donghua et al. 2017. "Analysis and Design of Current Control Schemes for LCL-Type Grid-Connected Inverter Based on a General Mathematical Model." *IEEE Transactions on Power Electronics* 32(6): 4395–4410.

Phuong, Le Minh, Phan Quoc Dzung, and Nguyen Minh Huy. 2012. "A Three-Phase Grid-Connected Photovoltaic System with Reactive Power Control." In *The 2012 International Conference on Green Technology and Sustainable Development (GTSD2012)*, , 1–8.

Phurailatpam, C, B S Rajpurohit, and N M Pindoriya. 2011. "Embracing Microgrids : Applications for Rural and Urban India." *Reserachgate* (May): 1–10.

Planas, Estefanía et al. 2013. "General Aspects, Hierarchical Controls and Droop Methods in Microgrids: A Review." *Renewable and Sustainable Energy Reviews* 17: 147–59.

Prakash, Ravi, and Sandeep Singh. 2016. "Designing and Modelling of Solar Photovoltaic Cell and Array." 11(2): 35–40.

Qazi, Salahuddin. 2017. "PV Systems Affordability , Community Solar , and Solar Microgrids." In *Standalone Photovoltaic (PV) Systems for Disaster Relief and Remote Areas*, , 177–202.

Reed, Gregory F., Brandon M. Grainger, Adam R. Sparacino, and Zhi-Hong Mao. 2012. "Ship to Grid." *IEEE Power and Energy Magazine* (november/december): 70–79.

Reyes-Garcia, Carlos A., and Alejandro A. Torres-Garcia. 2022. "Fuzzy Logic and Fuzzy Systems." In *Biosignal Processing and Classification Using Computational Learning and Intelligence*, , 153–76. https://www.sciencedirect.com/science/article/pii/B9780128201251000208.

Rizzo, Maria L., and Gábor J. Székely. 2016. "Energy Distance." *Wiley Interdisciplinary Reviews: Computational Statistics* 8(1): 27–38.

Sadeghi, M., and G. Abdollahi Sarvi. 2009. "Determination of ZIP Parameters with Least Squares Optimization Method." *2009 IEEE Electrical Power and Energy Conference, EPEC 2009*: 1–6.

Sahoo, Ashish Kumar, Arushi Shahani, Kaushik Basu, and Ned Mohan. 2014. "LCL Filter Design for Grid-Connected Inverters by Analytical Estimation of PWM Ripple Voltage." *Conference Proceedings - IEEE Applied Power Electronics Conference and Exposition - APEC*: 1281–86.

Salomonsson, Daniel, Lennart Söder, and Ambra Sannino. 2009. "Protection of Low-Voltage DC Microgrids." *IEEE Transactions on Power Delivery* 24(3): 1045–53.

Sampath, Kumar V, Jagdish Prasad, and Ravi Samikannu. 2018. "Barriers to Implementation of Smart Grids and Virtual Power Plant in Sub-Saharan Region — Focus Botswana." *Energy Reports* 4: 119–28. https://doi.org/10.1016/j.egyr.2018.02.001.

Sarwar, Adil, and Mohammad S J Asghar. 2011. "Simulation and Analysis of a Multilevel Converter Topology for Solar PV Based Grid Connected Inverter." *Smart Grid and Renewable Ene* 2011(February): 56–62.

Saxena, Nupur, Ikhlaq Hussain, Bhim Singh, and A. L. Vyas. 2017. "Solar PV Interfaced to Multifunctional VSC with a Battery Support." *2016 IEEE 7th Power India International Conference, PIICON 2016*: 1–6.

Schonardie, Mateus F., Roberto F. Coelho, Romulo Schweitzer, and Denizar C. Martins. 2012. "Control of the Active and Reactive Power Using Dq0 Transformation in a Three-Phase Grid-Connected PV System." *IEEE International Symposium on Industrial Electronics*: 264–69.

Shintre, Priyanka, and A M Mulla. 2016. "Study of Micro Grid Topology and Design of Voltage Source Inverter and Charge Controller." *International Research Journal of Engineering and Technology (IRJET)* 3(3).

Shrivastwa, Ritu Raj, Ahmad Hably, Kaouthar Melizi, and Seddik Bacha. 2019. "Understanding Microgrids and Their Future Trends." *Proceedings of the IEEE International Conference on Industrial Technology* 2019-Febru: 1723–28.

Shuai, Zhikang, Junbin Fang, Fenggen Ning, and Z. John Shen. 2018. "Hierarchical Structure and Bus Voltage Control of DC Microgrid." *Renewable and Sustainable Energy Reviews* 82(2): 3670–82. https://doi.org/10.1016/j.rser.2017.10.096.

Sivarasu, S. R., E. Chandira Sekaran, and P. Karthik. 2015. "Development of Renewable Energy Based Microgrid Project Implementations for Residential Consumers in India: Scope, Challenges and Possibilities." *Renewable and Sustainable Energy Reviews* 50: 256–69.

Siwakoti, Yam P, Mojtaba Forouzesh, and Ngoc Ha Pham. 2018. "Power Electronics Converters — An Overview." In *Control of Power Electronic Converters and*

*Systems*, Elsevier Inc., 3–29. http://dx.doi.org/10.1016/B978-0-12-805245-7.00001-9.

Soon, Jing Jun, and Kay Soon Low. 2015. "Optimizing Photovoltaic Model for Different Cell Technologies Using a Generalized Multidimension Diode Model." *IEEE Transactions on Industrial Electronics* 62(10): 6371–80.

Tang, Yi, Liangliang Zhu, Jia Ning, and Qi Wang. 2019. "A Data-Driven Approach for Online Aggregated Load Modeling through Intelligent Terminals." *International Journal of Distributed Sensor Networks* 15(1).

Tayab, Usman Bashir, Mohd Azrik Bin Roslan, Leong Jenn Hwai, and Muhammad Kashif. 2017. "A Review of Droop Control Techniques for Microgrid." *Renewable and Sustainable Energy Reviews* 76(May 2016): 717–27. http://dx.doi.org/10.1016/j.rser.2017.03.028.

Tremblay, Olivier, Louis A. Dessaint, and Abdel Illah Dekkiche. 2007. "A Generic Battery Model for the Dynamic Simulation of Hybrid Electric Vehicles." *VPPC 2007 - Proceedings of the 2007 IEEE Vehicle Power and Propulsion Conference* (V): 284–89.

Unruh, Peter, Maria Nuschke, Philipp Strauß, and Friedrich Welck. 2020. "Overview on Grid-Forming Inverter Control Methods." *Energies* 13(10).

Ustun, Taha Selim, Cagil Ozansoy, and Aladin Zayegh. 2011. "Recent Developments in Microgrids and Example Cases around the World - A Review." *Renewable and Sustainable Energy Reviews* 15(8): 4030–41. http://dx.doi.org/10.1016/j.rser.2011.07.033.

Vazquez, N. et al. 2012. "Parallel DC/Ac Converters under Connection/Disconnection of Power Modules." *Proceedings of the 6th Andean Region International Conference, Andescon 2012*: 21–24.

Vetter, Matthias, and Lukas Rohr. 2014. "Lithium-Ion Batteries for Storage of Renewable Energies and Electric Grid Backup." In *Lithium-Ion Batteries Advances and Applications*, Elsevier, 293–309. http://dx.doi.org/10.1016/B978-0-444-59513-3.00013-3.

Villalva, Marcelo Gradella, Jonas Rafael Gazoli, and Ernesto Ruppert Filho. 2009. "Comprehensive Approach to Modeling and Simulation of Photovoltaic Arrays." *IEEE Transactions on Power Electronics* 24(5): 1198–1208.

Wang, Fu, Yingming Zhu, and Jinyue Yan. 2018. "Performance of Solar PV Micro-Grid Systems : A Comparison Study." *Energy Procedia* 145: 570–75. https://doi.org/10.1016/j.egypro.2018.04.083.

Wang, Xuejie et al. 2020. "Optimal Energy Management of Microgrid Based on Multi-Parameter Dynamic Programming." *International Journal of Distributed Sensor Networks* 16(6).

Wang, Yi, Qixin Chen, Tao Hong, and Chongqing Kang. 2019. "Review of Smart Meter Data Analytics: Applications, Methodologies, and Challenges." *IEEE Transactions*

*on Smart Grid* 10(3): 3125–48.

Wanitschke, Alexander, Norman Pieniak, and Florian Schaller. 2017. "Economic and Environmental Cost of Self-Sufficiency-Analysis of an Urban Micro Grid." *Energy Procedia* 135: 445–51.

Wen, Lulu, Kaile Zhou, Shanlin Yang, and Lanlan Li. 2018. "Compression of Smart Meter Big Data : A Survey." *Renewable and Sustainable Energy Reviews* 91(January 2017): 59–69.

Woyte, A., and S. Goy. 2017. The Performance of Photovoltaic (PV) Systems: Modelling, Measurement and Assessment *Large Grid-Connected Photovoltaic Power Plants: Best Practices for the Design and Operation of Large Photovoltaic Power Plants*. Elsevier Ltd. http://dx.doi.org/10.1016/B978-1-78242-336-2.00011-2.

Xia, Tian et al. 2015. "Modeling and Simulation of Battery Energy Storage System ( BESS ) Used in Power System." *2015 5th International Conference on Electric Utility Deregulation and Restructuring and Power Technologies (DRPT)*: 2120–25.

Yamashita, K. et al. 2012. "Modelling and Aggregation of Loads in Flexible Power Networks." *IFAC Proceedings Volumes (IFAC-PapersOnline)* 8(PART 1): 405–10.

Yang, Yongheng, Katherine A. Kim, Frede Blaabjerg, and Ariya Sangwongwanich. 2019. "PV System Modeling, Monitoring, and Diagnosis." In *Advances in Grid-Connected Photovolatic Power Conversion Systems*, , 45–71.

Yekini, Mohammed et al. 2013. "Power Sector Renewable Energy Integration for Expanding Access to Electricity in Sub-Saharan Africa." *Renewable and Sustainable Energy Reviews* 25: 630–42. http://dx.doi.org/10.1016/j.rser.2013.04.033.

Yildiz, B, J I Bilbao, J Dore, and A B Sproul. 2017. "Recent Advances in the Analysis of Residential Electricity Consumption and Applications of Smart Meter Data." *Applied Energy* 208(October): 402–27. https://doi.org/10.1016/j.apenergy.2017.10.014.

Zainal, N.A, A.R Yusoff, and Ajisman. 2016. "Modelling of Photovoltaic Module Using Matlab Simulink." In *IOP Conf. Series: Materials Science and Engineering 114*,.

Zammit, Daniel, Cyril Spiteri Staines, Maurice Apap, and Alexander Micallef. 2018. "Control Of Buck and Boost Converters For Stand-Alone DC Microgrids." (August).

Zhang, Xiaoou Monica, Katarina Grolinger, Miriam A.M. Capretz, and Luke Seewald. 2019. "Forecasting Residential Energy Consumption: Single Household Perspective." *Proceedings - 17th IEEE International Conference on Machine Learning and Applications, ICMLA 2018*: 110–17.

Zhao, Bing, Yong Tang, Wen Chao Zhang, and Q. Wang. 2010. "Modeling of Common Load Components in Power System Based on Dynamic Simulation Experiments." *2010 International Conference on Power System Technology: Technological*

*Innovations Making Power Grid Smarter, POWERCON2010.*

## 9    APPENDIX A – ELECTRICITY USAGE RAW DATA

| MONTH | DATE | ELECTRICITY USAGE (kWh) | Daily Peak Electricity (kW) | Peak power (KW) | Peak Demand (kWh) | Peak demand time |
|---|---|---|---|---|---|---|
| AUGUST | Thursday, 20 August 2020 | 19.515 | 0.813 | 9.249 | 1.881 | 17:48:00 |
| | Friday, 21 August 2020 | 29.238 | 1.218 | 4.808 | 0.867 | 13:33:00 |
| | Saturday, 22 August 2020 | 18.890 | 0.787 | 4.840 | 0.803 | 20:48:00 |
| | Sunday, 23 August 2020 | 17.717 | 0.738 | 3.762 | 0.831 | 20:18:00 |
| | Monday, 24 August 2020 | 26.024 | 1.084 | 5.223 | 0.812 | 20:03:00 |
| | Tuesday, 25 August 2020 | 22.985 | 0.958 | 5.112 | 0.839 | 19:33:00 |
| | Wednesday, 26 August 2020 | 22.521 | 0.938 | 5.201 | 0.841 | 20:03:00 |
| | Thursday, 27 August 2020 | 23.239 | 0.968 | 4.994 | 0.840 | 17:48:00 |
| | Friday, 28 August 2020 | 26.514 | 1.105 | 5.382 | 0.855 | 19:18:00 |
| | Saturday, 29 August 2020 | 19.094 | 0.796 | 4.894 | 0.832 | 18:18:00 |
| | Sunday, 30 August 2020 | 17.595 | 0.733 | 3.765 | 0.817 | 19:33:00 |
| | Monday, 31 August 2020 | 28.101 | 1.171 | 5.090 | 0.809 | 14:48:00 |
| SEPTEMBER | Tuesday, 01 September 2020 | 29.804 | 1.242 | 4.919 | 0.822 | 12:48:00 |
| | Wednesday, 02 September 2020 | 28.857 | 1.202 | 4.956 | 0.810 | 18:03:00 |
| | Thursday, 03 September 2020 | 37.986 | 1.583 | 6.817 | 1.661 | 08:18:00 |
| | Friday, 04 September 2020 | 24.576 | 1.024 | 5.118 | 0.823 | 19:18:00 |

| | | | | | |
|---|---|---|---|---|---|
| Saturday, 05 September 2020 | 17.281 | 0.720 | 5.081 | 0.851 | 19:33:00 |
| Sunday, 06 September 2020 | 22.535 | 0.939 | 3.785 | 0.824 | 18:48:00 |
| Monday, 07 September 2020 | 27.748 | 1.156 | 6.697 | 0.825 | 19:18:00 |
| Tuesday, 08 September 2020 | 20.651 | 0.860 | 5.203 | 0.803 | 20:03:00 |
| Wednesday, 09 September 2020 | 23.648 | 0.985 | 5.380 | 0.864 | 09:33:00 |
| Thursday, 10 September 2020 | 21.439 | 0.893 | 5.077 | 0.835 | 14:48:00 |
| Friday, 11 September 2020 | 27.357 | 1.140 | 5.125 | 0.855 | 09:33:00 |
| Saturday, 12 September 2020 | 17.445 | 0.727 | 3.684 | 0.860 | 19:48:00 |
| Sunday, 13 September 2020 | 18.831 | 0.785 | 4.282 | 0.806 | 12:48:00 |
| Monday, 14 September 2020 | 22.134 | 0.922 | 4.826 | 0.815 | 11:33:00 |
| Tuesday, 15 September 2020 | 16.824 | 0.701 | 4.938 | 0.785 | 14:48:00 |
| Wednesday, 16 September 2020 | 18.803 | 0.783 | 4.950 | 0.809 | 09:33:00 |
| Thursday, 17 September 2020 | 17.187 | 0.716 | 4.864 | 0.813 | 19:03:00 |
| Friday, 18 September 2020 | 15.697 | 0.654 | 5.394 | 0.830 | 10:48:00 |
| Saturday, 19 September 2020 | 19.078 | 0.795 | 5.855 | 1.044 | 23:33:00 |
| Sunday, 20 September 2020 | 41.633 | 1.735 | 6.290 | 2.198 | 15:03:00 |
| Monday, 21 September 2020 | 41.747 | 1.739 | 9.212 | 2.320 | 22:18:03 |
| Tuesday, 22 September 2020 | 21.841 | 0.910 | 4.836 | 0.800 | 21:48:03 |
| Wednesday, 23 September 2020 | 18.994 | 0.791 | 5.252 | 0.809 | 09:18:02 |
| Thursday, 24 September 2020 | 20.795 | 0.866 | 4.544 | 0.796 | 11:03:01 |
| Friday, 25 September 2020 | 19.819 | 0.826 | 4.732 | 1.138 | 11:18:01 |
| Saturday, 26 September 2020 | 33.019 | 1.376 | 4.855 | 1.342 | 15:03:01 |

| | | | | | |
|---|---|---|---|---|---|
| | Sunday, 27 September 2020 | 31.157 | 1.298 | 6.772 | 1.670 | 22:02:59 |
| | Monday, 28 September 2020 | 26.493 | 1.104 | 5.335 | 0.969 | 11:32:59 |
| | Tuesday, 29 September 2020 | 16.288 | 0.679 | 4.934 | 0.840 | 23:47:00 |
| | Wednesday, 30 September 2020 | 10.486 | 0.437 | 5.282 | 0.629 | 09:17:00 |
| OCTOBER | Thursday, 01 October 2020 | 13.510 | 0.563 | 3.976 | 0.828 | 17:47:00 |
| | Friday, 02 October 2020 | 14.567 | 0.607 | 4.348 | 1.056 | 09:02:00 |
| | Saturday, 03 October 2020 | 23.517 | 0.980 | 5.229 | 0.848 | 08:02:00 |
| | Sunday, 04 October 2020 | 19.039 | 0.793 | 5.511 | 0.841 | 08:17:00 |
| | Monday, 05 October 2020 | 17.972 | 0.749 | 3.729 | 0.844 | 01:02:00 |
| | Tuesday, 06 October 2020 | 28.456 | 1.186 | 5.270 | 1.489 | 08:47:00 |
| | Wednesday, 07 October 2020 | 25.519 | 1.063 | 5.087 | 0.837 | 10:17:00 |
| | Thursday, 08 October 2020 | 23.915 | 0.996 | 4.928 | 0.834 | 15:02:00 |
| | Friday, 09 October 2020 | 15.988 | 0.666 | 4.780 | 0.810 | 08:02:00 |
| | Saturday, 10 October 2020 | 21.062 | 0.878 | 4.734 | 1.353 | 16:32:00 |
| | Sunday, 11 October 2020 | 20.785 | 0.866 | 4.485 | 0.829 | 01:32:00 |
| | Monday, 12 October 2020 | 22.698 | 0.946 | 4.792 | 0.793 | 08:02:00 |
| | Tuesday, 13 October 2020 | 20.883 | 0.870 | 5.691 | 0.816 | 08:17:00 |
| | Wednesday, 14 October 2020 | 18.115 | 0.755 | 3.703 | 0.808 | 18:17:00 |
| | Thursday, 15 October 2020 | 15.927 | 0.664 | 4.937 | 0.827 | 08:47:00 |
| | Friday, 16 October 2020 | 14.956 | 0.623 | 4.779 | 0.723 | 10:02:00 |
| | Saturday, 17 October 2020 | 30.075 | 1.253 | 5.702 | 1.379 | 23:47:00 |
| | Sunday, 18 October 2020 | 43.795 | 1.825 | 8.787 | 2.205 | 16:17:00 |

| | | | | | |
|---|---|---|---|---|---|
| | Monday, 19 October 2020 | 51.386 | 2.141 | 8.750 | 2.418 | 14:02:00 |
| | Tuesday, 20 October 2020 | 73.797 | 3.075 | 6.778 | 2.041 | 21:32:00 |
| | Wednesday, 21 October 2020 | 32.898 | 1.371 | 4.927 | 1.224 | 00:02:00 |
| | Thursday, 22 October 2020 | 36.893 | 1.537 | 5.876 | 1.667 | 22:47:00 |
| | Friday, 23 October 2020 | 33.476 | 1.395 | 6.603 | 1.847 | 15:17:00 |
| | Saturday, 24 October 2020 | 44.231 | 1.843 | 5.326 | 1.652 | 16:02:00 |
| | Sunday, 25 October 2020 | 51.107 | 2.129 | 6.782 | 1.841 | 21:32:00 |
| | Monday, 26 October 2020 | 56.788 | 2.366 | 6.669 | 1.656 | 00:02:00 |
| | Tuesday, 27 October 2020 | 46.359 | 1.932 | 6.774 | 1.763 | 21:47:00 |
| | Wednesday, 28 October 2020 | 51.027 | 2.126 | 6.726 | 1.823 | 23:17:00 |
| | Thursday, 29 October 2020 | 54.252 | 2.260 | 6.640 | 1.733 | 01:17:00 |
| | Friday, 30 October 2020 | 20.091 | 0.837 | 5.101 | 1.363 | 13:47:00 |
| | Saturday, 31 October 2020 | 6.076 | 0.253 | 3.199 | 0.639 | 04:47:00 |
| November | Sunday, 01 November 2020 | 11.380 | 0.474 | 3.737 | 0.790 | 21:17:00 |
| | Monday, 02 November 2020 | 17.020 | 0.709 | 4.843 | 0.776 | 06:47:00 |
| | Tuesday, 03 November 2020 | 18.561 | 0.773 | 4.731 | 0.834 | 09:17:00 |
| | Wednesday, 04 November 2020 | 22.854 | 0.952 | 5.216 | 1.635 | 06:47:00 |
| | Thursday, 05 November 2020 | 18.776 | 0.782 | 4.733 | 0.769 | 10:17:00 |
| | Friday, 06 November 2020 | 44.538 | 1.856 | 6.064 | 1.876 | 16:47:00 |
| | Saturday, 07 November 2020 | 64.165 | 2.674 | 6.279 | 1.705 | 19:02:00 |
| | Sunday, 08 November 2020 | 73.421 | 3.059 | 6.323 | 2.163 | 15:32:00 |
| | Monday, 09 November 2020 | 70.243 | 2.927 | 7.012 | 2.430 | 23:32:00 |

| | | | | | |
|---|---|---|---|---|---|
| | Tuesday, 10 November 2020 | 31.243 | 1.302 | 5.216 | 1.406 | 09:02:00 |
| | Wednesday, 11 November 2020 | 17.446 | 0.727 | 4.926 | 0.851 | 18:17:00 |
| | Thursday, 12 November 2020 | 19.195 | 0.800 | 3.650 | 0.798 | 00:32:00 |
| | Friday, 13 November 2020 | 17.913 | 0.746 | 5.780 | 0.803 | 13:32:00 |
| | Saturday, 14 November 2020 | 23.656 | 0.986 | 4.279 | 1.090 | 20:47:00 |
| | Sunday, 15 November 2020 | 20.025 | 0.834 | 4.782 | 1.110 | 23:47:00 |
| | Monday, 16 November 2020 | 53.723 | 2.238 | 6.236 | 2.114 | 21:17:00 |
| | Tuesday, 17 November 2020 | 40.762 | 1.698 | 6.132 | 1.771 | 22:47:00 |
| | Wednesday, 18 November 2020 | 44.926 | 1.872 | 6.908 | 1.766 | 13:02:00 |
| | Thursday, 19 November 2020 | 44.122 | 1.838 | 4.772 | 1.910 | 00:17:00 |
| | Friday, 20 November 2020 | 20.459 | 0.852 | 4.851 | 0.821 | 02:02:00 |
| | Saturday, 21 November 2020 | 17.815 | 0.742 | 3.643 | 0.811 | 19:02:00 |
| | Sunday, 22 November 2020 | 19.029 | 0.793 | 4.928 | 1.045 | 21:47:00 |
| | Monday, 23 November 2020 | 40.688 | 1.695 | 5.426 | 1.476 | 19:47:00 |
| | Tuesday, 24 November 2020 | 45.321 | 1.888 | 5.360 | 0.497 | 18:14:00 |
| | Wednesday, 25 November 2020 | 28.471 | 1.186 | 5.451 | 2.411 | 13:22:00 |
| | Thursday, 26 November 2020 | 46.006 | 1.917 | 6.100 | 1.917 | 15:07:00 |
| | Friday, 27 November 2020 | 34.325 | 1.430 | 5.226 | 1.188 | 13:52:00 |
| | Saturday, 28 November 2020 | 28.671 | 1.195 | 4.955 | 1.012 | 00:22:00 |
| | Sunday, 29 November 2020 | 28.764 | 1.198 | 5.438 | 1.469 | 20:22:00 |
| | Monday, 30 November 2020 | 20.171 | 0.840 | 5.660 | 1.336 | 20:52:00 |
| December | Tuesday, 01 December 2020 | 22.346 | 0.931 | 5.195 | 1.395 | 23:07:00 |

| | | | | | |
|---|---|---|---|---|---|
| Wednesday, 02 December 2020 | 15.983 | 0.666 | 5.176 | 0.825 | 08:37:00 |
| Thursday, 03 December 2020 | 17.175 | 0.716 | 4.831 | 0.784 | 08:22:00 |
| Friday, 04 December 2020 | 17.645 | 0.735 | 3.705 | 0.804 | 21:37:00 |
| Saturday, 05 December 2020 | 14.330 | 0.597 | 3.579 | 0.820 | 21:07:00 |
| Sunday, 06 December 2020 | 16.670 | 0.695 | 3.803 | 0.832 | 21:37:00 |
| Monday, 07 December 2020 | 19.988 | 0.833 | 4.919 | 0.844 | 14:07:00 |
| Tuesday, 08 December 2020 | 24.957 | 1.040 | 5.092 | 0.862 | 09:22:00 |
| Wednesday, 09 December 2020 | 18.848 | 0.785 | 5.292 | 0.814 | 09:37:00 |
| Thursday, 10 December 2020 | 41.610 | 1.734 | 6.371 | 2.279 | 20:22:00 |
| Friday, 11 December 2020 | 52.700 | 2.196 | 6.842 | 1.788 | 22:22:00 |
| Saturday, 12 December 2020 | 46.300 | 1.929 | 7.093 | 1.906 | 21:07:00 |
| Sunday, 13 December 2020 | 34.153 | 1.423 | 6.826 | 1.673 | 01:37:00 |
| Monday, 14 December 2020 | 20.640 | 0.860 | 6.009 | 0.889 | 07:22:00 |
| Tuesday, 15 December 2020 | 20.559 | 0.857 | 5.929 | 0.839 | 08:22:00 |
| Wednesday, 16 December 2020 | 22.804 | 0.950 | 5.043 | 0.868 | 08:22:00 |
| Thursday, 17 December 2020 | 26.532 | 1.106 | 5.142 | 0.883 | 13:22:00 |
| Friday, 18 December 2020 | 20.901 | 0.871 | 5.041 | 0.840 | 08:37:00 |
| Saturday, 19 December 2020 | 22.020 | 0.918 | 5.232 | 0.917 | 19:22:00 |
| Sunday, 20 December 2020 | 19.793 | 0.825 | 6.003 | 0.874 | 08:37:00 |
| Monday, 21 December 2020 | 20.418 | 0.851 | 5.025 | 0.845 | 18:44:00 |
| Tuesday, 22 December 2020 | 27.209 | 1.134 | 8.534 | 1.734 | 08:14:00 |
| Wednesday, 23 December 2020 | 32.525 | 1.355 | 6.789 | 1.938 | 21:29:00 |

| | | | | | |
|---|---|---|---|---|---|
| | Thursday, 24 December 2020 | 22.264 | 0.928 | 5.870 | 0.814 | 08:29:00 |
| | Friday, 25 December 2020 | 19.168 | 0.799 | 5.988 | 1.187 | 10:29:00 |
| | Saturday, 26 December 2020 | 44.450 | 1.852 | 6.424 | 1.752 | 13:59:00 |
| | Sunday, 27 December 2020 | 46.870 | 1.953 | 6.933 | 2.130 | 17:44:00 |
| | Monday, 28 December 2020 | 29.519 | 1.230 | 5.159 | 1.590 | 15:59:00 |
| | Tuesday, 29 December 2020 | 17.242 | 0.718 | 4.015 | 0.844 | 23:29:00 |
| | Wednesday, 30 December 2020 | 16.954 | 0.706 | 4.022 | 0.781 | 22:59:00 |
| January | Thursday, 31 December 2020 | 32.359 | 1.348 | 6.762 | 1.859 | 22:29:00 |
| | Friday, 01 January 2021 | 41.714 | 1.738 | 6.600 | 1.920 | 23:44:00 |
| | Saturday, 02 January 2021 | 23.065 | 0.961 | 4.777 | 1.457 | 05:59:00 |
| | Sunday, 03 January 2021 | 16.847 | 0.702 | 4.858 | 0.808 | 20:44:00 |
| | Monday, 04 January 2021 | 19.136 | 0.797 | 5.208 | 1.333 | 08:59:00 |
| | Tuesday, 05 January 2021 | 35.827 | 1.493 | 6.002 | 1.695 | 20:44:00 |
| | Wednesday, 06 January 2021 | 44.848 | 1.869 | 5.901 | 1.822 | 20:59:00 |
| | Thursday, 07 January 2021 | 26.026 | 1.084 | 4.782 | 0.982 | 02:44:00 |
| | Friday, 08 January 2021 | 23.868 | 0.995 | 4.769 | 1.048 | 11:14:00 |
| | Saturday, 09 January 2021 | 20.554 | 0.856 | 5.640 | 1.344 | 07:14:00 |
| | Sunday, 10 January 2021 | 43.135 | 1.797 | 6.691 | 1.712 | 20:44:00 |
| | Monday, 11 January 2021 | 29.100 | 1.212 | 4.966 | 1.101 | 18:29:00 |
| | Tuesday, 12 January 2021 | 31.768 | 1.324 | 5.859 | 1.478 | 20:29:00 |
| | Wednesday, 13 January 2021 | 33.604 | 1.400 | 6.655 | 1.462 | 19:14:00 |
| | Thursday, 14 January 2021 | 34.099 | 1.421 | 6.565 | 1.817 | 20:44:00 |

| | | | | | |
|---|---|---|---|---|---|
| | Friday, 15 January 2021 | 39.328 | 1.639 | 6.744 | 1.769 | 13:14:00 |
| | Saturday, 16 January 2021 | 26.242 | 1.093 | 5.877 | 1.281 | 20:59:00 |
| | Sunday, 17 January 2021 | 50.050 | 2.085 | 6.691 | 1.725 | 21:29:00 |
| | Monday, 18 January 2021 | 20.179 | 0.841 | 4.930 | 0.889 | 19:14:00 |
| | Tuesday, 19 January 2021 | 18.651 | 0.777 | 4.974 | 0.811 | 21:14:00 |
| | Wednesday, 20 January 2021 | 22.074 | 0.920 | 5.254 | 1.331 | 20:14:00 |
| | Thursday, 21 January 2021 | 19.236 | 0.801 | 6.418 | 0.870 | 08:44:00 |
| | Friday, 22 January 2021 | 20.372 | 0.849 | 5.238 | 1.337 | 19:59:00 |
| | Saturday, 23 January 2021 | 22.300 | 0.929 | 4.863 | 1.199 | 07:29:00 |
| | Sunday, 24 January 2021 | 27.231 | 1.135 | 5.953 | 1.206 | 09:14:00 |
| | Monday, 25 January 2021 | 17.269 | 0.720 | 4.996 | 0.814 | 08:14:00 |
| | Tuesday, 26 January 2021 | 16.587 | 0.691 | 4.667 | 0.834 | 13:44:00 |
| | Wednesday, 27 January 2021 | 17.033 | 0.710 | 4.895 | 1.012 | 08:14:00 |
| | Thursday, 28 January 2021 | 17.033 | 0.710 | 4.792 | 1.012 | 01:49:00 |
| | Friday, 29 January 2021 | 21.506 | 0.896 | 4.413 | 1.150 | 20:46:00 |
| February | Saturday, 30 January 2021 | 14.695 | 0.612 | 4.847 | 0.835 | 11:46:00 |
| | Sunday, 31 January 2021 | 19.897 | 0.829 | 4.830 | 1.190 | 21:16:00 |
| | Monday, 01 February 2021 | 21.828 | 0.909 | 6.574 | 1.598 | 09:16:00 |
| | Tuesday, 02 February 2021 | 19.819 | 0.826 | 4.928 | 0.808 | 14:31:00 |
| | Wednesday, 03 February 2021 | 18.315 | 0.763 | 3.902 | 0.810 | 20:46:00 |
| | Thursday, 04 February 2021 | 15.749 | 0.656 | 4.963 | 0.820 | 08:31:00 |
| | Friday, 05 February 2021 | 14.477 | 0.603 | 5.737 | 1.153 | 08:16:00 |

| | | | | | |
|---|---|---|---|---|---|
| Saturday, 06 February 2021 | 12.340 | 0.514 | 4.607 | 0.751 | 20:46:00 |
| Sunday, 07 February 2021 | 18.482 | 0.770 | 4.153 | 0.823 | 20:31:00 |
| Monday, 08 February 2021 | 16.337 | 0.681 | 4.866 | 0.827 | 19:31:00 |
| Tuesday, 09 February 2021 | 16.695 | 0.696 | 4.029 | 0.781 | 14:01:00 |
| Wednesday, 10 February 2021 | 16.784 | 0.699 | 5.984 | 0.759 | 13:16:00 |
| Thursday, 11 February 2021 | 14.499 | 0.604 | 3.916 | 0.775 | 13:16:00 |
| Friday, 12 February 2021 | 19.872 | 0.828 | 4.803 | 1.194 | 09:01:00 |
| Saturday, 13 February 2021 | 51.447 | 2.144 | 8.267 | 1.956 | 20:31:00 |
| Sunday, 14 February 2021 | 31.961 | 1.332 | 5.286 | 1.721 | 14:01:00 |
| Monday, 15 February 2021 | 36.171 | 1.507 | 6.104 | 1.737 | 15:16:00 |
| Tuesday, 16 February 2021 | 22.683 | 0.945 | 5.082 | 0.903 | 18:16:00 |
| Wednesday, 17 February 2021 | 19.608 | 0.817 | 4.477 | 0.826 | 07:01:00 |
| Thursday, 18 February 2021 | 28.624 | 1.193 | 6.753 | 1.494 | 16:46:00 |
| Friday, 19 February 2021 | 53.214 | 2.217 | 5.722 | 1.507 | 22:46:00 |
| Saturday, 20 February 2021 | 39.207 | 1.634 | 6.719 | 1.677 | 22:46:00 |
| Sunday, 21 February 2021 | 34.042 | 1.418 | 5.089 | 1.213 | 20:16:00 |
| Monday, 22 February 2021 | 28.291 | 1.179 | 6.003 | 1.010 | 08:01:00 |
| Tuesday, 23 February 2021 | 25.141 | 1.048 | 5.125 | 0.988 | 12:01:00 |
| Wednesday, 24 February 2021 | 25.255 | 1.052 | 6.734 | 2.204 | 20:46:00 |
| Thursday, 25 February 2021 | 22.904 | 0.954 | 5.046 | 0.852 | 12:46:00 |
| Friday, 26 February 2021 | 18.406 | 0.767 | 4.918 | 0.960 | 12:31:00 |
| Saturday, 27 February 2021 | 16.396 | 0.683 | 5.003 | 0.850 | 18:16:00 |

| | | | | | |
|---|---|---|---|---|---|
| | Sunday, 28 February 2021 | 21.970 | 0.915 | 5.450 | 1.160 | 20:42:00 |
| March | Monday, 01 March 2021 | 22.590 | 0.941 | 5.690 | 1.101 | 09:35:00 |
| | Tuesday, 02 March 2021 | 24.000 | 1.000 | 5.430 | 0.906 | 11:43:00 |
| | Wednesday, 03 March 2021 | 16.558 | 0.690 | 5.025 | 0.847 | 21:03:00 |
| | Thursday, 04 March 2021 | 25.747 | 1.073 | 5.268 | 1.548 | 14:33:00 |
| | Friday, 05 March 2021 | 19.347 | 0.806 | 4.933 | 0.807 | 19:03:00 |
| | Saturday, 06 March 2021 | 13.251 | 0.552 | 4.138 | 0.797 | 02:18:00 |
| | Sunday, 07 March 2021 | 16.267 | 0.678 | 4.907 | 0.812 | 20:18:00 |
| | Monday, 08 March 2021 | 25.211 | 1.050 | 5.156 | 1.110 | 08:33:00 |
| | Tuesday, 09 March 2021 | 25.029 | 1.043 | 6.758 | 1.726 | 21:37:00 |
| | Wednesday, 10 March 2021 | 33.100 | 1.379 | 5.862 | 1.565 | 20:22:00 |
| | Thursday, 11 March 2021 | 35.597 | 1.483 | 5.526 | 1.868 | 08:37:00 |
| | Friday, 12 March 2021 | 22.596 | 0.942 | 5.327 | 1.703 | 22:07:00 |
| | Saturday, 13 March 2021 | 19.666 | 0.819 | 5.068 | 0.878 | 21:37:00 |
| | Sunday, 14 March 2021 | 20.666 | 0.861 | 4.821 | 0.835 | 22:22:00 |
| | Monday, 15 March 2021 | 23.915 | 0.996 | 6.147 | 1.522 | 22:22:00 |
| | Tuesday, 16 March 2021 | 22.828 | 0.951 | 5.296 | 1.607 | 19:52:00 |
| | Wednesday, 17 March 2021 | 19.128 | 0.797 | 5.616 | 1.370 | 22:37:00 |
| | Thursday, 18 March 2021 | 28.156 | 1.173 | 5.917 | 1.559 | 21:07:00 |
| | Friday, 19 March 2021 | 25.139 | 1.047 | 6.576 | 1.713 | 20:52:00 |
| | Saturday, 20 March 2021 | 21.840 | 0.910 | 4.786 | 0.797 | 11:22:00 |
| | Sunday, 21 March 2021 | 19.089 | 0.795 | 5.067 | 1.010 | 11:37:00 |

| | | | | | |
|---|---|---|---|---|---|
| | Monday, 22 March 2021 | 17.568 | 0.732 | 4.697 | 0.836 | 08:07:00 |
| | Tuesday, 23 March 2021 | 18.626 | 0.776 | 4.581 | 0.844 | 10:37:00 |
| | Wednesday, 24 March 2021 | 19.104 | 0.796 | 5.189 | 0.827 | 18:37:00 |
| | Thursday, 25 March 2021 | 22.049 | 0.919 | 4.859 | 0.848 | 13:22:00 |
| | Friday, 26 March 2021 | 22.768 | 0.949 | 3.596 | 0.848 | 19:22:00 |
| | Saturday, 27 March 2021 | 14.876 | 0.620 | 4.637 | 0.871 | 20:07:00 |
| | Sunday, 28 March 2021 | 13.806 | 0.575 | 3.587 | 0.060 | 20:07:00 |
| | Monday, 29 March 2021 | 24.112 | 1.005 | 5.084 | 0.822 | 13:37:00 |
| | Tuesday, 30 March 2021 | 18.859 | 0.786 | 5.262 | 0.808 | 08:52:00 |
| | Wednesday, 31 March 2021 | 15.932 | 0.664 | 3.549 | 0.771 | 20:37:00 |
| APRIL | Thursday, 01 April 2021 | 14.725 | 0.614 | 4.887 | 0.842 | 08:37:00 |
| | Friday, 02 April 2021 | 16.006 | 0.667 | 4.768 | 0.874 | 09:52:00 |
| | Saturday, 03 April 2021 | 28.010 | 1.167 | 6.059 | 1.407 | 20:07:00 |
| | Sunday, 04 April 2021 | 11.691 | 0.487 | 4.614 | 0.642 | 00:52:00 |
| | Monday, 05 April 2021 | 15.696 | 0.654 | 4.846 | 0.797 | 20:52:00 |
| | Tuesday, 06 April 2021 | 20.348 | 0.848 | 8.061 | 0.952 | 08:22:00 |
| | Wednesday, 07 April 2021 | 20.018 | 0.834 | 5.176 | 0.845 | 10:37:00 |
| | Thursday, 08 April 2021 | 17.318 | 0.722 | 4.862 | 0.776 | 13:19:00 |
| | Friday, 09 April 2021 | 16.770 | 0.699 | 4.957 | 0.843 | 18:19:00 |
| | Saturday, 10 April 2021 | 15.292 | 0.637 | 3.617 | 0.844 | 16:19:00 |
| | Sunday, 11 April 2021 | 18.803 | 0.783 | 4.652 | 1.031 | 19:04:00 |
| | Monday, 12 April 2021 | 21.678 | 0.903 | 5.390 | 1.024 | 21:34:00 |

| | | | | | |
|---|---|---|---|---|---|
| | Tuesday, 13 April 2021 | 20.690 | 0.862 | 6.582 | 1.086 | 09:34:00 |
| | Wednesday, 14 April 2021 | 16.998 | 0.708 | 5.158 | 1.034 | 20:34:00 |
| | Thursday, 15 April 2021 | 22.274 | 0.928 | 6.418 | 1.026 | 09:49:00 |
| | Friday, 16 April 2021 | 20.996 | 0.875 | 4.404 | 1.119 | 19:49:00 |
| | Saturday, 17 April 2021 | 17.996 | 0.750 | 4.948 | 0.855 | 17:34:00 |
| | Sunday, 18 April 2021 | 17.099 | 0.712 | 5.247 | 0.907 | 18:19:00 |
| | Monday, 19 April 2021 | 24.490 | 1.020 | 5.050 | 0.850 | 12:19:00 |
| | Tuesday, 20 April 2021 | 25.191 | 1.050 | 6.455 | 0.863 | 08:34:00 |
| | Wednesday, 21 April 2021 | 22.228 | 0.926 | 5.061 | 0.841 | 18:34:00 |
| | Thursday, 22 April 2021 | 20.968 | 0.874 | 5.102 | 0.888 | 19:19:00 |
| | Friday, 23 April 2021 | 26.491 | 1.104 | 5.040 | 0.888 | 09:34:00 |
| | Saturday, 24 April 2021 | 11.414 | 0.476 | 3.501 | 0.757 | 00:34:00 |
| | Sunday, 25 April 2021 | 18.284 | 0.762 | 4.972 | 0.863 | 18:19:00 |
| | Monday, 26 April 2021 | 19.986 | 0.833 | 4.844 | 0.807 | 08:19:00 |
| | Tuesday, 27 April 2021 | 20.740 | 0.864 | 4.913 | 0.841 | 08:19:00 |
| | Wednesday, 28 April 2021 | 15.582 | 0.649 | 4.986 | 0.821 | 18:19:00 |
| | Thursday, 29 April 2021 | 22.447 | 0.935 | 4.860 | 0.851 | 12:19:00 |
| | Friday, 30 April 2021 | 23.269 | 0.970 | 4.863 | 0.841 | 13:04:00 |
| MAY | Saturday, 01 May 2021 | 13.052 | 0.544 | 3.652 | 0.803 | 19:34:00 |
| | Sunday, 02 May 2021 | 18.891 | 0.787 | 4.799 | 0.815 | 11:04:00 |
| | Monday, 03 May 2021 | 19.099 | 0.796 | 4.831 | 0.839 | 17:49:00 |
| | Tuesday, 04 May 2021 | 28.207 | 1.175 | 8.049 | 1.846 | 08:19:00 |

| | | | | | |
|---|---|---|---|---|---|
| Wednesday, 05 May 2021 | 30.320 | 1.263 | 6.189 | 1.311 | 08:34:00 |
| Thursday, 06 May 2021 | 34.337 | 1.431 | 8.038 | 1.407 | 09:19:00 |
| Friday, 07 May 2021 | 29.884 | 1.245 | 7.993 | 1.866 | 08:34:00 |
| Saturday, 08 May 2021 | 28.864 | 1.203 | 5.886 | 1.723 | 08:19:00 |
| Sunday, 09 May 2021 | 26.949 | 1.123 | 5.837 | 1.789 | 16:23:00 |
| Monday, 10 May 2021 | 32.114 | 1.338 | 6.412 | 1.302 | 09:08:00 |
| Tuesday, 11 May 2021 | 28.748 | 1.198 | 5.853 | 1.618 | 08:08:00 |
| Wednesday, 12 May 2021 | 28.290 | 1.179 | 6.163 | 1.944 | 09:08:00 |
| Thursday, 13 May 2021 | 24.273 | 1.011 | 4.740 | 0.975 | 19:38:00 |
| Friday, 14 May 2021 | 24.355 | 1.015 | 4.935 | 0.955 | 09:38:00 |
| Saturday, 15 May 2021 | 21.158 | 0.882 | 4.787 | 0.921 | 21:53:00 |
| Sunday, 16 May 2021 | 21.619 | 0.901 | 4.792 | 0.986 | 20:53:00 |
| Monday, 17 May 2021 | 23.587 | 0.983 | 5.005 | 1.000 | 20:23:00 |
| Tuesday, 18 May 2021 | 21.838 | 0.910 | 6.277 | 1.117 | 08:38:00 |
| Wednesday, 19 May 2021 | 26.532 | 1.106 | 4.715 | 0.856 | 22:08:00 |
| Thursday, 20 May 2021 | 21.625 | 0.901 | 4.604 | 0.955 | 19:08:00 |
| Friday, 21 May 2021 | 24.486 | 1.020 | 5.005 | 0.995 | 20:08:00 |
| Saturday, 22 May 2021 | 24.788 | 1.033 | 5.060 | 0.874 | 18:23:00 |
| Sunday, 23 May 2021 | 17.920 | 0.747 | 3.917 | 1.679 | 13:38:00 |
| Monday, 24 May 2021 | 37.465 | 1.561 | 5.712 | 1.814 | 07:08:00 |
| Tuesday, 25 May 2021 | 36.498 | 1.521 | 6.934 | 1.547 | 09:04:00 |
| Wednesday, 26 May 2021 | 32.357 | 1.348 | 6.682 | 1.418 | 08:19:00 |

| | | | | | |
|---|---|---|---|---|---|
| | Thursday, 27 May 2021 | 40.102 | 1.671 | 7.913 | 1.934 | 08:19:00 |
| | Friday, 28 May 2021 | 37.884 | 1.578 | 6.997 | 1.774 | 08:19:00 |
| | Saturday, 29 May 2021 | 24.774 | 1.032 | 4.585 | 1.244 | 20:49:00 |
| | Sunday, 30 May 2021 | 31.128 | 1.297 | 7.870 | 1.693 | 09:19:00 |
| | Monday, 31 May 2021 | 27.543 | 1.148 | 6.486 | 1.220 | 17:04:00 |
| JUNE | Tuesday, 01 June 2021 | 40.015 | 1.667 | 6.556 | 1.901 | 08:04:00 |
| | Wednesday, 02 June 2021 | 38.626 | 1.609 | 6.907 | 1.664 | 09:04:00 |
| | Thursday, 03 June 2021 | 44.170 | 1.840 | 6.678 | 1.923 | 07:04:00 |
| | Friday, 04 June 2021 | 45.360 | 1.890 | 7.813 | 2.128 | 18:49:00 |
| | Saturday, 05 June 2021 | 35.362 | 1.473 | 7.703 | 2.109 | 18:49:00 |
| | Sunday, 06 June 2021 | 38.470 | 1.603 | 7.671 | 2.124 | 18:49:00 |
| | Monday, 07 June 2021 | 52.057 | 2.169 | 6.805 | 2.129 | 18:34:00 |
| | Tuesday, 08 June 2021 | 49.576 | 2.066 | 7.611 | 1.931 | 09:04:00 |
| | Wednesday, 09 June 2021 | 48.164 | 2.007 | 6.851 | 1.963 | 08:19:00 |
| | Thursday, 10 June 2021 | 47.819 | 1.992 | 6.991 | 1.610 | 06:49:00 |
| | Friday, 11 June 2021 | 47.192 | 1.966 | 7.534 | 2.193 | 09:19:00 |
| | Saturday, 12 June 2021 | 35.027 | 1.459 | 5.913 | 2.016 | 07:49:00 |
| | Sunday, 13 June 2021 | 33.703 | 1.404 | 6.182 | 1.547 | 08:34:00 |
| | Monday, 14 June 2021 | 47.427 | 1.976 | 7.493 | 2.047 | 08:18:00 |
| | Tuesday, 15 June 2021 | 41.760 | 1.740 | 7.431 | 1.995 | 09:34:00 |
| | Wednesday, 16 June 2021 | 36.355 | 1.515 | 6.756 | 1.669 | 09:03:00 |
| | Thursday, 17 June 2021 | 34.611 | 1.442 | 6.607 | 1.339 | 06:48:00 |

| | | | | | |
|---|---|---|---|---|---|
| | Friday, 18 June 2021 | 36.510 | 1.521 | 5.889 | 5.080 | 09:48:00 |
| | Saturday, 19 June 2021 | 31.205 | 1.300 | 7.386 | 1.929 | 18:03:00 |
| | Sunday, 20 June 2021 | 35.407 | 1.475 | 5.855 | 1.714 | 08:48:00 |
| | Monday, 21 June 2021 | 59.253 | 2.469 | 7.366 | 1.948 | 09:18:00 |
| | Tuesday, 22 June 2021 | 50.626 | 2.109 | 6.996 | 1.892 | 09:03:00 |
| | Wednesday, 23 June 2021 | 37.103 | 1.546 | 7.336 | 1.390 | 09:49:00 |
| | Thursday, 24 June 2021 | 39.265 | 1.636 | 5.502 | 1.388 | 09:03:00 |
| | Friday, 25 June 2021 | 27.610 | 1.150 | 4.976 | 0.814 | 12:48:00 |
| | Saturday, 26 June 2021 | 20.237 | 0.843 | 4.853 | 0.827 | 15:48:00 |
| | Sunday, 27 June 2021 | 16.316 | 0.680 | 5.982 | 0.857 | 08:48:00 |
| | Monday, 28 June 2021 | 26.281 | 1.095 | 6.273 | 0.978 | 09:33:00 |
| | Tuesday, 29 June 2021 | 25.071 | 1.045 | 4.993 | 0.830 | 20:18:00 |
| | Wednesday, 30 June 2021 | 25.556 | 1.065 | 5.515 | 0.814 | 00:03:00 |
| | Thursday, 01 July 2021 | 18.767 | 0.841 | 4.929 | 0.841 | 18:33:00 |
| | Friday, 02 July 2021 | 26.226 | 0.833 | 4.908 | 0.833 | 19:18:00 |
| | Saturday, 03 July 2021 | 21.214 | 0.831 | 3.707 | 0.831 | 18:48:00 |
| | Sunday, 04 July 2021 | 24.016 | 2.884 | 4.884 | 2.884 | 17:03:00 |
| | Monday, 05 July 2021 | 30.258 | 1.380 | 5.477 | 1.380 | 08:49:00 |
| | Tuesday, 06 July 2021 | 30.455 | 0.840 | 5.020 | 0.840 | 15:03:00 |
| | Wednesday, 07 July 2021 | 30.783 | 1.275 | 6.344 | 1.275 | 09:18:00 |
| | Thursday, 08 July 2021 | 21.107 | 0.977 | 5.161 | 0.977 | 18:33:00 |
| | Friday, 09 July 2021 | 23.094 | 0.993 | 6.416 | 0.993 | 06:48:00 |

| | | | | | |
|---|---|---|---|---|---|
| | Saturday, 10 July 2021 | 22.939 | 0.858 | 5.761 | 0.858 | 11:03:00 |
| | Sunday, 11 July 2021 | 18.243 | 0.850 | 4.939 | 0.850 | 18:19:00 |
| | Monday, 12 July 2021 | 24.903 | 0.860 | 3.805 | 0.860 | 19:49:00 |
| | Tuesday, 13 July 2021 | 24.173 | 0.853 | 5.409 | 0.853 | 10:19:00 |
| | Wednesday, 14 July 2021 | 25.786 | 0.941 | 4.896 | 0.941 | 20:19:00 |
| | Thursday, 15 July 2021 | 36.022 | 1.360 | 5.874 | 1.929 | 17:49:00 |
| | Friday, 16 July 2021 | 24.261 | 0.873 | 4.838 | 1.082 | 14:49:00 |
| | Saturday, 17 July 2021 | 38.613 | 1.400 | 7.283 | 1.973 | 09:34:00 |
| | Sunday, 18 July 2021 | 28.234 | 1.381 | 6.134 | 1.956 | 09:19:00 |
| | Monday, 19 July 2021 | 50.068 | 1.577 | 7.245 | 2.035 | 12:49:00 |
| | Tuesday, 20 July 2021 | 36.198 | 1.377 | 6.435 | 1.956 | 08:04:00 |
| | Wednesday, 21 July 2021 | 60.461 | 1.702 | 7.187 | 2.275 | 18:34:00 |
| | Thursday, 22 July 2021 | 44.190 | 1.474 | 6.286 | 1.474 | 20:34:00 |
| | Friday, 23 July 2021 | 49.788 | 1.650 | 6.245 | 2.416 | 22:49:00 |
| | Saturday, 24 July 2021 | 32.388 | 1.399 | 6.284 | 1.399 | 22:04:00 |
| | Sunday, 25 July 2021 | 31.074 | 1.442 | 6.313 | 1.442 | 22:19:00 |
| | Monday, 26 July 2021 | 41.872 | 1.806 | 7.187 | 2.398 | 18:49:00 |
| | Tuesday, 27 July 2021 | 38.746 | 1.328 | 6.242 | 1.328 | 19:04:00 |
| | Wednesday, 28 July 2021 | 30.709 | 1.417 | 6.416 | 1.417 | 21:19:00 |
| August | Thursday, 29 July 2021 | 39.283 | 1.394 | 6.488 | 1.394 | 19:34:00 |
| | Friday, 30 July 2021 | 39.994 | 1.265 | 6.525 | 1.265 | 20:49:00 |
| | Saturday, 31 July 2021 | 26.264 | 1.398 | 6.478 | 1.398 | 21:19:00 |

| | | | | | |
|---|---|---|---|---|---|
| Sunday, 01 August 2021 | 30.659 | 1.397 | 7.149 | 1.397 | 20:34:00 |
| Monday, 02 August 2021 | 31.685 | 1.228 | 6.199 | 1.228 | 22:04:00 |
| Tuesday, 03 August 2021 | 29.385 | 1.167 | 7.115 | 1.167 | 20:34:00 |
| Wednesday, 04 August 2021 | 32.455 | 1.057 | 6.374 | 1.057 | 20:19:00 |
| Thursday, 05 August 2021 | 33.756 | 1.208 | 6.433 | 1.208 | 20:19:00 |
| Friday, 06 August 2021 | 27.453 | 0.887 | 5.040 | 0.887 | 21:49:00 |
| Saturday, 07 August 2021 | 25.909 | 0.898 | 5.033 | 0.898 | 20:19:00 |
| Sunday, 08 August 2021 | 23.063 | 0.881 | 6.363 | 0.881 | 22:04:00 |
| Monday, 09 August 2021 | 30.164 | 0.952 | 6.577 | 0.952 | 20:34:00 |
| Tuesday, 10 August 2021 | 24.425 | 1.377 | 6.562 | 1.377 | 19:34:00 |
| Wednesday, 11 August 2021 | 31.913 | 0.987 | 6.319 | 0.987 | 18:34:00 |
| Thursday, 12 August 2021 | 26.162 | 0.861 | 5.132 | 0.861 | 20:19:00 |
| Friday, 13 August 2021 | 23.574 | 1.204 | 6.328 | 1.204 | 18:49:00 |
| Saturday, 14 August 2021 | 28.656 | 1.404 | 6.239 | 1.404 | 12:49:00 |
| Sunday, 15 August 2021 | 37.035 | 1.341 | 6.363 | 1.341 | 17:19:00 |
| Monday, 16 August 2021 | 34.316 | 1.347 | 7.111 | 1.347 | 19:49:00 |
| Tuesday, 17 August 2021 | 36.618 | 1.412 | 6.424 | 1.412 | 19:34:00 |
| Wednesday, 18 August 2021 | 28.755 | 0.956 | 5.639 | 0.956 | 12:49:00 |
| Thursday, 19 August 2021 | 25.966 | 1.050 | 6.520 | 1.050 | 19:49:00 |
| Friday, 20 August 2021 | | | | | |
| Saturday, 21 August 2021 | | | | | |
| | | | | | |

|  |  |  |  |  |  |  |
|---|---|---|---|---|---|---|
|  |  |  |  |  |  |  |
|  |  |  |  |  |  |  |
|  |  |  |  |  |  |  |
|  |  |  |  |  |  |  |

## 10 APPENDIX B – MATLAB CODE

### 10.1 MPPT Algorithm

```
function duty= MPPT(vpv,ipv,delta_in)
duty_init=0.05;
duty_min=0;
duty_max=0.85;

persistent Vold Pold duty_old;
if isempty(Vold)
    Vold=0;
    Pold=0;
    duty_old=duty_init;
end
P= vpv*ipv;
dV= vpv-Vold;
dP= P-Pold;
duty = duty_old;
delta= delta_in;

if dP~= 0
```

```matlab
if dP<0
    if dV<0
        duty=duty_old - delta;
    else
        duty=duty_old + delta;
    end
else
    if dV<0
        duty=duty_old + delta;

    else
        duty= duty_old - delta;
    end
end
if duty>=duty_max;
    duty=duty_max;
elseif duty<duty_min
    duty=duty_min;
end
duty_old=duty;
Vold=vpv;
```

```
   Pold=P;
```

## 10.2  Community solar PV microgrid component code

```
%Boost Converter Filter Design

P=250e3;      %Rated power

U=460; %Inverter phase2phase voltage

f=50;         %grid frequency

fsw=5e3;    %switching frequency

Ts=1e-6;      %Sampling time


Lf=((0.1*(U^2))/(2*pi*f*(P/3)));  %Filter inductance for inverter


%Design of boost converter

Vmpp=546.75;

V_bus_ref=835;

Vin=Vmpp;      %input voltage of boost converter
```

Vo=V_bus_ref;   %output voltage of boost converter

fsw_boost=5e3; %switching frequency of boost converter

D= 1-(Vin/Vo);

L_bound= ((1-D)^2)*D*(Vo^2)/(2*fsw_boost*P);

C_boost_min= (D*P)/(0.1*Vo^2*fsw_boost);

L_boost = 10*L_bound; %Boost converter inductor

C_boost= 1000e-6;


%LCL Filter for grid-connected inverter

fres=fsw/10;

Ig= P/(3*U);

Igsw =0.003*Ig;

Vgsw=0.9*U;

Wsw=2*pi*fsw;

Wres=2*pi*fres;

Lmin=abs((1)/(((Wsw*(Igsw/Vgsw))*(1-((Wsw^2)/(Wres^2))))));

Lmin_value= Lmin/2;

C= ((0.05*P)/(3*((U^2)*2*pi*f)));

Lmax=((0.2*U)/(2*pi*f*Ig));

Lmax_value=Lmax/2;

R= Vo^2/P;

### 10.3  Data preprocessing

Due to power outages in the area, there are missing gaps in the annual power usages.

#### 10.3.1  Missing data

Through the MATLAB live script, the linear interpolation method was utilized to fill the missing data. The code used to fill in the missing data is shown below.

```
% Fill missing data
[cleanedData,missingIndices] = fillmissing(new1.ActivePowerkW,'linear');
% Display results
clf
plot(cleanedData,'Color',[0 114 189]/255,'LineWidth',1.5,...
    'DisplayName','Cleaned data')
```

```matlab
hold on
% Plot filled missing entries
plot(find(missingIndices),cleanedData(missingIndices),'.','MarkerSize',12,...
    'Color',[217 83 25]/255,'DisplayName','Filled missing entries')
title(['Number of filled missing entries: ' num2str(nnz(missing indices))])
hold off
legend
clear missing indices
```

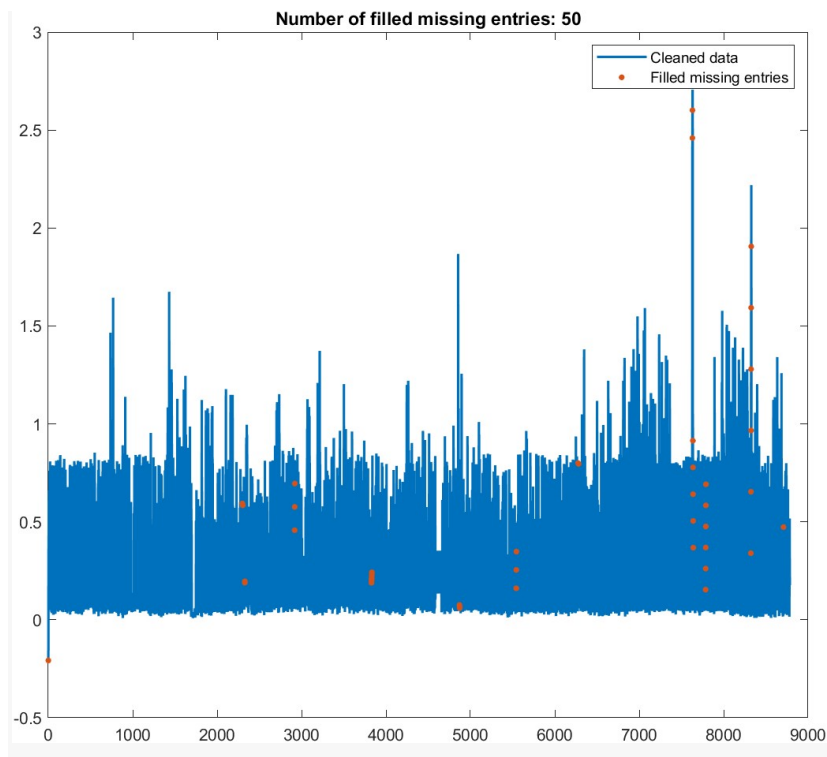Figure 10.1 is a graph of filled missing entries in the dataset.

Figure 10.1: Missing entries filled in the daily energy consumption dataset

### 10.3.2  Remove outliers

The exceptional values in the dataset have the possibility of distorting statistical analysis. Thereby they must be removed. Below is the MATLAB live script code to remove the outliers

```
% Remove outliers
[cleanedData2,outlierIndices] = rmoutliers(new1.ActivePowerkW,'mean');
```

```matlab
% Display results
clf
plot(new1.ActivePowerkW,'Color',[109 185 226]/255,'DisplayName','Input data')
hold on
plot(find(~outlierIndices),cleanedData2,'Color',[0 114 189]/255,'LineWidth',1.5,...
    'DisplayName','Cleaned data')


% Plot outliers
plot(find(outlierIndices),new1.ActivePowerkW(outlierIndices),'x',...
    'Color',[64 64 64]/255,'DisplayName','Outliers')
title(['Number of outliers: ' num2str(nnz(outlierIndices))])
% Compute thresholds and center
[~,thresholdLow,thresholdHigh] = isoutlier(new1.ActivePowerkW,'mean');
% Plot outlier thresholds
plot([xlim missing xlim],[thresholdLow*[1 1] NaN thresholdHigh*[1 1]],...
    'Color',[145 145 145]/255,'DisplayName','Outlier thresholds')
hold off
legend
clear threshold low threshold high
```
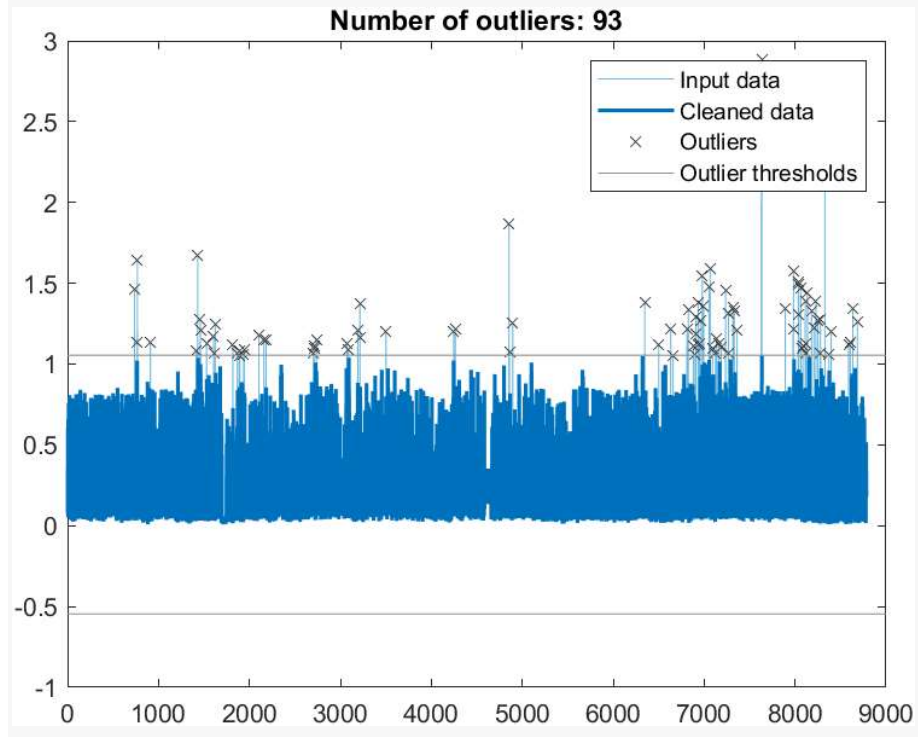
Figure 10.2 represents the number of outliers in the dataset



Figure 10.2: Number of outliers in the large dataset